NASA CR 54825
AGC 8800-28

ANALYSIS OF

THE M-1 LIQUID HYDROGEN TURBOPUMP SHAFT

CRITICAL WHIRLING SPEED AND BEARING LOADS

By

L. K. Severud
H. G. Reeser

Prepared for

National Aeronautics and Space Administration

Contract NAS 3-2555

AEROJET
GENERAL TIRE
GENERAL

AEROJET-GENERAL CORPORATION

SACRAMENTO, CALIFORNIA

Requests for copies of this report should be referred to:

National Aeronautics and Space Administration
Office of Scientific and Technical Information
Attention: AFSS-A
Washington, D. C. 20546

TECHNOLOGY REPORT

ANALYSIS OF
THE M-1 LIQUID HYDROGEN TURBOPUMP SHAFT
CRITICAL WHIRLING SPEED AND BEARING LOADS

Prepared for

NATIONAL AERONAUTICS AND SPACE ADMINISTRATION

December 20, 1965

CONTRACT NAS 3-2555

Prepared by:

AEROJET-GENERAL CORPORATION
LIQUID ROCKET OPERATIONS
SACRAMENTO, CALIFORNIA

AUTHORS: L. K. Severud and
            H. G. Reeser

APPROVED: W. E. Campbell
            Manager
            M-1 Turbopump Project

Technical Management:

NASA LEWIS RESEARCH CENTER
CLEVELAND, OHIO

NASA TECHNICAL MANAGER: W. W. Wilcox

APPROVED: W. F. Dankhoff
                M-1 Project Manager

ABSTRACT

19689

The shaft whirling critical speeds for the M-1 fuel turbopump assembly are presented in this report. The roller bearing loads caused by shaft whirling and other sources are also discussed.

The predicted critical speeds are 16,000 rpm for the Model I turbopump, 15,700 rpm for the Model II turbopump with an interim inducer, and 18,000 rpm for the Model II turbopump with the final inducer. Nominal operating speeds for the Model I and Model II turbopumps are 11,700 rpm and 13,225 rpm, respectively.

TABLE OF CONTENTS

TABLE OF CONTENTS (Cont.)

APPENDICES

LIST OF TABLES

LIST OF FIGURES

I. SUMMARY

The analytical determination of shaft whirling critical speeds and bearing loads for the Model I and Model II fuel turbopumps is delineated herein. The Model I is basically the same as the Model II except for the turbine end in that the Model I turbopump has one turbine wheel while the Model II has two turbine wheels.

The nominal operating shaft speeds for both turbopumps (Model I and Model II) are 11,700 and 13,225 rpm, respectively. These are sufficiently below their first critical speed to preclude bearing loads of magnitude in excess of the roller bearing capacities. The critical speeds predicted are 16,000 rpm for the Model I, 15,700 rpm for the Model II with interim inducer, and 18,000 rpm for the Model II with final inducer.

Bearing loads from sources other than shaft whirling (e.g., engine accelerations, gimbal snubbing, decelerations, etc.) are presented and combined into the total predicted reactions. As the total reactions on the roller bearings are less than the predicted and test demonstrated capacities, they should not cause bearing failure during the required life of the turbopump.

Experimental and theoretical evaluation and correlation of roller bearing spring rate-load relationships was accomplished. The turbine bearing support housing spring constant was also evaluated both experimentally and analytically.

The analyses were accomplished using digital computer programs, which are capable of accounting for the effects of non-linear load-deflection characteristics of the bearings, gyroscopic and inertia forces, shear and flexural deflections of the shaft, rotor misalignment and bearing clearances, and dynamic coupling of the housing and rotor.

II. INTRODUCTION

The lateral vibration and roller bearing load analysis for the M-1 fuel turbopump assembly for both the Model I (single turbine wheel) and Model II (two turbine wheels) configurations is delineated in this report.

In addition to the computation of the natural frequencies and roller bearing loads, the following areas were also investigated: shaft elastic curves (for evaluation of rotor blade clearances) shaft bending stresses caused by conical whirling, bearing capacities, and operating Hertz stress levels.

The analysis was made in support of the design of the M-1 fuel turbopump which was designed, fabricated, assembled, and tested by the Aerojet-General Corp. at its Sacramento Plant under Contract NAS 3-2555 for the National Aeronautics and Space Administration Lewis Research Center, Cleveland, Ohio.

Much of the analysis was performed using computer programs developed for the dynamic analysis of the fuel turbopump assembly. In addition to providing a capability for evaluating the natural frequencies of complex

multi-degree-of-freedom models, these programs were also used to determine the mode shapes and associated shear and moment distributions, as well as the slopes and deflections caused by harmonic forcing functions.

III.   DESCRIPTION OF OVER-ALL CONFIGURATION

The fuel turbopump assembly is a 10-stage axial flow unit designed to deliver liquid hydrogen at a high flowrate. The 10 stages consist of a first-stage mixed flow inducer and stator, a second-stage axial inducer and stator, and eight axial mainstages. Each mainstage consists of a row of rotating blades and a row of stator blades. Power is supplied by a single- or double-stage turbine, which is coupled directly to the pump rotating assembly. The fuel turbopump assembly, in its transport stand, is shown in Figure No. 1.

The fuel turbopump assembly is an integrated design in that no separate pump assembly, power transmission assembly, or turbine assembly exist as completely independent units. The bearings are contained within the pump envelope. The turbine shaft, which carries the turbine-end roller bearing, is installed directly into the pump rotor by using a series of pilot diameters and a spline. This coupling is designed so that a rigid joint is formed at operating temperature, which results in a single rotating assembly comprised of turbine and pump components.

A more complete description of the turbopump is provided in other NASA Contractor Reports.(1)(2)

A.   MODEL I AND MODEL II TURBOPUMP UNITS

There are three versions of the M-1 fuel turbopump assembly. The bearings are identical in each unit. The only differences occur in the first-stage inducer and turbine areas. The Model I has a single-stage turbine and exhaust cone, and an interim inducer. Most of the rotating system for the single stage turbine configuration is shown in Figure No. 2. The Model II has a two-stage turbine and the same exhaust cone and inducer as the Model I. The Model II-B unit is identical to the Model II-A except that the interim inducer is replaced with a lighter final inducer and the exhaust cone is replaced with a hemispherical exhaust manifold.

The Model I and Model II-A are intended for component testing only. The Model I is designed to operate up to three-fourths of design speed while the Model II-A is capable of full speed operation. It is the Model II-B that is intended for use in the engine system.

---

(1)   "Mechanical Design of a Two Stage Impulse Turbine for the Liquid Hydrogen Turbopump of the M-1 Engine," NASA CR-54821,   1966.

(2)   "Mechanical Design of the M-1 Axial Flow Liquid Hydrogen Pump," NASA CR-54823,   1966.
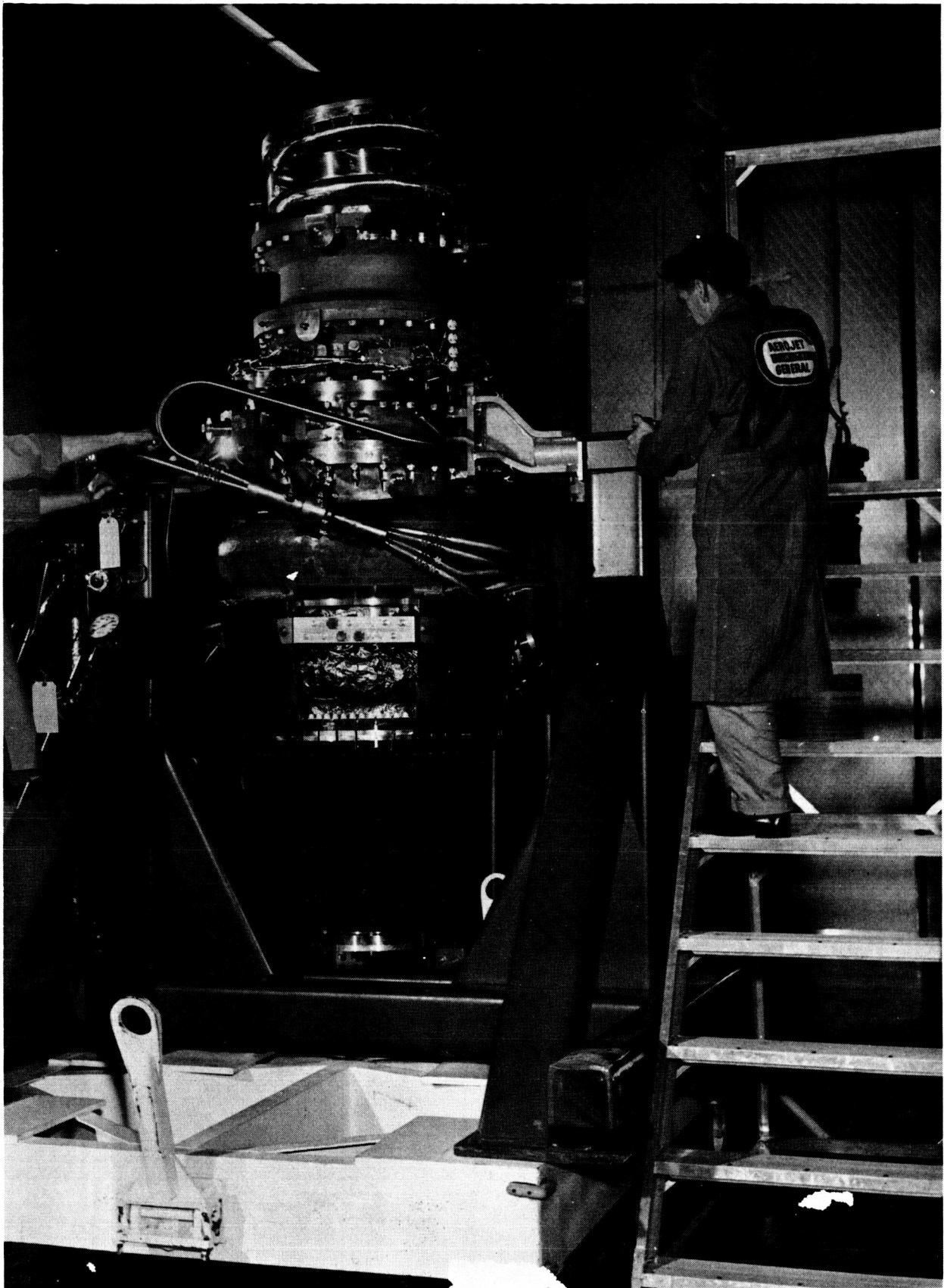
Figure 1

Model I Fuel Turbopump Assembly
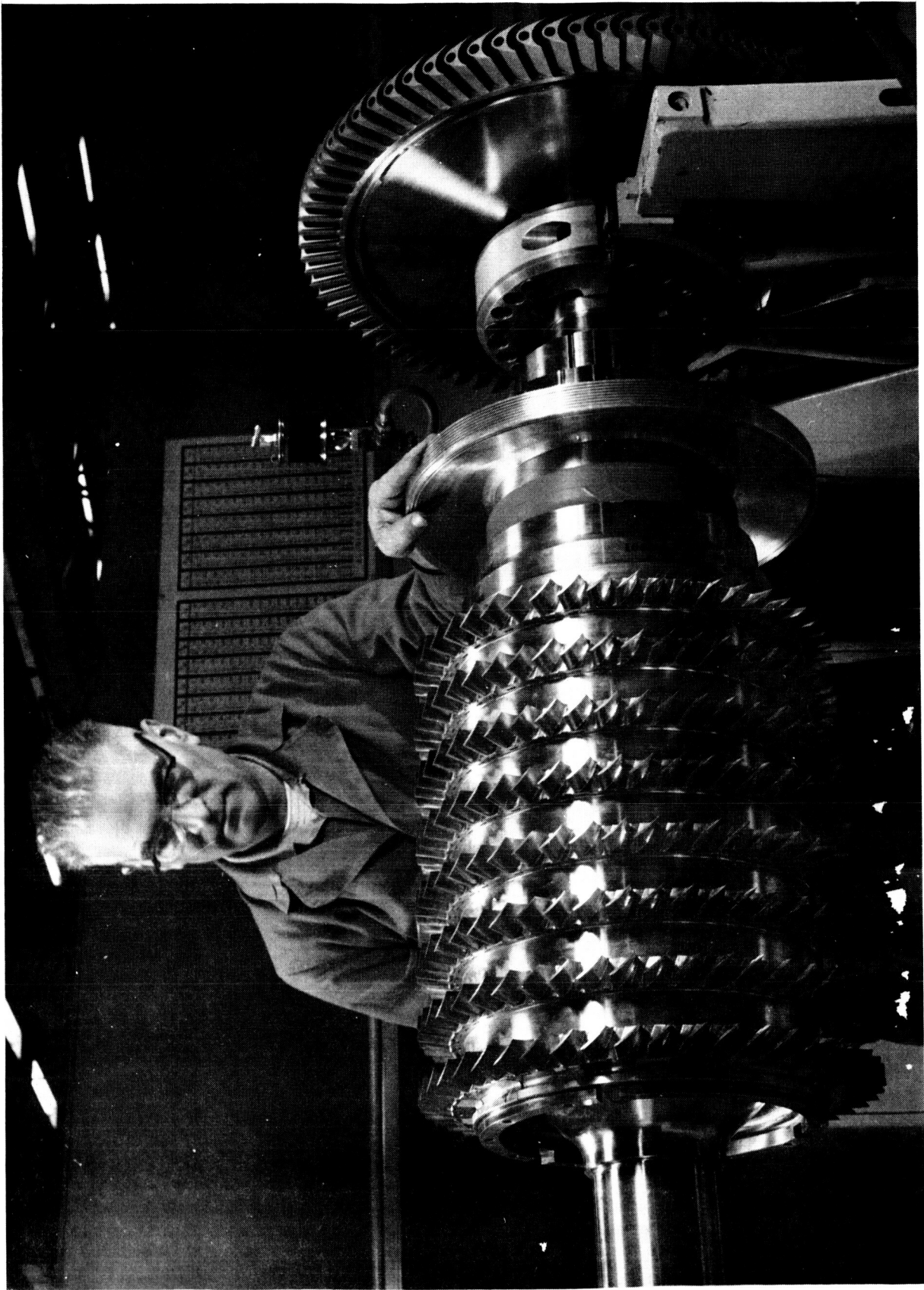
Figure 2

Model I Rotor

B.   STATIONARY PARTS (FUEL TURBOPUMP ASSEMBLY HOUSING)

The guide vane housing, located directly above the ball bearings (Figure No. 3), serves two functions. It provides a set of guide vanes that direct the fluid flow from the first-stage inducer to the second-stage inducer and it serves as a bearing housing, which supports the pump-end bearing package. All thrust loads and pump end radial loads are transmitted through this housing, which also contains passages for bearing coolant flow, both in and out of the bearing package. This housing contains passages used for routing instrumentation wires which originate within the bearing package.

The stationary components at the turbine end consist of the turbine bearing housing support frame, inlet manifold, and exhaust cone.

The turbine bearing housing transmits the radial loads from the turbine bearing to the pump discharge housing. Coolant passages for the bearing are located in the housing.

The support frame is made up of three conical segments that are fabricated from sheet stock. Each segment is continuous for approximately 72-degrees of the circumference. The openings between the segments are required for the turbine manifold, coolant lines, and instrumentation.

The turbine inlet manifold is a constant area torus containing 37 nozzle vanes. The manifold is insulated to minimize the transfer of heat to pump components. Heat shields and a metal seal are provided to confine all hot gas flow to the turbine area and exhaust system.

The exhaust cone is fabricated from sheet metal and is designed to direct the exhaust gases into a test stand exhaust line. The model II-B has a hemispherical exhaust manifold, which has outlets for ducts that route the exhaust gases to the oxidizer pump turbine inlet manifold.

C.   WEIGHT

All rotating components are of flight-weight design. Weight reduction became a vital factor in obtaining an acceptable calculated critical speed for the fuel turbopump assembly.

In contrast to the lightweight rotating components, the exterior housing, which are machined from castings, are of heavy construction. Component weight was only a minor consideration when function and schedule lead time were considered.

D.   METHOD OF SUPPORT FOR ROTATING SYSTEM

The fuel turbopump assembly rotor support system is designed so that the radial loads are transmitted from the rotor, through the roller bearings, to the housing. The thrust loads are transmitted from the rotor, through the ball bearings, to the housing.
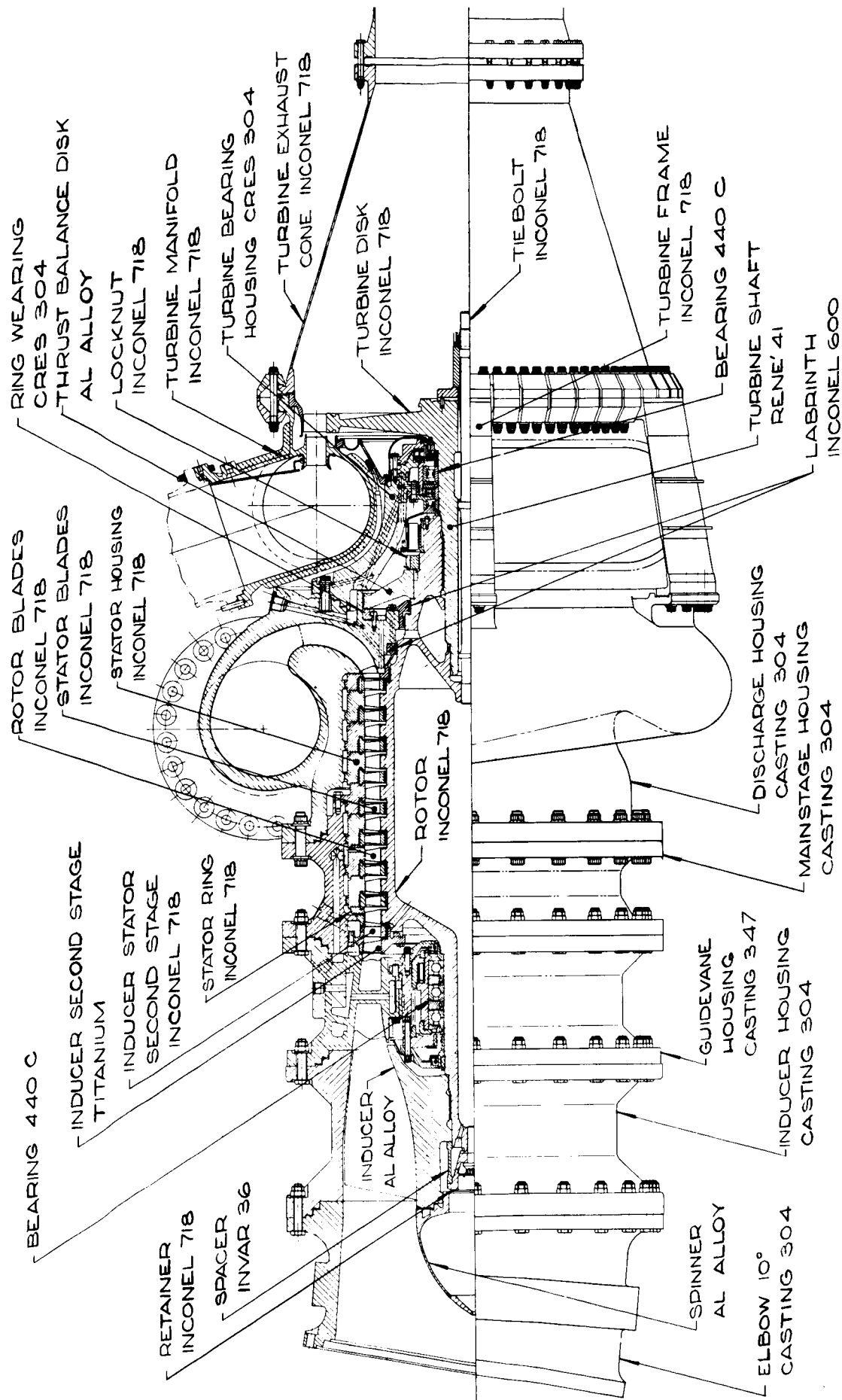
Figure 3

Model I Turbopump Cross-Section

The ball bearings are ground as a set to guarantee proportionate load sharing. The thrust bearing system is designed so that the ball bearings can transmit a maximum radial load of approximately 200 lb. This is accomplished by mounting the thrust bearings in a radially flexible housing, which ensures that the roller bearings carry virtually all of the radial loads.

E. METHOD OF SUPPORT FOR FUEL TURBOPUMP ASSEMBLY HOUSING

The fuel turbopump assembly is secured to the test stand or engine by supporting struts (see Figures No. 4, 5, and 6) which are connected to the engine at three points. Two of the connection points are located in a plane near the pump center of gravity and the third acts as a stabilizer.

The method of attaching the fuel turbopump assembly to the engine or test stand defines the spring system between the turbopump and its reference plane (i.e., ground). Because the stiffness of the supporting struts has some effect upon the critical speeds and bearing reactions, the strut stiffness was evaluated.

IV. OPERATING CONDITIONS

A. PURPOSE OF FUEL TURBOPUMP ASSEMBLY

The purpose of the M-1 fuel turbopump is to supply liquid hydrogen to the engine system. The turbopump consists of a 10-stage axial flow, reaction-type pump that is directly driven by a two-stage, axial flow impulse type, gas turbine (see Figure No. 7).

B. PUMP DESIGN CRITERIA[3]

The pump nominal design flowrate is approximately 60,000 gal per minute. Its nominal inlet pressure is 30.8 psia for -421°F liquid hydrogen temperature, and nominal discharge pressure is 1800 psia at nominal operating shaft speed of 13,225 rpm. The maximum design shaft speed is 14,550 rpm. At the engine nominal operating speed, the pump shaft power is 74,138 horsepower. The maximum design shaft power is 119,725 horsepower.

C. TURBINE DESIGN CRITERIA[4]

The turbine nominal design flowrate is 99.3 lb/sec at a nominal design gas inlet temperature of 1000°F. Nominal design turbine inlet pressure is 1020 psia and nominal design turbine exit pressure is 214 psia. The turbine drive gas is furnished by the engine system gas generator and consists of approximately 90% gaseous hydrogen and 10% steam.

---

(3) <u>M-1 Engine Design Information Report</u>, Aerojet-General Report No. 9430-DIR-1, 16 Oct 1964.

(4) <u>ibid</u>.

Page 7
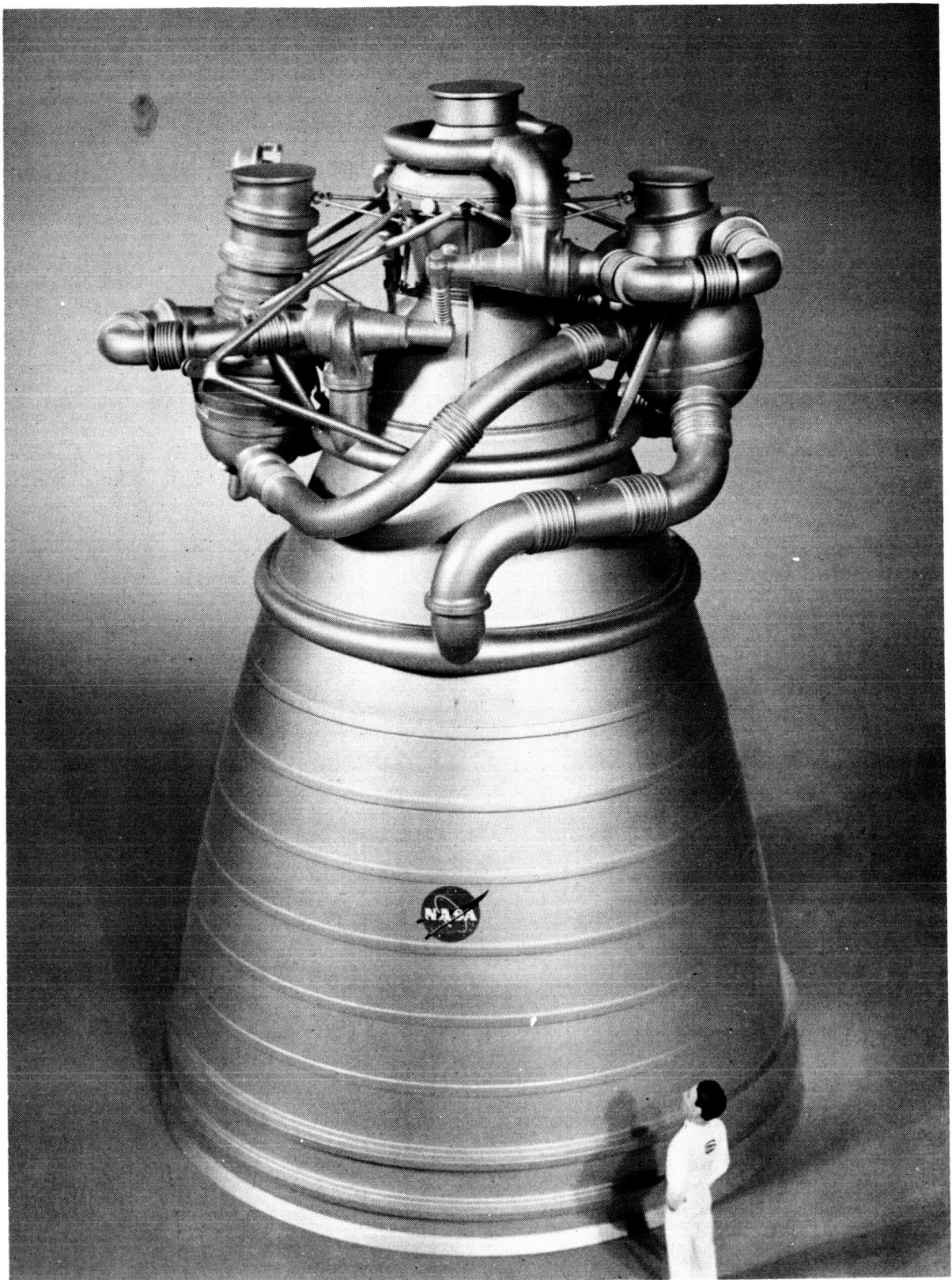
Figure 4

M-1 Engine With FTPA Support System
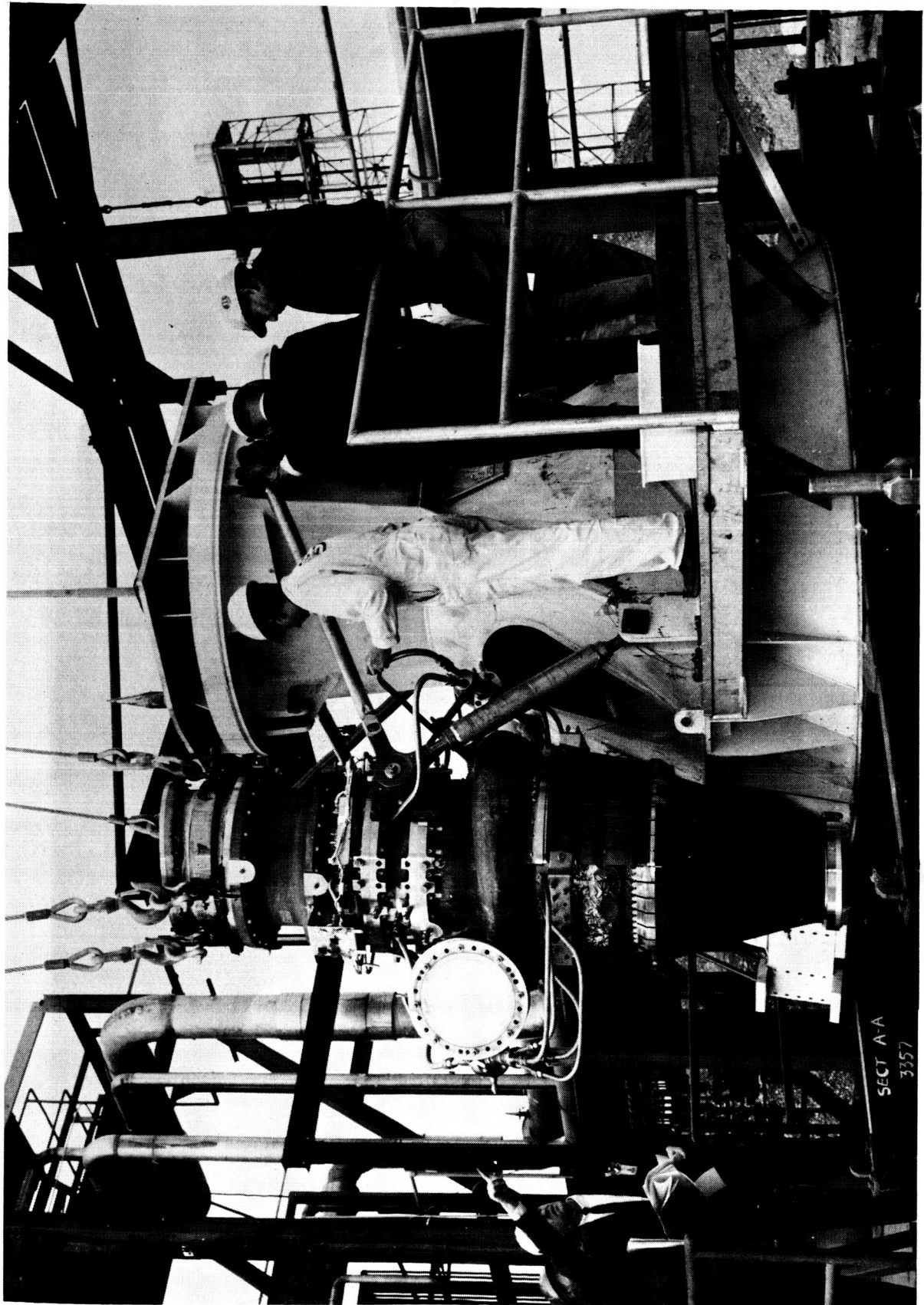
Figure 5

FTPA Test Stand Support System
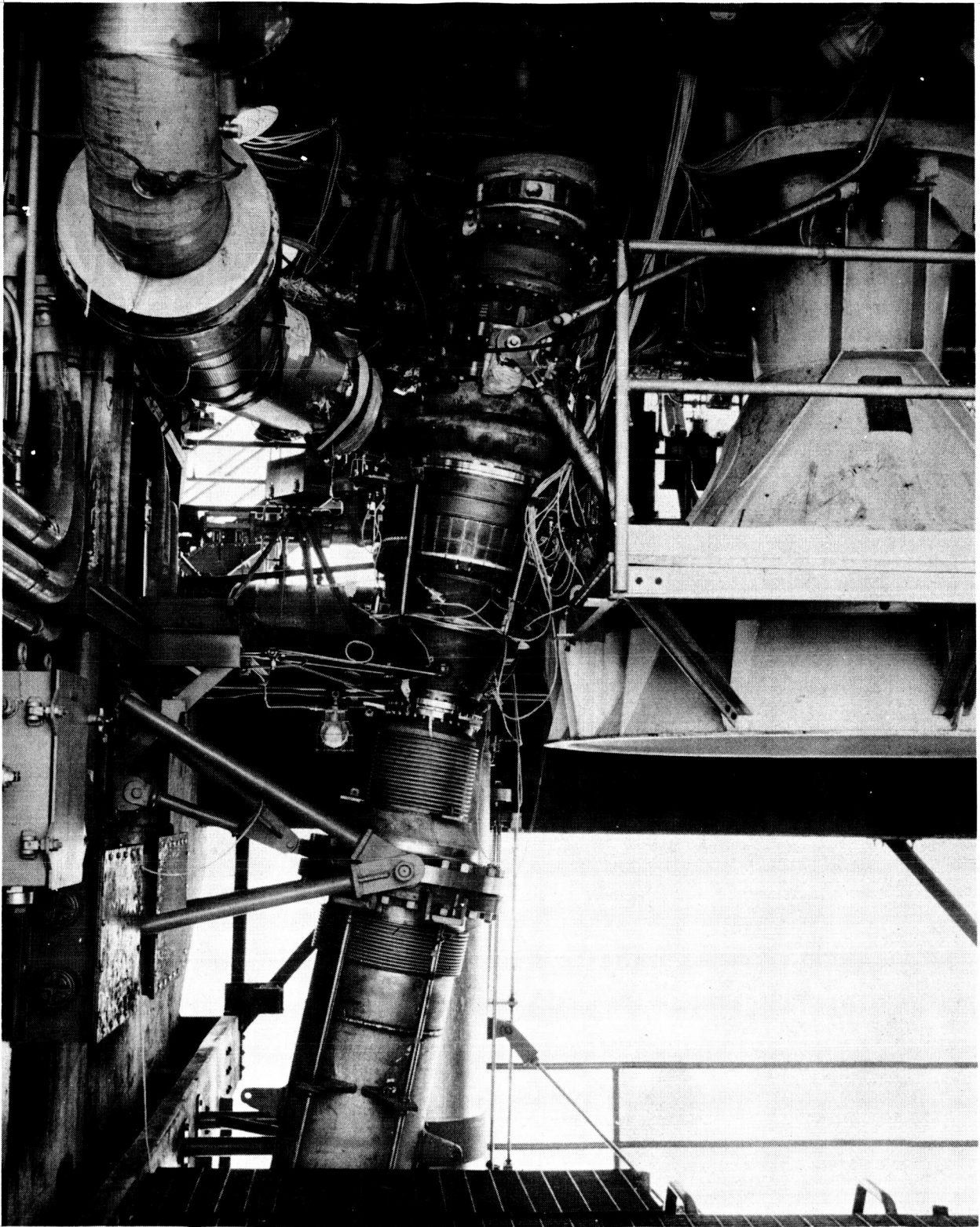
Figure 6

FTPA Installed in Test Stand E-1
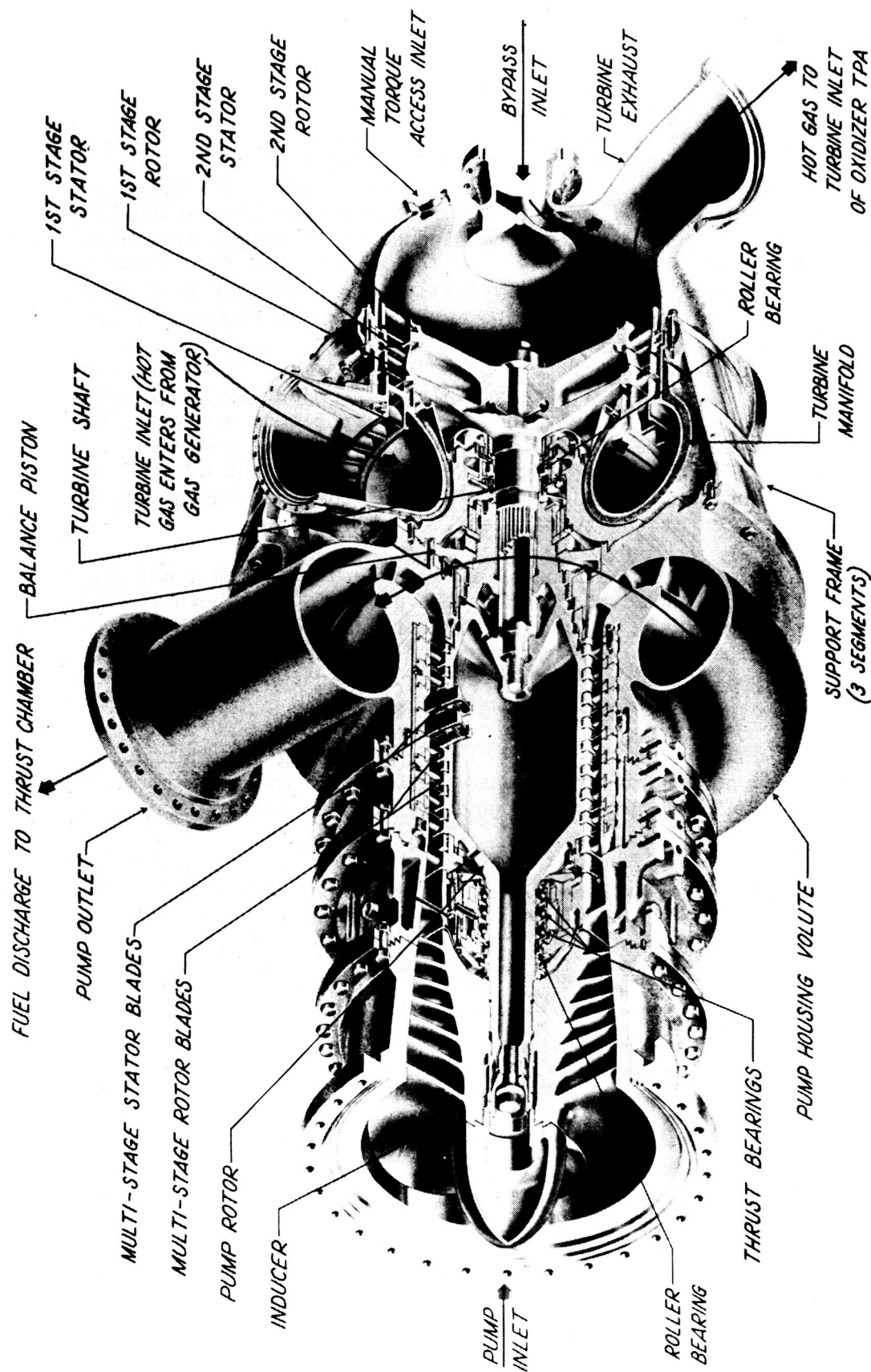
Figure 7

Model II Turbopump Cross-Section

V. LATERAL VIBRATION MODEL

A. MATHEMATICAL MODEL

The lateral vibration and bearing load characteristics of three fuel turbopump assembly configurations were evaluated. The first configuration is a Model I design that has a 93 lb interim inducer and a 215 lb first-stage turbine wheel. A cross-section of the Model I turbopump is shown in Figure No. 3. The second and third configurations are Model II designs. The second model has an interim inducer with first- and second-stage turbine wheels that weigh 180 lb and 128 lb, respectively. The third has a final inducer that weighs approximately 73 lb with the same turbine wheels being used. The feasibility and structural integrity of the final inducer has been proven analytically but it has not been fabricated. An axial section view of the Model II turbopump is shown in Figure No. 7.

The ratio of the mass of the housing to the mass of the rotating system was sufficiently low (approximately 7.5 to 1) to justify the inclusion of stator effects in the mathematical model. For purposes of analysis, the housing is assumed to terminate at the 10 degree elbow at the pump end and to the right of the turbine inlet manifold (Figure No. 3). The weight of the turbine inlet torus, part of the turbine inlet line, and the turbine exhaust housing are assumed to be concentrated at the turbine end.

A cross-section of the Model I fuel turbopump assembly and the lumped-mass parameter model that was used in the analysis are shown in Figure No. 8. The mass of the rotating system and the housing are considered to be concentrated at discrete points (lumped-mass) and the elements that connect the lumped masses are considered to be beam elements that have flexural and shear stiffnesses but no mass.

The rotating system is connected to the housing by springs (K_p) and $K_t)$. These represent the stiffnesses of the bearings and some parts of the housing (e.g., inducer guide vanes and the turbine bearing housing).

Springs connecting the stator to ground were not included in this model as they were found to have negligible influence upon the whirling critical speeds. This is discussed further in Section V.C.3.

The mechanical and physical properties of each bay are itemized in Table I. A bay consists of a lumped mass and one-half of the elastic element on each side that connects the masses to the left and right of the mass being considered (see Figure No. 9).

B. METHOD OF ANALYSIS

The method that was used to analyze the lateral vibration characteristics of the fuel turbopump assembly is detailed in Appendix A. Briefly, this method is a modified Myklestad-Thomson type solution facilitated by a matrix formulation and programed for digital computer application. Free, forced, and forced-damped vibration programs were developed; however, only the first two were utilized for the analyses presented in this report.

Table I

Model Physical Properties Used in Analysis

Bays 1–20

Bay	Rotor L* (in)	W (lb)	EI (lb-in²)	I_J (lb-in-sec²)	C (in⁻²)	Housing L* (in)	W (lb)	EI (lb-in²)	I_J (lb-in-sec²)	C (in⁻²)
1	0.0	0.0	1.00	0.0	0.0	1.30	65.6	380.(10^9)	11.8	.011
2	0.0	0.0	1.00	0.0	0.0	0.20	38.8	119.(10^9)	5.84	.029
3	0.0	0.0	1.00	0.0	0.0	3.40	66.7	101.	9.89	.033
4	0.0	0.0	1.00	0.0	0.0	2.30	56.2	111.	7.98	.023
5	0.0	0.0	1.00	0.0	0.0	2.70	247.	69.6	46.4	.006
6	0.0	0.0	1.00	0.0	0.0	2.40	93.1	239.	44.1	.015
7	0.0	133.+	1.00	0.0	0.0	4.50	73.9	95.0	10.3	.033
8	1.95	7.40	.183(10^9)	1.56	.344	1.60	59.3	209.	8.24	.015
9	3.24	0.0	.718(10^9)	0.0	.134	2.50	248.	722.	44.6	.005
10	1.28	9.20	.718	0.0	.134	0.85	0.0	302.	0.0	.011
11	1.60	10.3	.718	0.0	.134	1.90	88.1	302.	12.9	.011
12	3.20	9.78	.958	0.0	.111	1.70	33.6	93.7	8.51	.060
13	2.37	20.5	3.80	0.0	.060	1.90	30.5	91.9	7.58	.060
14	1.15	13.3	6.56	0.0	.060	1.90	117.	339.	15.9	.009
15	0.62	22.3	26.5	0.0	.034	2.60	315.	830.	53.5	.004
16	0.96	17.9	11.4	0.0	.096	1.30	81.6	221.	7.05	.015
17	1.15	16.0	11.4	0.0	.096	1.35	76.4	180.	5.96	.018
18	1.58	22.5	11.4	0.0	.096	1.35	76.4	180.	5.96	.018
19	2.30	22.5	11.4	0.0	.096	1.55	206.	736.	28.2	.006
20	2.30	22.5	11.4(10^9)	0.0	.096	1.55	206.	736(10^9)	28.2	.006

Bays 21–39

Bay	Rotor L* (in)	W (lb)	EI (lb-in²)	I_J (lb-in-sec²)	C (in⁻²)	Housing L* (in)	W (lb)	EI (lb-in²)	I_J (lb-in-sec²)	C (in⁻²)
21	2.30	22.5	11.4(10^9)	0.0	.096	1.00	45.3	135.(10^9)	2.82	.028
22	2.30	22.5	11.4(10^9)	0.0	.096	1.00	45.3	135.(10^9)	2.82	.028
23	2.30	22.5	11.4	0.0	.096	1.70	72.2	328	13.8	.011
24	1.86	19.9	13.4	0.0	.079	0.90	102.	180.	7.96	.018
25	1.31	15.3	12.2	0.0	.078	0.85	38.1	107.	2.22	.028
26	1.50	21.7	8.21	0.0	.099	0.85	38.1	107	2.16	.028
27	1.00	24.4	7.56	0.0	.079	0.80	36.1	110.	2.16	.028
28	0.70	17.2	5.39	0.0	.093	0.80	36.1	110.	7.86	.015
29	1.64	38.5	7.67	0.0	.030	1.05	66.2	226.	7.86	.015
30	1.70	39.6	5.16	0.0	.037	1.05	66.2	226.	32.4	.006
31	2.04	21.2	3.51	0.0	.047	2.10	204.	627.	29.6	.007
32	2.97	22.3	1.10	0.0	.100	2.70	211.	443.	0.0	.007
33	1.60	0.0	1.10	0.0	.100	0.85	0.0	397.	52.8	.007
34	1.37	17.8	1.10	0.0	.100	0.85	395.	397.	20.8	.007
35	1.87	8.60	30.5	0.0	.044	1.30	395.	96.7	14.7	.091
36	1.00	130.++	30.5	9.36	.044	0.20	1750.	288.(10^9)	0.0	.022
37	1.25	0.0	2.75	0.0	.125	0.0	0.0	1.00	0.0	0.0
38	1.25	0.0	30.5	0.0	.139	0.0	0.0	1.00	0.0	0.0
39	0.50	128.+	10.0(10^9)	8.87	0.0	0.0	0.0	1.00	0.0	0.0

* L is total length of bay

+ For Mod II with final inducer, this weight is 97.3 lbs.

++ For Mod I analysis, bay 36 weight is 165 lbs and bay 39 is zero.

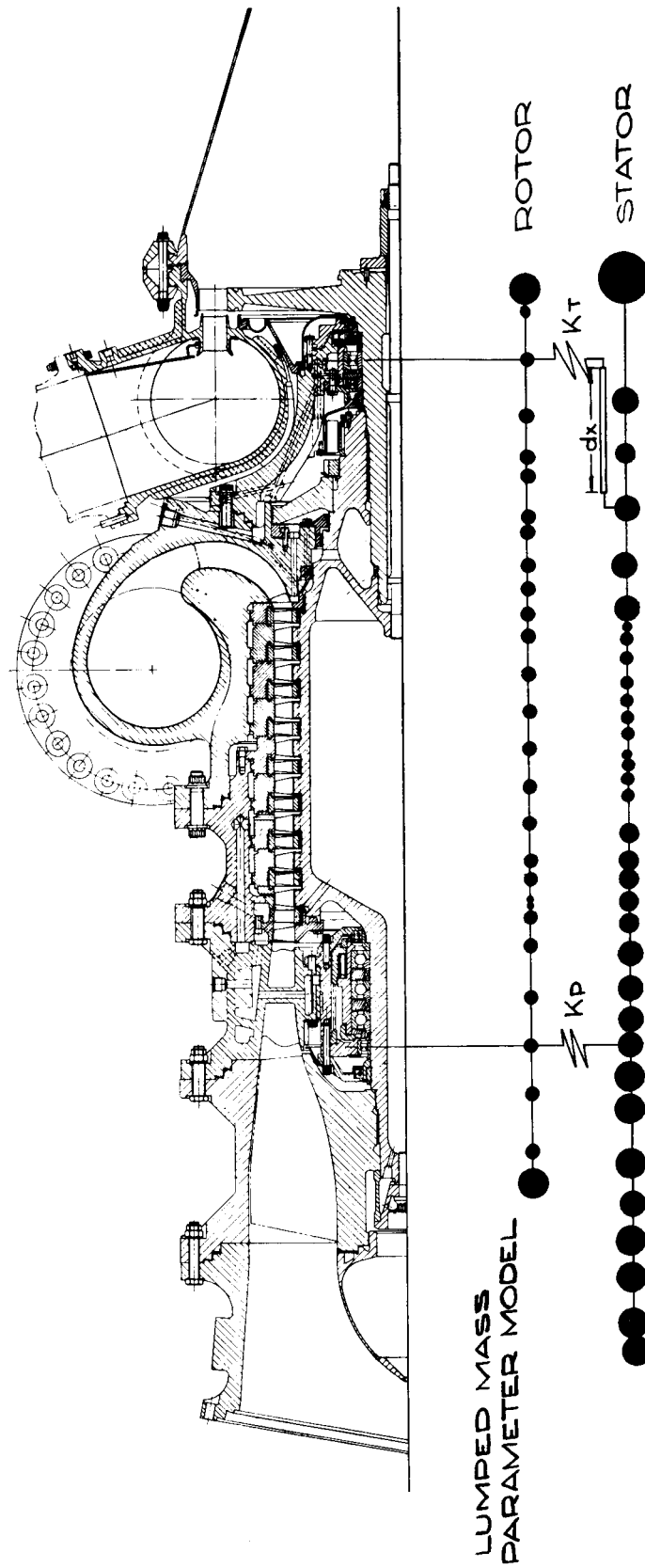Note: The nomenclature is defined in appendix A.

Figure 8

Cross-Section of Model I Turbopump
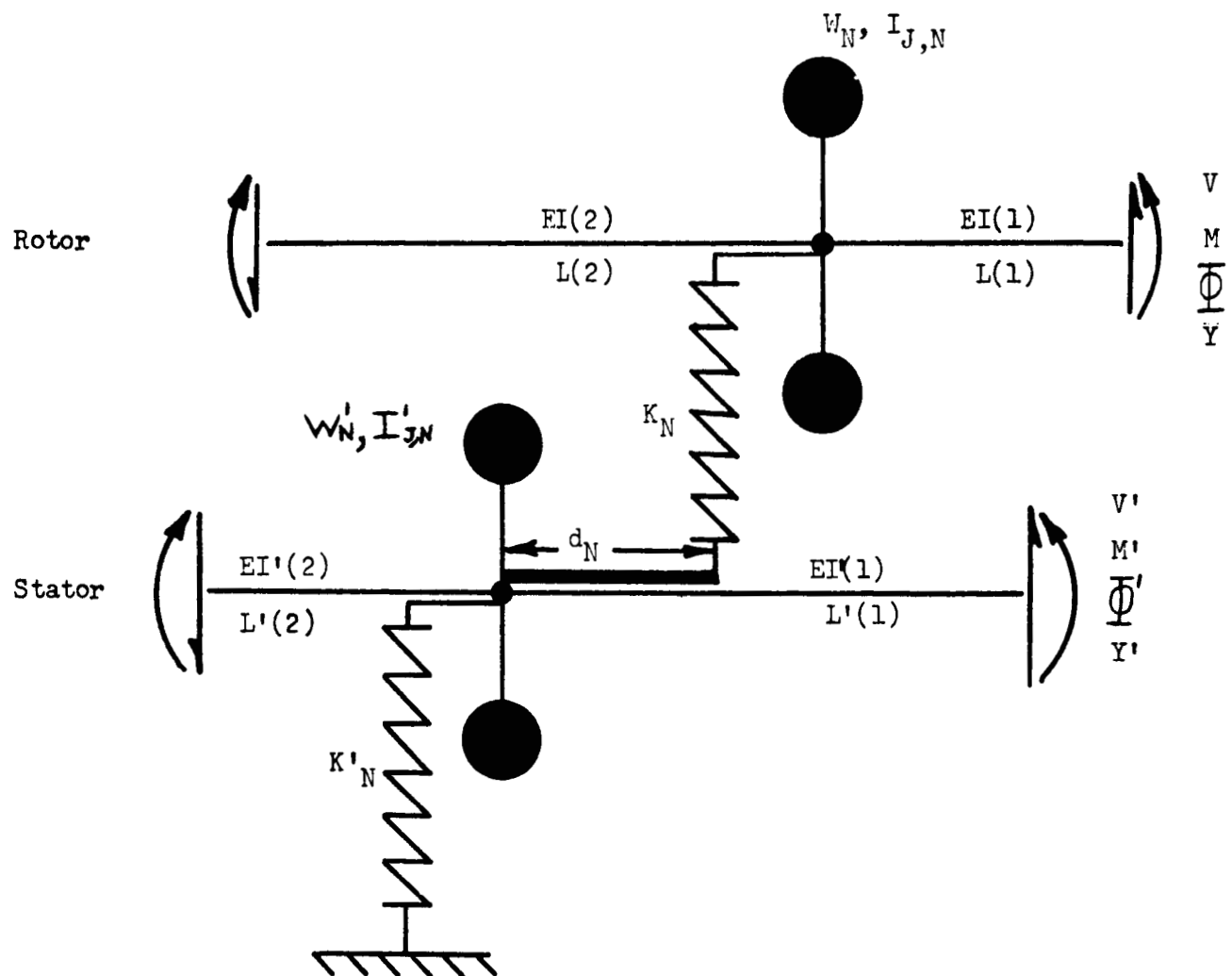and Lumped-Mass Parameter Model

Figure 9

Typical Bay of Lumped Mass Parameter Model

C. SPECIAL CONSIDERATIONS

1. Roller Bearing Spring Rates

The influence of the roller bearing spring rates upon critical speed makes it imperative that exact value of spring rate be known. This is shown in Figures No. 10 and 11. The bearing spring rates have been experimentally and analytically evaluated. Generally, the experimental data and the theoretical results compared quite well. The theoretical and experimental spring rate – load relationships for both the pump and turbine roller bearings are shown in Figures No. 12 through 16. The basis for the derivation of the spring rates is presented in Appendix B.

2. Turbine Bearing Housing Spring Rate

The flexibility of the turbine bearing housing causes the apparent turbine bearing spring rate to be reduced. The equivalent spring rate is shown in Figure No. 17. Because the flexibility of the turbine bearing support significantly affects the critical speed, it is also necessary to evaluate the turbine bearing housing spring rate. The bearing housing stiffness has been analytically and experimentally examined. The theoretical and experimental analyses are presented in Appendices C and D.

3. Turbopump Assembly Support Flexibility

A description of the supporting struts were given in Section III.E. The spring rate of the supporting struts varies depending upon the direction of translation of the fuel turbopump assembly. For purposes of estimating the effects of the support flexibility upon the shaft critical speeds, an effective spring rate has been evaluated in the plane that contains the centerlines of the engine and fuel turbopump assembly as well as in the plane that is perpendicular to the first plane. Therefore, the values derived represent approximately maximum and minimum values of strut spring rate. This permits bounds to be placed regarding the effect of strut stiffness upon the fuel turbopump assembly critical speeds.

The effective strut spring rate[5], acting at the turbopump assembly center of gravity, and in the plane that contains the centerlines of the engine and fuel turbopump assembly is approximately 0.64 (10^6) lb/in. In the plane perpendicular to the first plane the spring rate is approximately 0.31 (10^6) lb/in. These spring rates were used in an analysis wherein the entire turbopump assembly was considered as a rigid body and the strut support system as springs.

The corresponding uncoupled natural frequencies are 25.0 and 17.5 cps (1500 and 1050 rpm). Thus, no significant change in the critical speed near the design operating range is expected. Subsequent to the analysis, a resonant survey was conducted of the Model I fuel turbopump assembly assembled in the test stand. Natural frequencies of the rigid body fuel turbopump assembly on its support

---

(5) Natural Frequency Analysis of the FTPA Rigid Body Strut Support System, Aerojet-General Report No. SA-FTPA-121, Rev. B, April 1965.
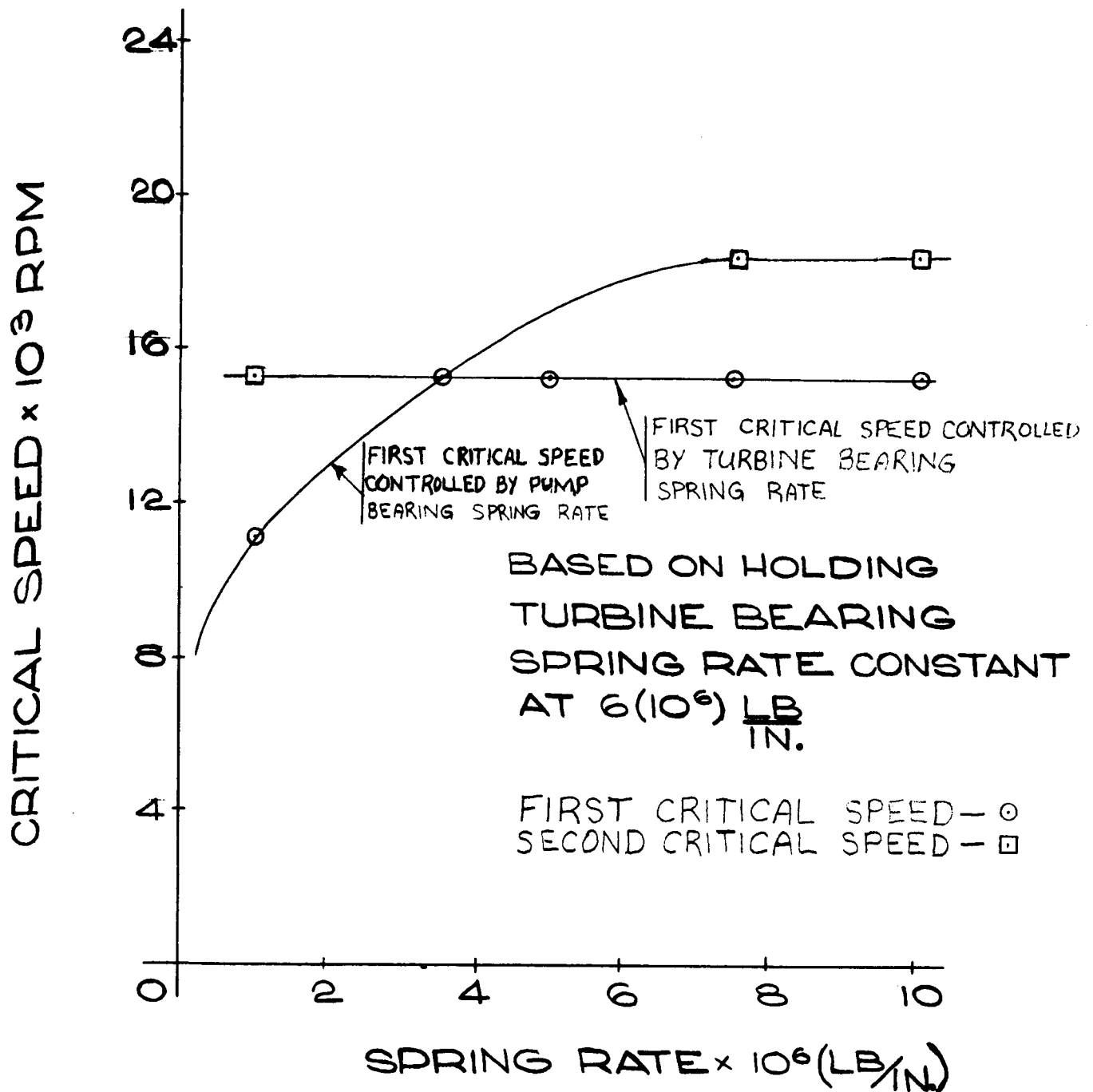
Figure 10

Model I FTPA Critical Speed vs. Pump Bearing Spring Rate
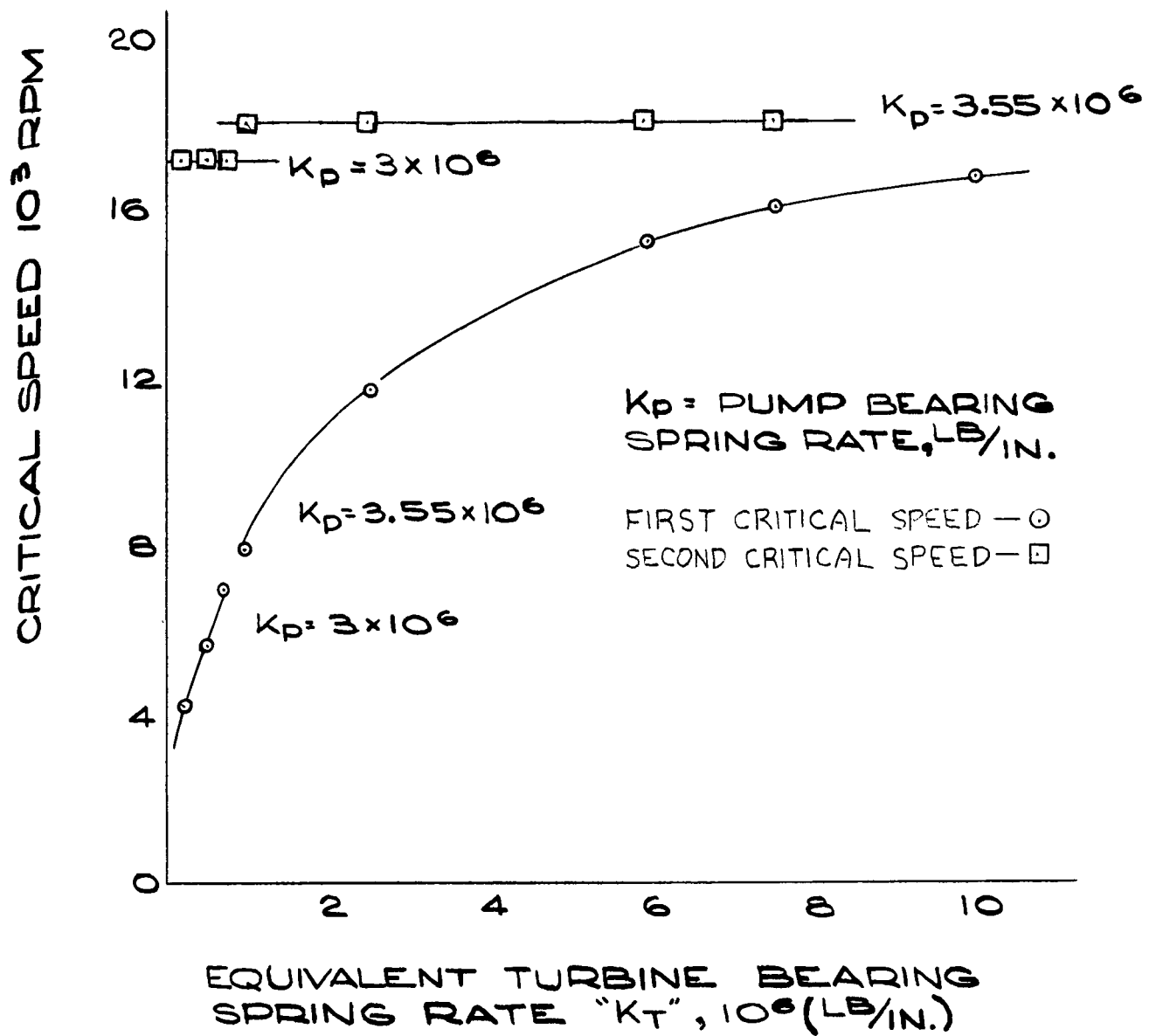
Figure 11

Model I FTPA Critical Speed
vs. Equivalent Turbine Bearing Spring Rate

ITI PUMP BEARING - 110 mm
P/N 288260
24 ROLLERS, PITCH DIA.=5.905 IN
LENGTH OF ROLLERS = .433 IN
SHAFT SPEED = 0 RPM

BEARING EFFECTIVE LENGTH (% OF TOTAL)

100%

PER PALMGRENS EQUATION

75%

50%

———— O RADIAL CLEARANCE
—·— .0005 RADIAL CLEARANCE
———— .001 RADIAL CLEARANCE
———— STD. PALMGREN FORMULA

$\delta = .89(10)^{-6} (\frac{5P}{n})^{.9} (\frac{1}{L})^{.8}$, $L_{EFF} = .433''$

⊙ S/N 307 { EXPERIMENTAL POINTS

SPRING RATE (10^6 LBS/IN)

TOTAL BEARING LOAD (10^3 LBS)
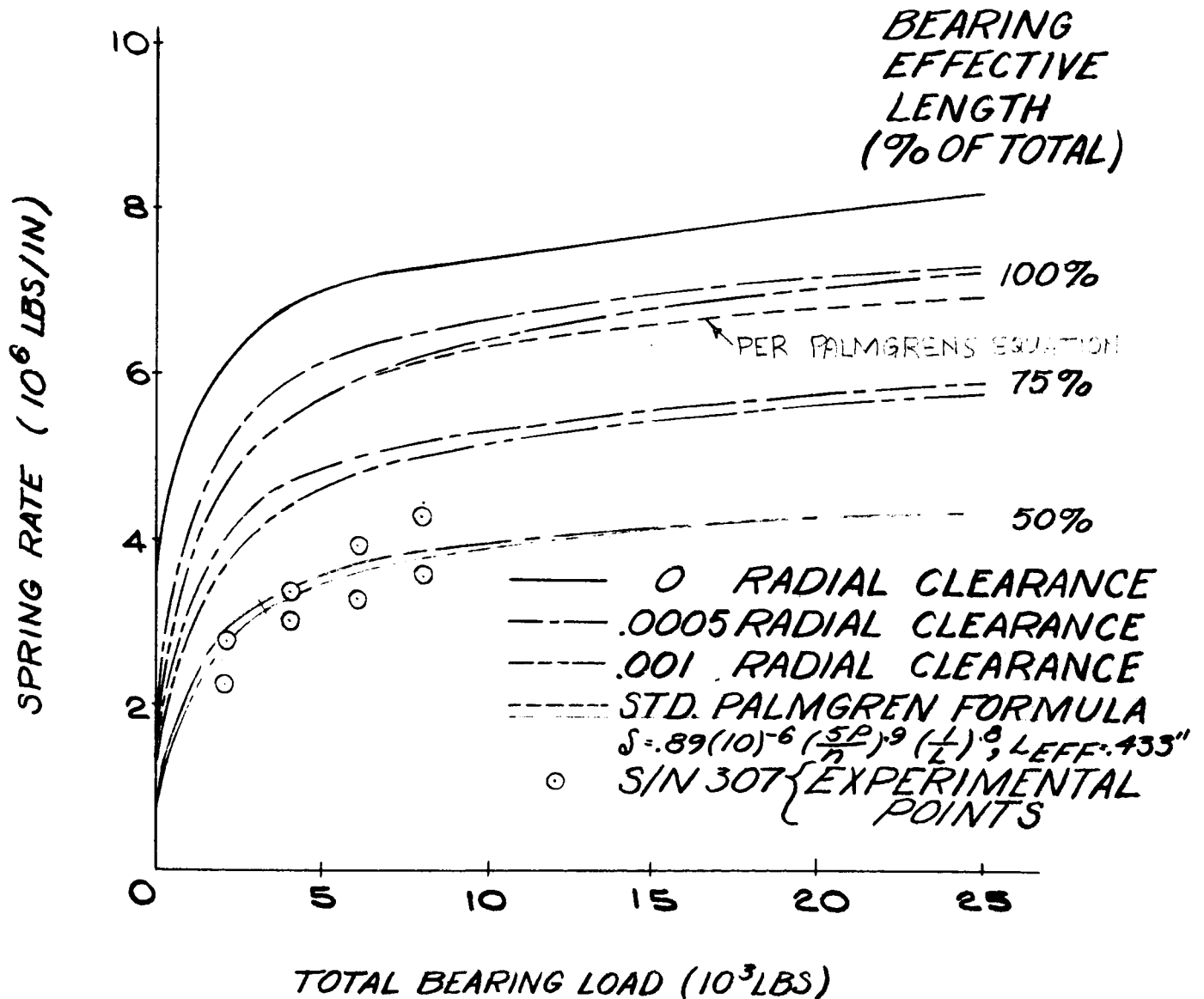
Figure 12

Pump Bearing Spring Rate
vs. Load - 24 Rollers (P/N 288260)

Page 19

PUMP BEARING -110 mm
P/N 288260
24 ROLLERS
LENGTH OF ROLLERS = .433 IN

$$K = 1.35(10)^6 p^{0.1}$$

⊙ EXPERIMENTAL POINTS.
—— NON-LINEAR SPRING-
RATE USED IN ANALYSIS.

SPRING RATE × 10⁶ (LB/IN)

BEARING LOAD × 10³ (LB)
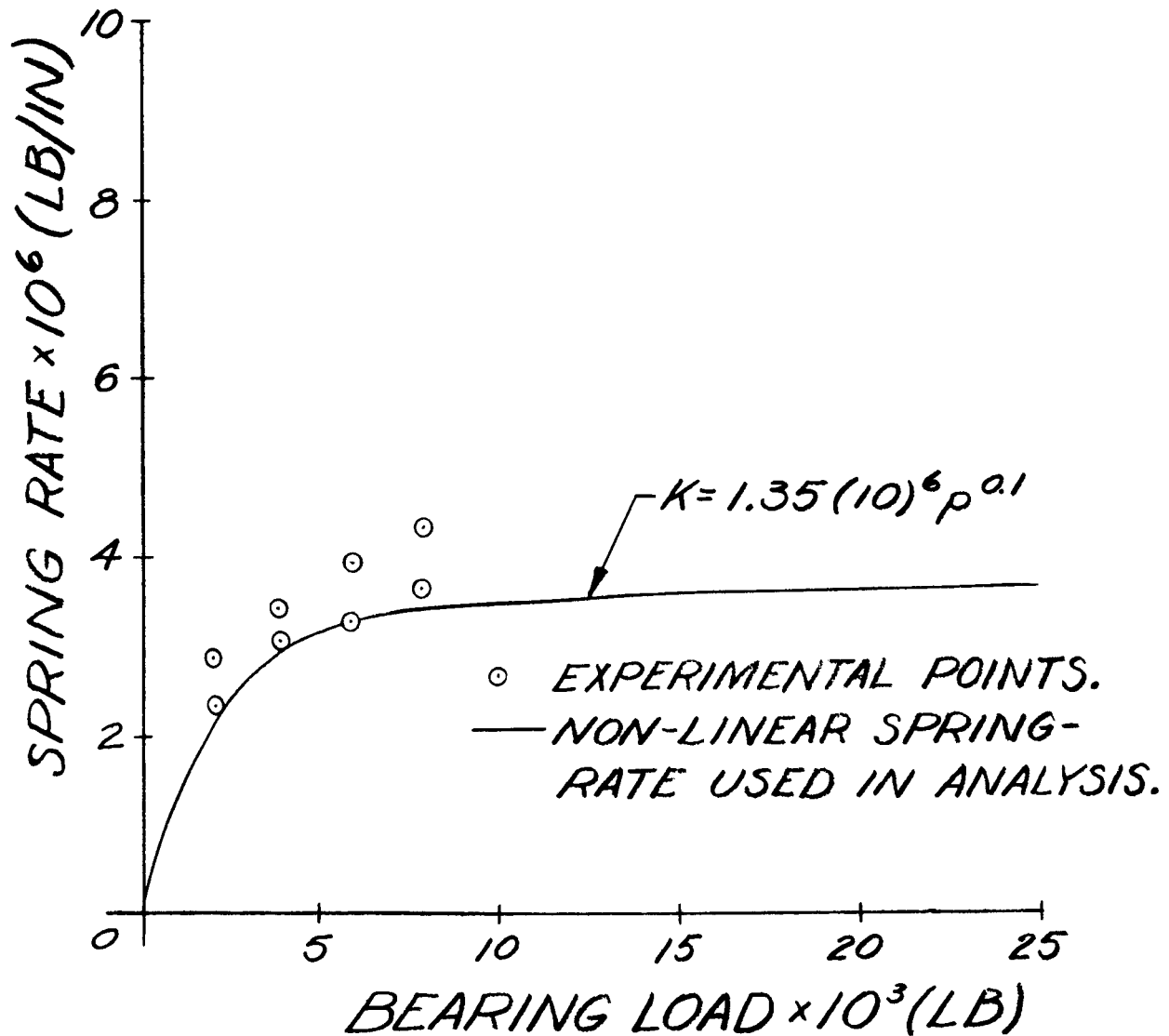
Figure 13

Spring Rate vs Load of 24 Roller Pump Bearing Used in Analysis

ITI TURBINE BEARING - 120 mm
P/N 288420
21 ROLLERS, PITCH DIA.=5.905 IN
LENGTH OF ROLLERS=.625 IN
SHAFT SPEED=0 RPM
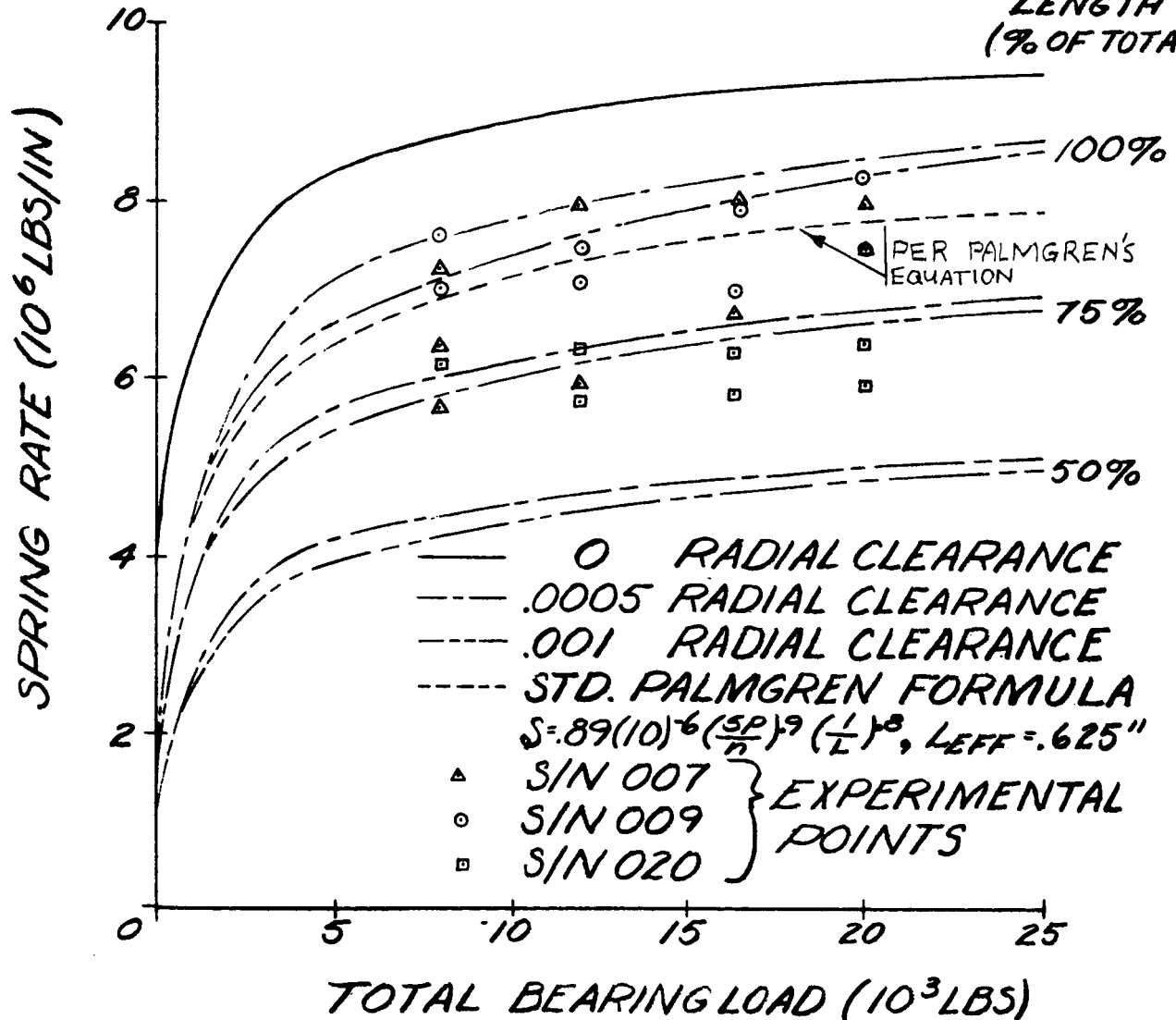
Figure 14

Turbine Bearing Spring Rate
vs. Load - 21 Rollers (P/N 288420)

BOWER TURBINE BEARING - 120 mm
P/N 288
26 ROLLERS, PITCH DIA. = 5.906 IN
LENGTH OF ROLLERS = .654 IN
SHAFT SPEED = 0 RPM

100%
87%
75%

BEARING
EFFECTIVE
LENGTH
(% OF TOTAL)

PER PALMGREN'S EQUATION

———— 0 RADIAL CLEARANCE
— — — .0005 RADIAL CLEARANCE
— · — .001 RADIAL CLEARANCE
— — — STD. PALMGREN FORMULA
$\delta = .89(10)^{-6} \left(\frac{SP}{n}\right)^{.9} \left(\frac{1}{L}\right)^{.8}$
▫ EXPERIMENTAL POINTS

SPRING RATE (10^6 LBS/IN)

TOTAL BEARING LOAD (10^3 LBS)
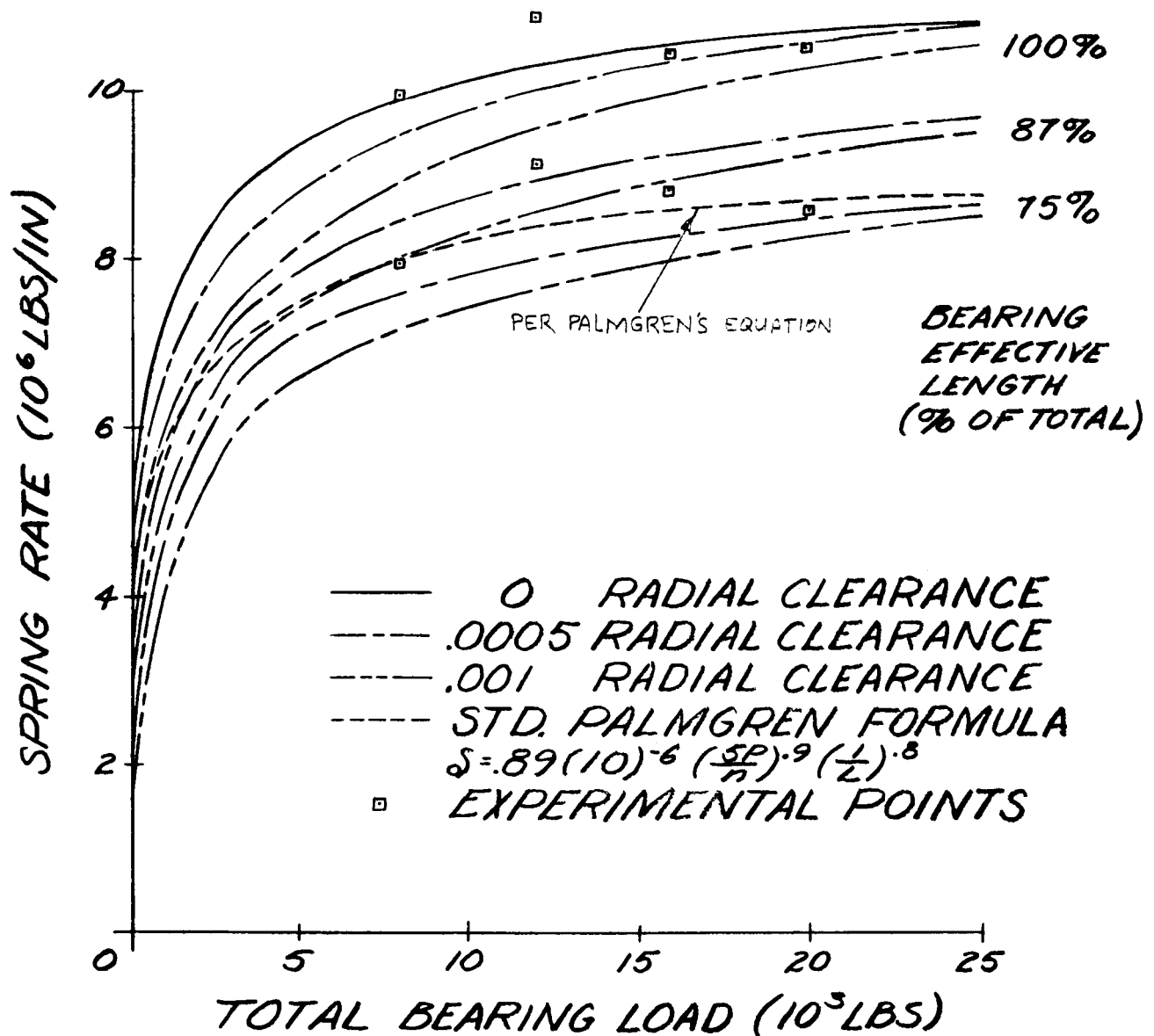
Figure 15

Turbine Bearing Spring Rate
vs. Load - 26 Rollers (P/N 288340)

Page 22

BOWER TURBINE BEARING - 120mm
P/N 288340
26 ROLLERS , PITCH DIA. = 5.906 IN.
LENGTH OF ROLLERS = .654 IN
SHAFT SPEED = 0 RRM

$$K = 0.713 (10)^6 \, p^{0.276}$$

□   EXPERIMENTAL POINTS
—— NON-LINEAR SPRING
         RATE USED IN ANALYSIS

SPRING RATE (10⁶ LB/IN)

TOTAL BEARING LOAD (10³ LBS)

Figure 16

Spring Rate vs. Load of 26 Roller Turbine Bearing Used in Analysis

Figure 17

Equivalent Turbine Bearing Spring Rate
Considering Flexibility of Turbine Bearing Housing

struts were found to be 6.5, 21, 24, 60, and 67 cps. Therefore, turbopump support flexibility should not significantly affect the shaft critical speed.

4. Residual Imbalance

The imbalance of each major component resulting from the limits in balancing capabilities is shown in Figure No. 18. Bearing reactions caused by the residual imbalances are given in Table II. Because the rotor is not balanced as a complete assembly, diametral runouts and tolerances of pilot diameters could cause some shaft misalignment. Following the analysis, it was decided to balance the turbine rotor and main pump rotor as a subassembly. Thus, the effects of the pilot runouts at the turbine end will be removed during this subassembly balancing. The resulting bearing loads, which are quite small, are given in Table II.

5. Damping

The effects of the various forms of damping upon rotating machinery include a slight shift in the critical speeds, a limit on shaft displacements, and a reduction in bearing reactions. Because the rotor is supported by rolling bearings and operates in a very low viscosity and light fluid medium (liquid hydrogen), damping of any significant magnitude is not expected. Therefore, it is not included in the analysis presented in this report.

6. Conical Whirl Mode of Motion Allowed by Bearing Clearances

A probable mode of motion of the rotor under operating conditions, is one of conical whirling[6][7], as indicated in Figure No. 19. Another possible motion is a cylindrical whirling mode, but because the resulting bearing loads will not be as severe as for the conical mode, due to the smaller overhung mass eccentricities, only the conical mode was evaluated. The resulting bearing loads are discussed in the ensuing section.
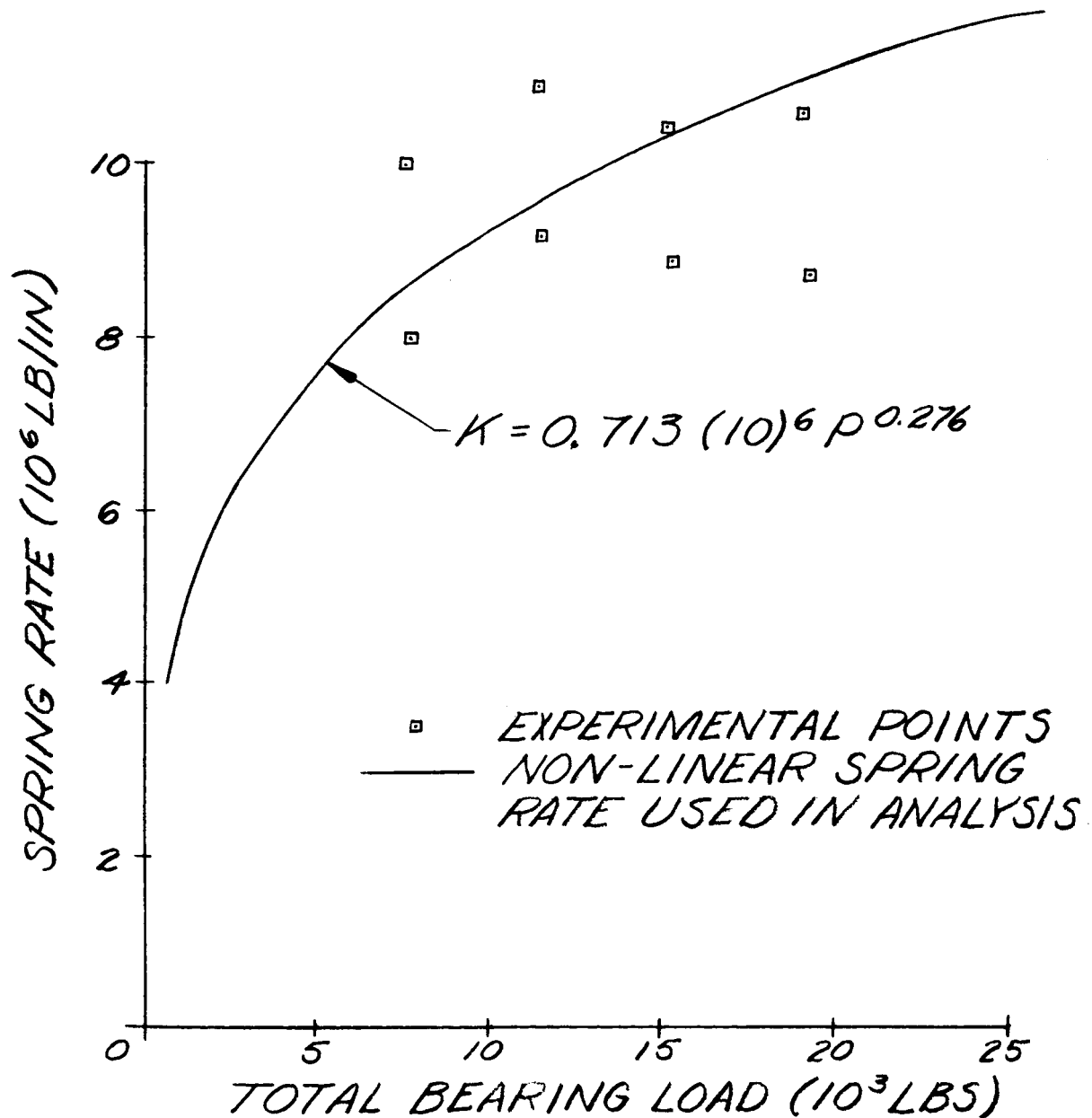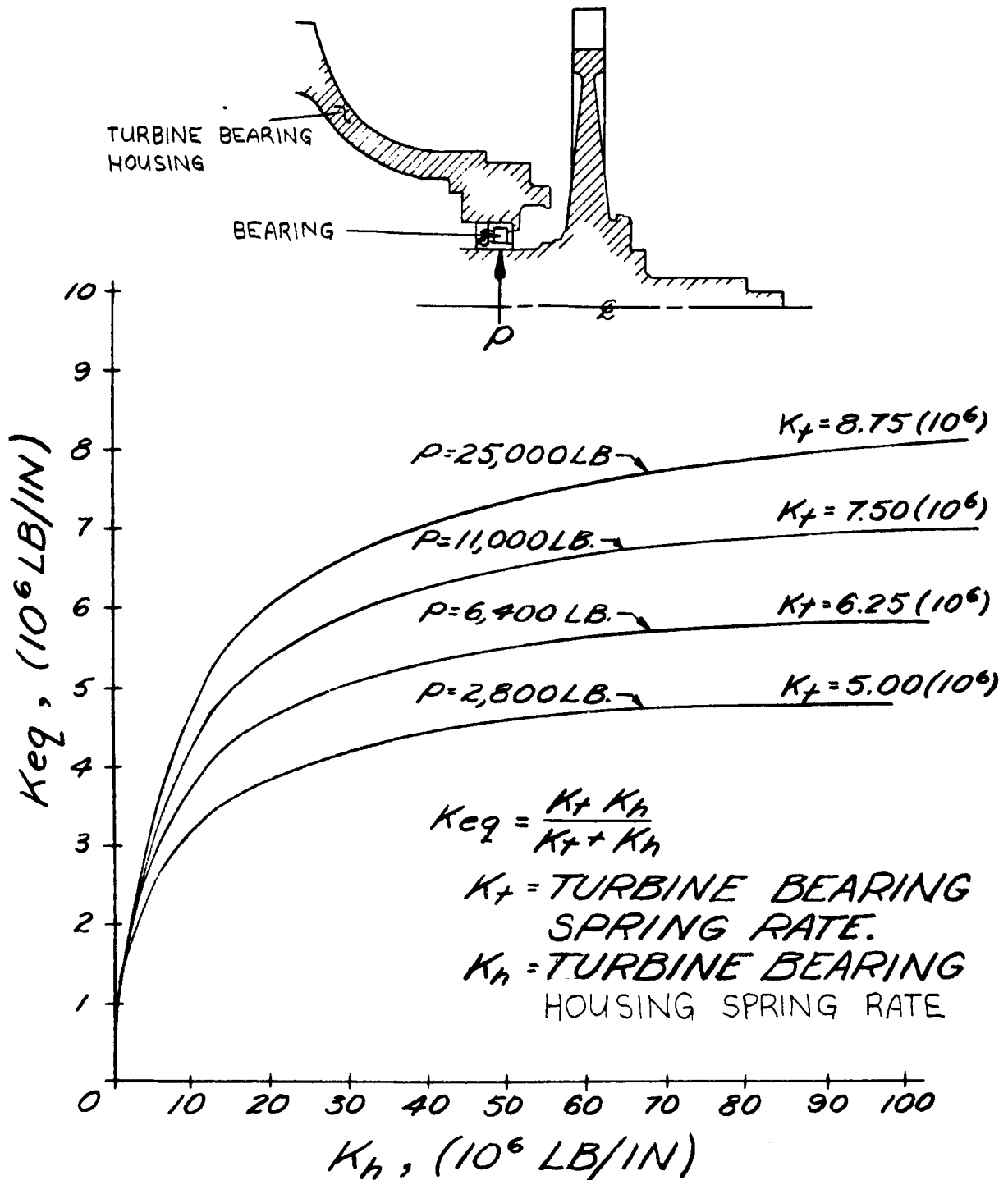
D. BEARING REACTIONS AND CRITICAL SPEED

Bearing clearances are the major source of bearing reactions. The clearances allow the rotor masses to rotate at some position other than the geometric center defined by the bearing axis. This type of rotation results in conical whirl. The rotor masses, which require an additional forcing function[8] to initiate a conical precession of the shaft axis, cause centrifugal forces that are balanced by the bearing reactions. This additional forcing function will most likely be caused by the imperfect mass balance of the rotor turbine wheels or inducer. Bearing clearances are discussed in Appendix E.

---

(6) Morris, J., "The Impact of Bearing Clearances on Shaft Stability" Aircraft Engineering, pp 382-383, December 1957.

(7) Den Hartog, J. P., Mechanical Vibrations, New York, McGraw-Hill, 1956, Fourth Edition, pp 252-265.

(8) Morris, J., loc. cit.

TABLE II

Model I TPA Bearing Reactions Resulting From Residual Imbalance		
Source	Reactions (lbs) at 12,000 rpm	
	Pump Bearing	Turbine Bearing
Balancing to .35 in-oz and .75 in-oz at planes I and II respectively (refer Figure 18)	100	300
Eccentricities in pilot diameters (refer Figure 18)	540	730
TOTAL	640	1030

NOTE: The Model I assembly first critical speed is calculated to be 16,000 rpm

(a.) DUE TO BALANCING LIMITS OF COMPONENTS

(b.) DUE TO ECCENTRICITIES OF PILOT DIAMETERS

BALANCE PLANE I

BALANCE PLANE II

PUMP BEARING

TURBINE BEARING

PUMP ROTOR RUNOUT .0005 T.I.R.

TURBINE ROTOR RUNOUT .0002 T.I.R.

BEARING INNER RACE ECCENTRICITY .0002 T.I.R.

CENTERLINE OF ROTOR

AXIS OF REVOLUTION

INDUCER RUNOUT .001 T.I.R.

SHAFT RUNOUT .001 T.I.R.

BEARING INNER RACE ECCENTRICITY .0002 T.I.R.
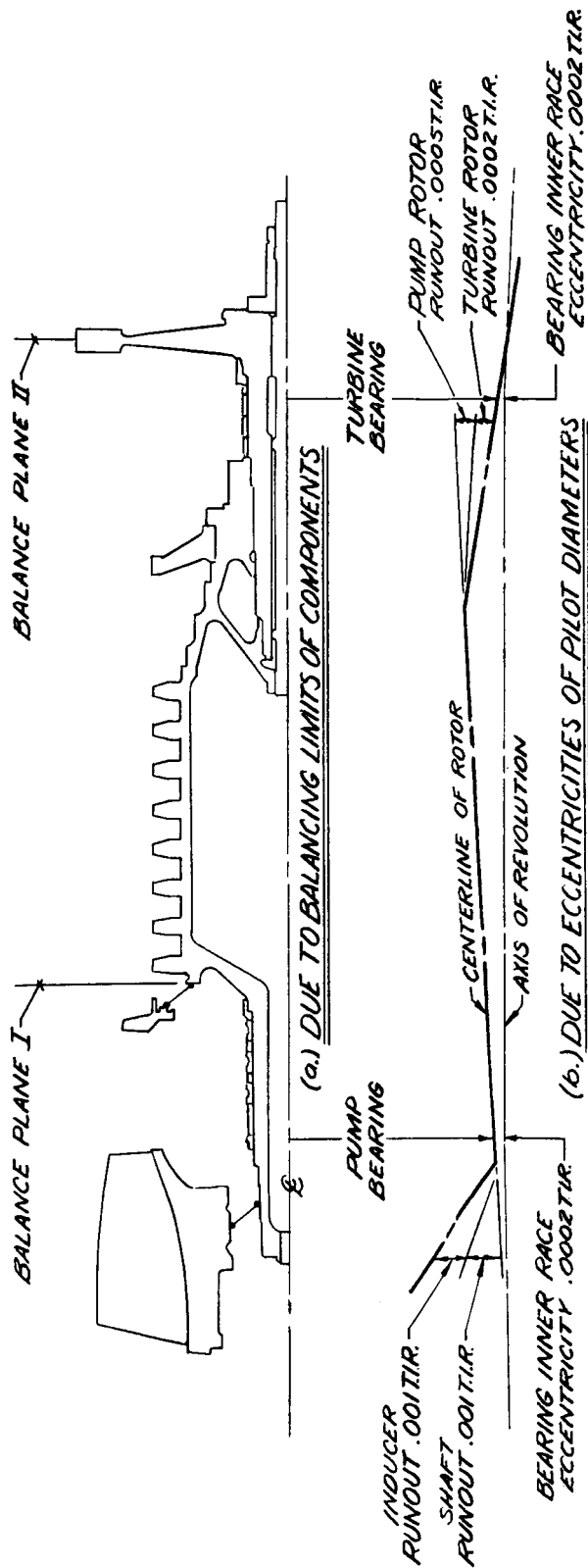
BALANCING LIMITS OF COMPONENTS

COMPONENTS	WEIGHT (LBS)	SPEC. (IN-OZ)
ROTOR & BLADES	380.0	0.02
1ST STAGE INDUCER	82.0	0.02
2ND STAGE INDUCER	9.3	0.02
THRUST BAL. DISK	19.3	0.01
TURBINE ROTOR	215.0	0.05
BALANCE PLANE I	SPEC. .35 IN-OZ. ;	.25 IN-OZ. ACTUAL
BALANCE PLANE II	SPEC. .75 IN-OZ. ;	.48 IN-OZ. ACTUAL

Figure 18

Residual Imbalance Sources
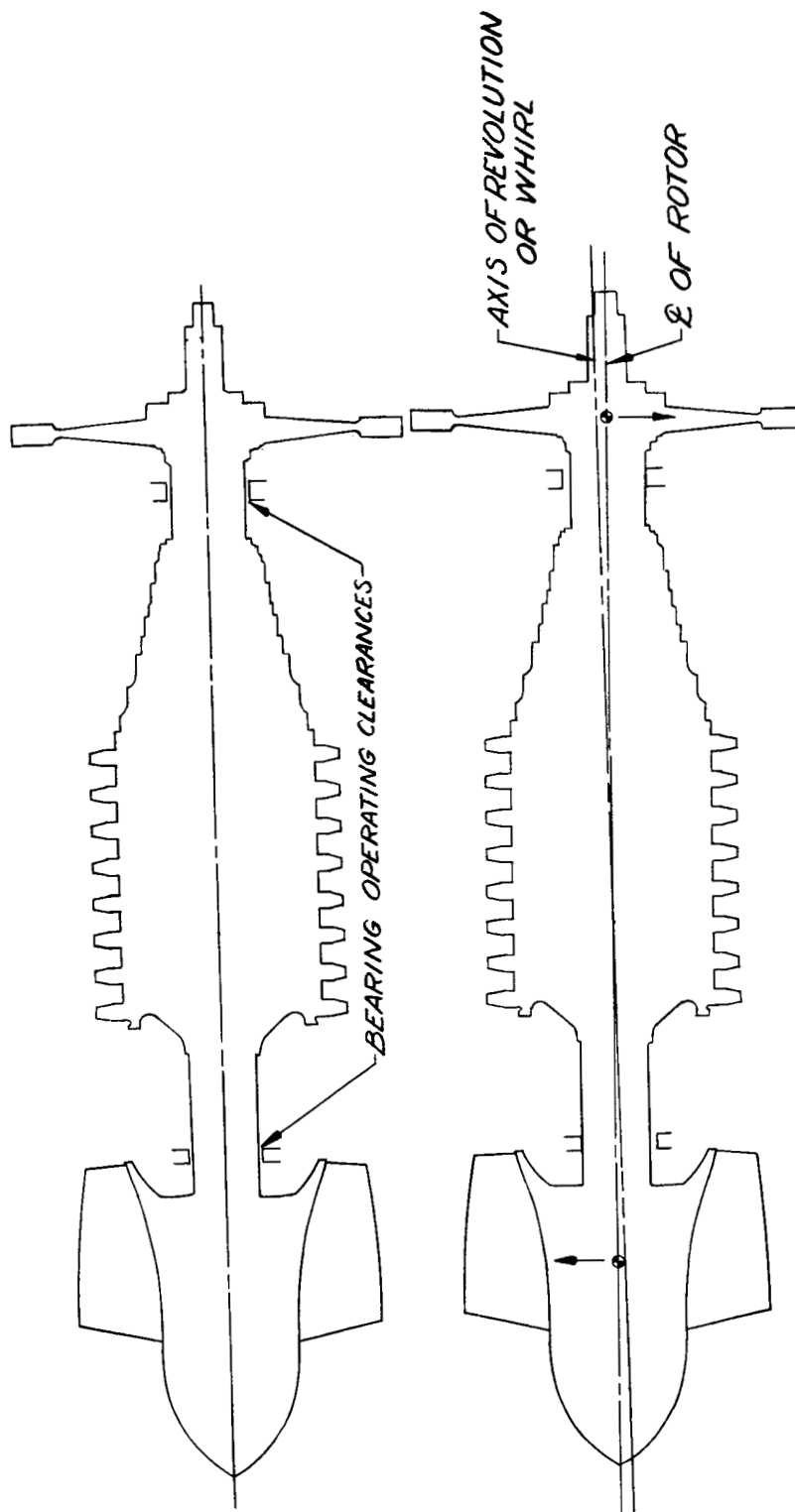
Figure 19

Conical Whirl Mode of Motion

As previously shown, the bearing spring rates are not constant (i.e., the load-deflection relationship is not linear). For purposes of comparison, the bearing reactions are shown in Figure No. 20 for both constant value and load dependent spring rates. Note that the linear treatment of a nonlinear system tends to give lower bearing reactions in the operating speed range. Also, the value of the first critical speed is somewhat underestimated. Bearing reactions for bearings that are represented by nonlinear springs for the Model II configurations are shown in Figures No. 21 and No. 22.

E. ADDITIONAL ANALYSIS DESIGN INFORMATION

The shaft bending stresses caused by conical whirling and associated unbalance forces are shown in Figure No. 23. Because they are very small, these stresses can be ignored in evaluating the structural integrity of the rotating system. Hoop stresses, caused by rotation, control the design structural integrity.

The shaft and stator elastic curves of the Model II turbopump assembly for various operating speeds are shown in Figure No. 24. The elastic curves are used to evaluate the rotor running clearances.

Hertz stresses as a function of bearing reaction are shown in Figures No. 25 and No. 26.

VI. OTHER SOURCES OF BEARING LOADS

Bearing loads from sources other than shaft whirling are shown in Table III (e.g., longitudinal and lateral accelerations, gimbal snubbing, gyroscopic reaction caused by gimbal angular velocity and hydraulic imbalance).

VII. CONCLUSIONS

The bearing loads for the pump and turbine roller bearings are given in Table IV. The total loads are caused by the centrifugal loads from the conical whirling mode of motion plus all other sources of bearing loads considered in this report.

Critical speed analyses typically tend to show higher results than are obtained experimentally. This is primarily because of the exclusion or approximate treatment of some potentially significant factors (i.e., bearing spring rate, dynamic coupling of rotor to housing, shear deflections, etc.).

In this report, a fairly rigorous method for prediction shaft whirling critical speeds and associated bearing reactions has been presented. Many factors found to be influential in the analysis have been experimentally and analytically investigated. The roller bearings, load-deflection relationships, their load capacities, and the turbine bearing support housing spring rate were determined by tests. Consequently, the predictions set forth in this report warrant a high degree of confidence.

TABLE III

Bearing Loads Attributable to Sources Other Than Shaft Whirl		
Source	Load at 14,550 rpm, Kips	
	Pump Bearing	Turbine Bearing
Pump Hydraulics	0.70	1.40

Engine Accelerations:
 	
  10 g's longitudinal
  1 g lateral
	0.80	1.64

Engine Gimbal Snubbing	1.03	1.92
Engine Gimballing Gyroscopic Action of Rotor	1.02	1.02
TOTAL	3.55	5.98

Table IV

Summary of Bearing Load and Whirl Critical Speeds

| Configuration | First Critical Speed, rpm | Radial Bearing Loads, kips | | | | | | | | Test Demonstrated Bearing Capacities (See Fig. 16) |
| | | Due to Conical Whirl at 13,225 rpm | | Due to Conical Whirl at 14,550 rpm | | Due to Other Sources at 14,550 rpm | | Total at 14,550 rpm | | |
		Pump Brg	Turb Brg	Pump Brg	Turb Brg	Pump Brg	Turb Brg	Pump Bearing	Turbine Bearing	
Mod II Turbopump Assembly, Interim Inducer	15,700	3.55	7.45	8.18	14.57	3.55	5.94	11.72	20.51	**Turbine Bearing:** Four (4) Brg's each have withstood 15.5 kips at 13,300 rpm for 88 minutes.
Mod II Turbopump Assembly, Final Inducer	18,000	2.30	7.00	3.55	11.86	3.55	5.94	7.10	17.80	
Mod I Turbopump Assembly (Interim Inducer)	16,000	at 12,000 rpm Pump Brg 0.87		at 12,000 rpm Turb Brg 2.38		0.70	1.40	at 12,000 rpm 1.57	3.78	**Pump Bearing:** One Brg has withstood 5 kips 14 minutes at 13,200 rpm

NOTE: Calculated pump bearing life is 11.4 hrs for a 12,000 lb load at 13,225 rpm.

Calculated turbine bearing life is 15.7 hrs for a 20,000 lb load at 13,225 rpm.

Total required life is approximately 2.08 hrs (Reference: DIR, Section 4.25 pg 1).
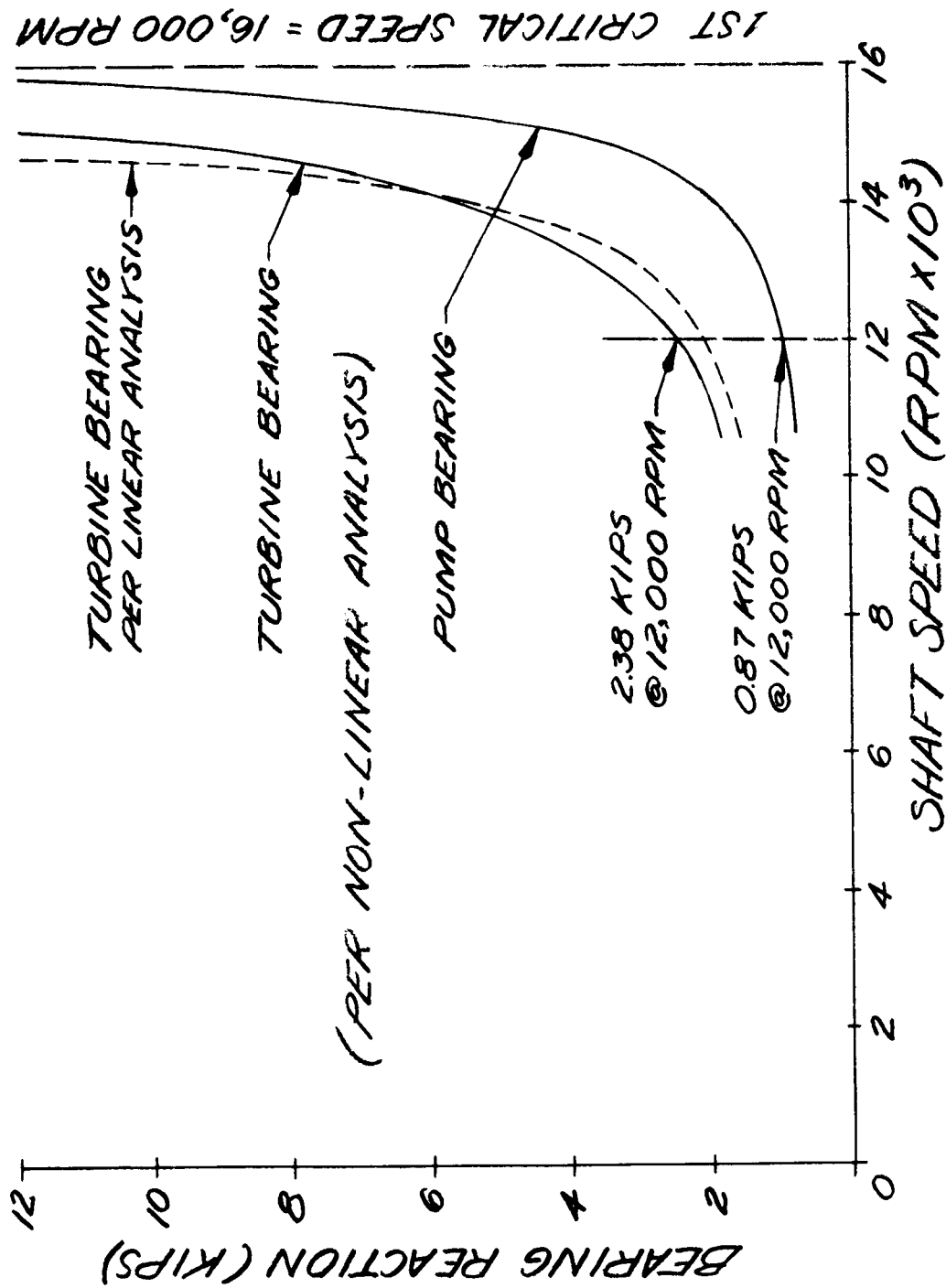
Figure 20

Bearing Reactions and Critical Speed for Model I TPA
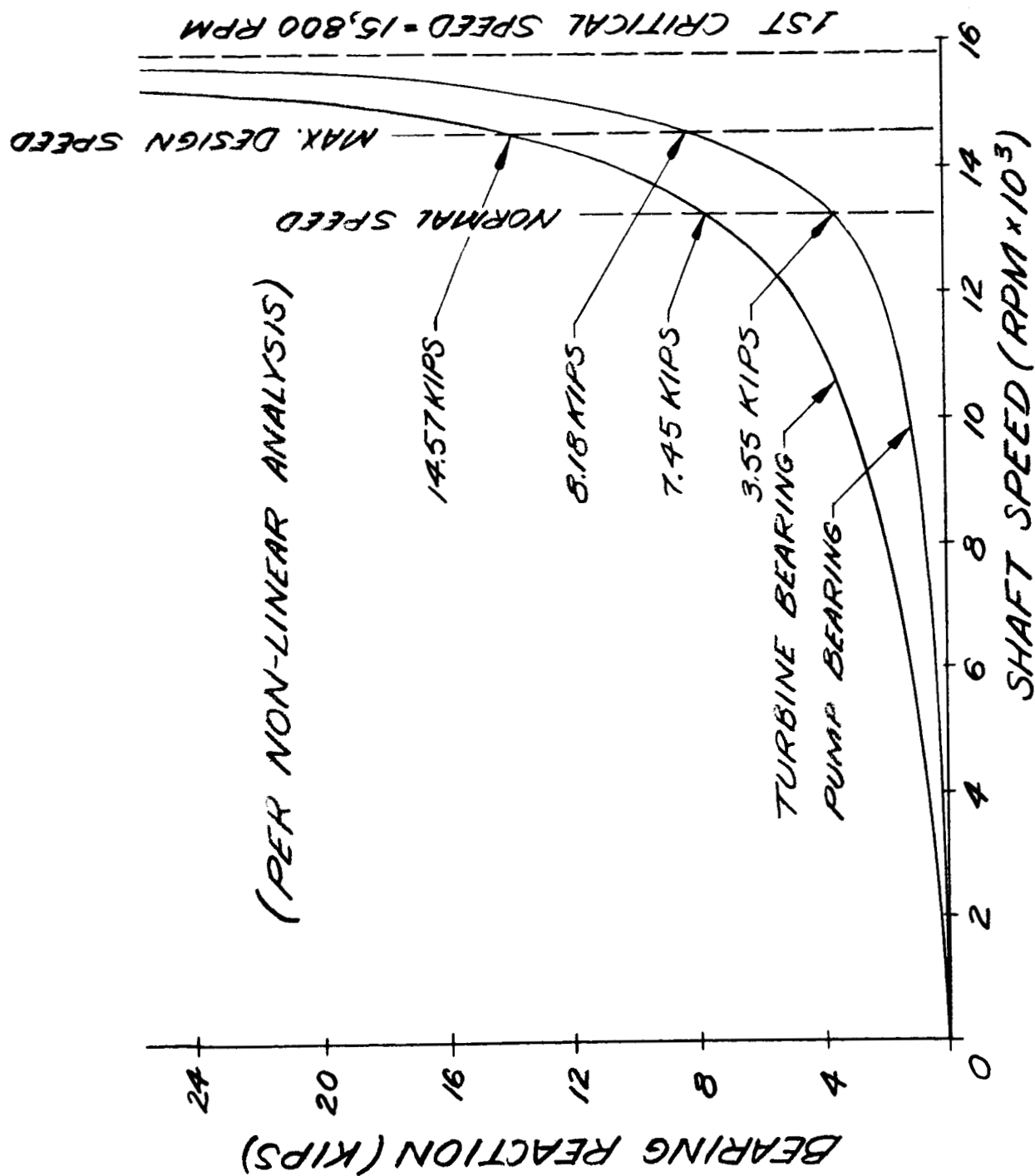
Figure 21

Bearing Reactions and Critical Speed
For Model II FTPA With Interim Inducer
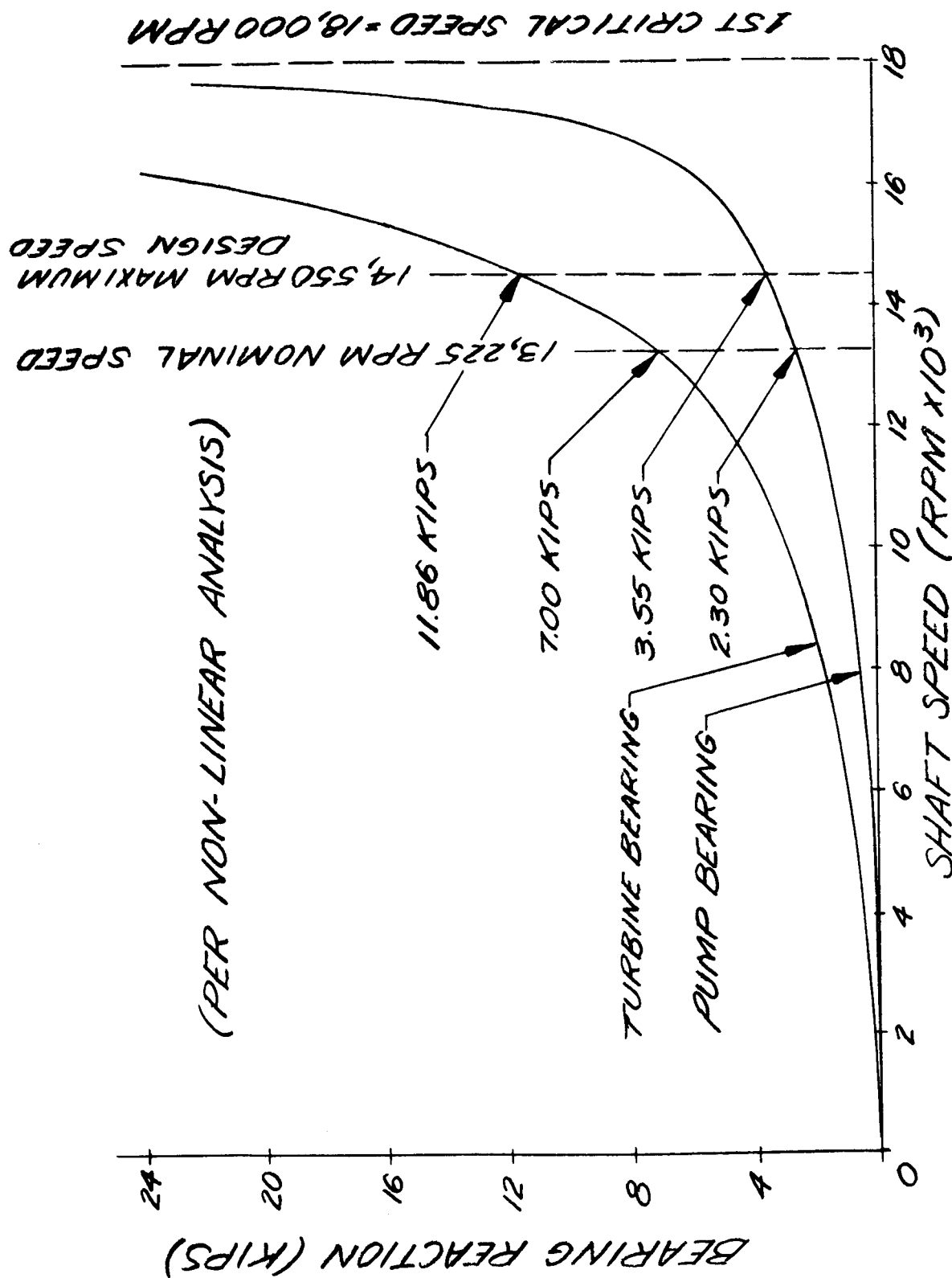
Figure 22

Bearing Reactions and Critical Speed
For Model II FTPA With Final Inducer

Page 34
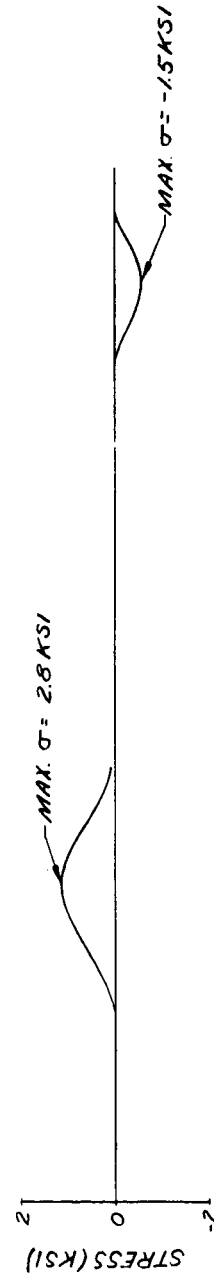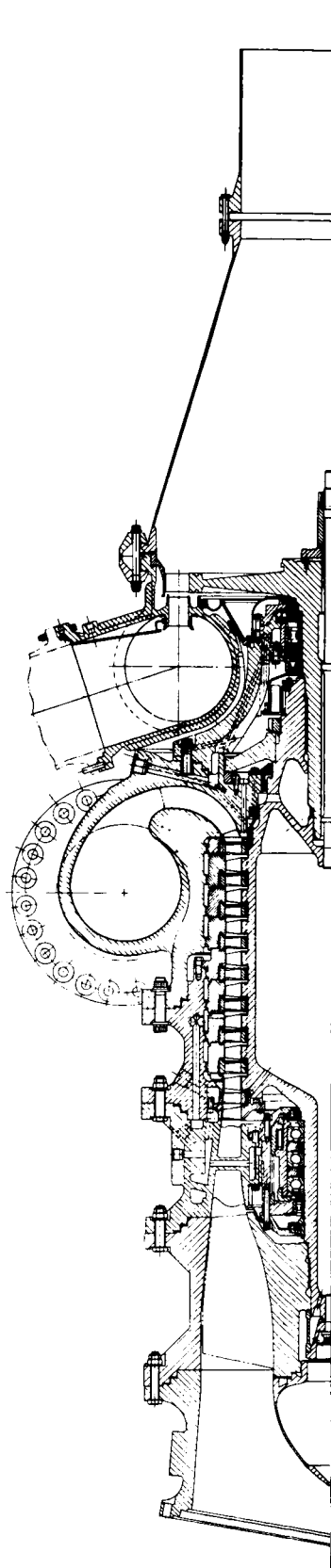
Figure 23

Shaft Bending Stresses Caused by Conical Whirling
and Associated Unbalance Forces at 14,500 RPM
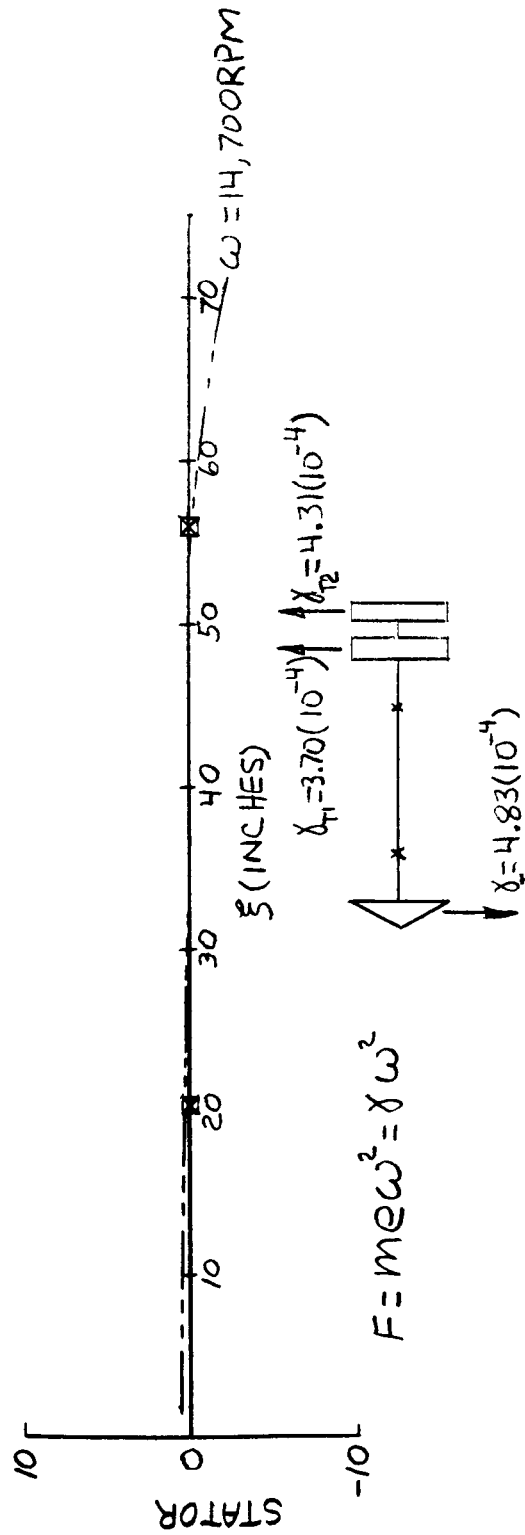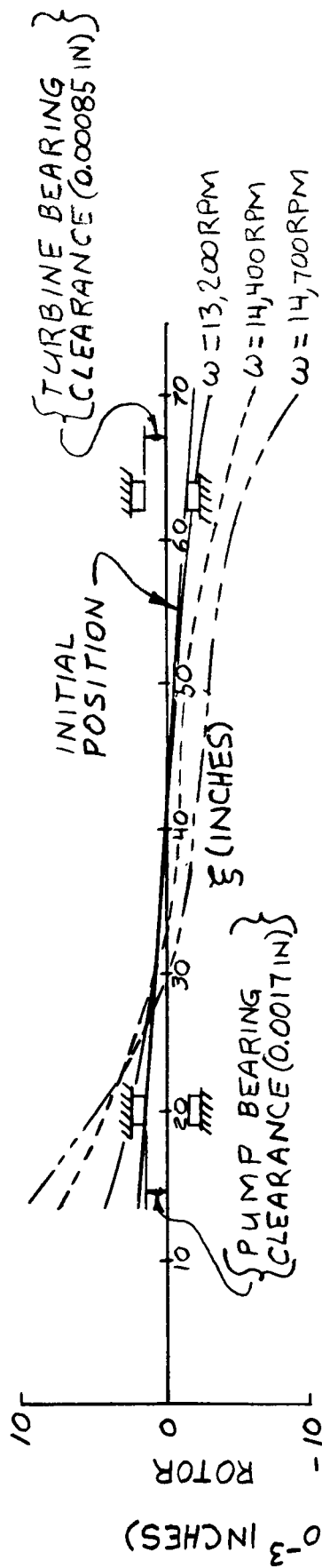
Figure 24

Shaft and Stator Elastic Curves of Model II FTPA
With Interim Inducer for Various Shaft Speeds
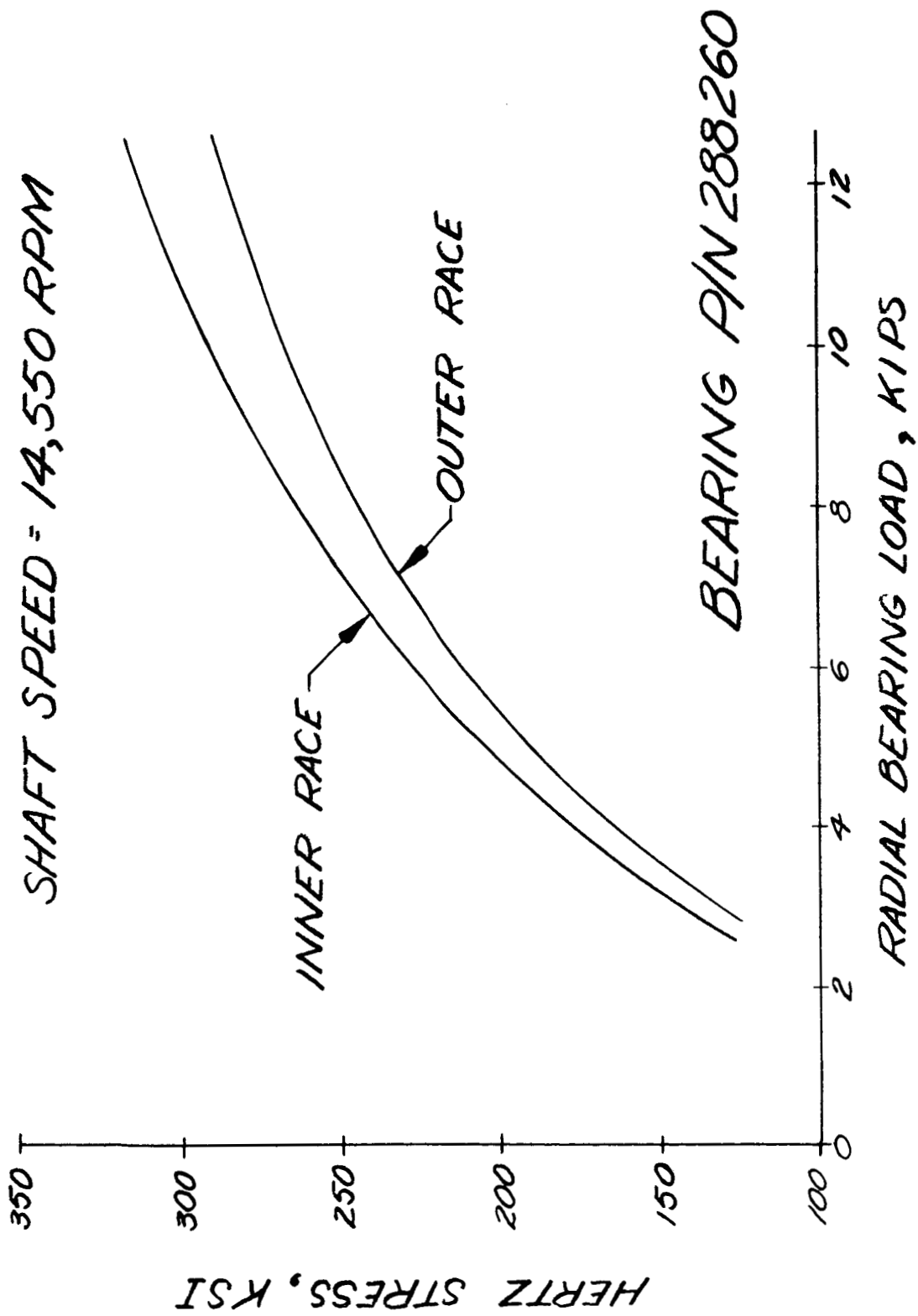
Figure 25

Hertz Stress vs. Pump Bearing Load (P/N 288260)
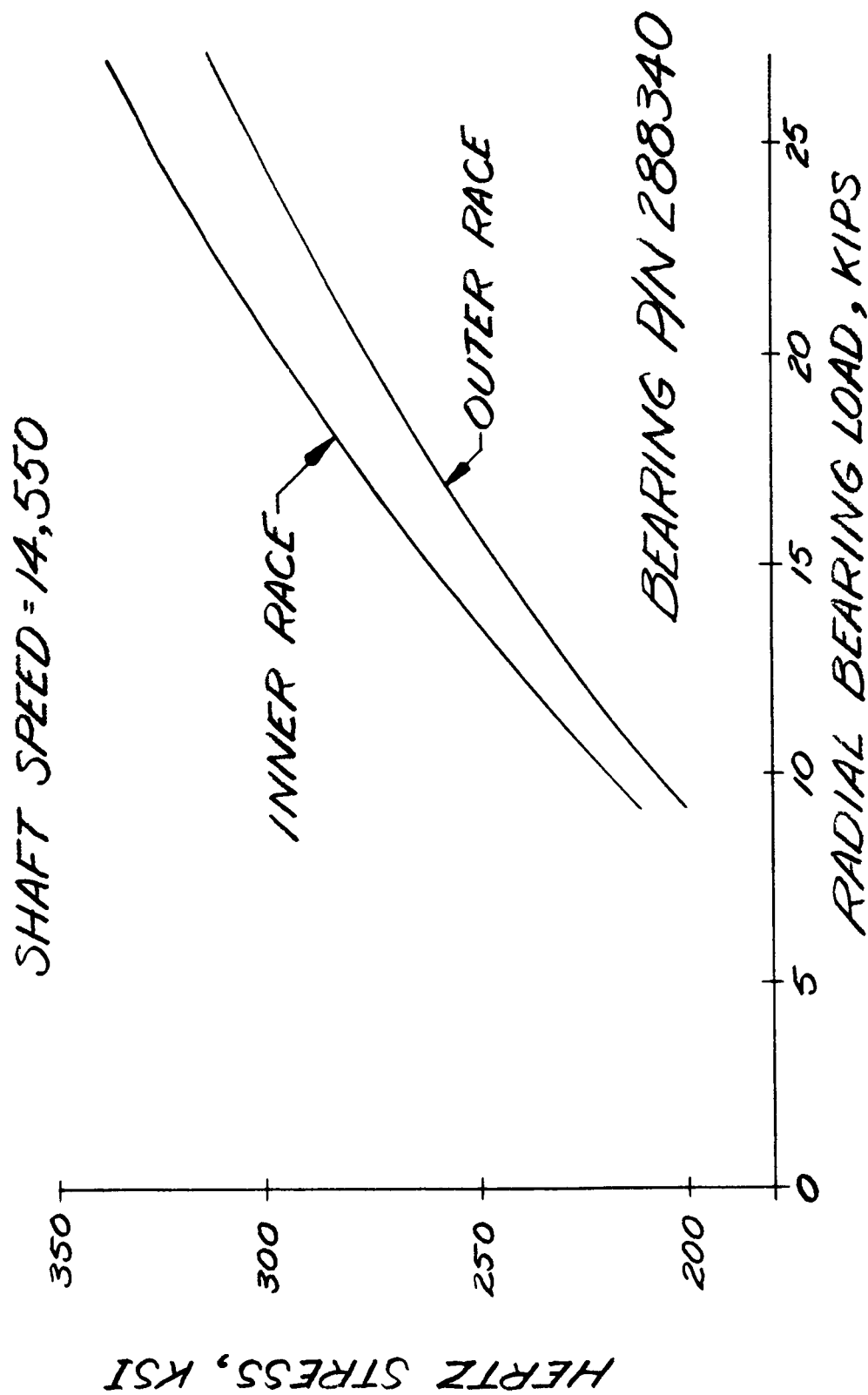
Figure 26

Hertz Stress vs. Turbine Bearing Load
(P/N 288340)

BIBILIOGRAPHY

1. Den Hartog, J. P., *Mechanical Vibrations*, New York, McGraw-Hill 1956, 4th ed., pp. 252-265 and pp. 270-373

2. Holister, G. S. and Zienkiewicz, O. D., *Stress Analysis*, London-New York-Sydney, John Wiley & Sons, 1965

3. Leckie, F. A. and Pestel, E. C., *Matrix Methods in Elastomechanics*, New York, McGraw-Hill, 1963

4. Leveille, A. R. and Ludwig, H. R., New Departure Consulting Services in Support of M-1 Engine Bearing Problems, Report to AGC from New Departure Division, Subcontract E290750, General Motors Corp., Bristol, Conn.

5. Morris, J., "The Impact of Bearing Clearances on Shaft Stability," *Aircraft Engineering*, pp. 382-383, December 1957

6. Palmgren, A., *Ball and Roller Bearing Engineering*, SKF Industries Inc., 1st ed. p. 47

7. Purdy, C. C., "Design and Development of Liquid Hydrogen Cooled 120mm Roller, 110mm Roller, and 110mm Tandem Ball Bearings for M-1 Fuel Turbopump," NASA CR-54826,

8. Regan, P. J., "Mechanical Design of the M-1 Axial Flow Liquid Hydrogen Pump," NASA CR-54823,

9. Reynolds, T. W., "Mechanical Design of a Two-Stage Impulse Turbine for the Liquid Hydrogen Turbopump of the M-1 Engine," NASA CR-54821,

10. Targoff, Walter P., *The Bending Vibrations of a Twisted Rotating Beam*, Proceedings of the Third Midwestern Conference on Solid Mechanics, pp. 177-194, University of Michigan Press, 1957

APPENDICES

APPENDIX A

METHOD OF ANALYSIS-DESCRIPTION

OF DIGITAL COMPUTER PROGRAM

I. INTRODUCTION

This program has the capability for analyzing the free or forced-undamped, lateral vibrations of two elastically coupled lumped parameter beams. Natural frequencies, mode shapes, as well as associated shear and moment distributions can be computed. The program can compute the amplitudes of the shears, moments, slopes, and deflections attributable to harmonic forcing functions. Shear deflections, rotary inertia, and gyroscopic effects for rotating shaft analyses are also included in the program capability.

The spring supports may be input as either constant values or load dependent functions defined by

$$K = A \cdot P^B$$

where A and B are constants and P is applied load, or by a table of P vs. K points.

The following is a list of appropriate nomenclature.

L   -   Length of Elasticity Element (in.)

E   -   Modulus of Elasticity (psi)

I   -   Area Moment of Inertia of Cross Section (in.^{4})

C   -   Shape Constant for Shear Deflection (in.$^{-2}$)

G   -   Modulus of Rigidity (psi)

W   -   Weight of Lumped Mass (lb)

I_J -   Polar Mass Moment of Inertia (lb-in-sec^2)

I_X -   Diametral Mass Moment of Inertia (lb-in-sec^2)

K   -   Spring Constant (lb/in.)

ω -   Shaft Whirl Frequency (cps)

$\Delta\omega$ -   Increment in Frequency (cps)

d   -   Offset Between Corresponding Stations in Two Beams (in.)

γ -   Forcing Function Coefficient of ω^2 (lb-sec^2)

Note: All unprimed quantities refer to top beam and springs between the beams. All primed quantities refer to the bottom beam and springs between it and ground.

V   -   Shear (lb)

M   -   Moment (in.-lb)

$\bar{\phi}$ -   Slope (rad)

Y   -   Deflection (in.)

[E]   -   Elasticity Transfer Matrix

[F]   -   Mass Transfer Matrix

{Δ}   -   State Vector

II.   GENERAL PROCEDURE

Analyses of complex multi-degree-of-freedom systems, of which the rotor-stator system is one, are commonly undertaken using matrix transfer techniques and the methods used herein are based upon this technique. The system is first reduced to an idealized mass-elastic model (see Figure 8 on page 15) and, then subdivided into bays of the type shown in Figure 9 on page 18.
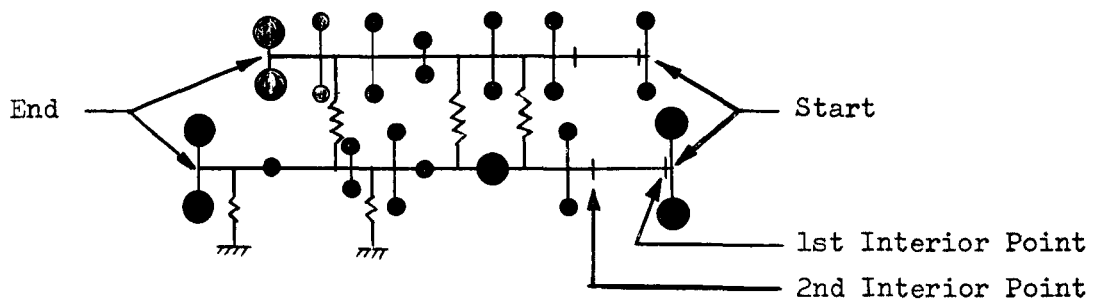
Then a column matrix containing all the types of load and deflection variables which can occur in the system is made. This column matrix is called the "state vector." At the start the state vector consists of the boundary conditions, both known and unknown. Next, a matrix equation is written which transforms the variables of the state vector from their values at the start to their values at the first interior point in the system. Further relating the conditions at the second interior point to the first interior point in-tern relates the second point to the start. Thus far, two matrix transformation equations are required: the first is for a transformation of variables across the idealized mass (Figure A-1 and A-2) and the second is for trans-formation of variables across the idealized elasticity (Figures A-3 and A-4). This procedure is continued until the last interior point and also the start is related to the end point. Then, by utilizing the boundary conditions at the end, the unknown conditions at the start and at the end can be evaluated. Once all the boundary conditions at the start are known, all interior conditions can be evaluated by re-walking through the system to the end.

At the start of the first bay N = 0, thus

$$\{\Delta_N\} = \{\Delta_0\}$$

Assuming the model starts with elastic elements we have going across the first elements in bay 1.

$$\{\Delta_1''\} = [E_1^1]\{\Delta_0\}$$

And across the first lumped masses in bay 1

$$\{\Delta_1'\} = [F_1]\{\Delta_1''\} = [F_1][E_1^1]\{\Delta_0\}$$

Next, across the second elasticity

$$\{\Delta_1\} = [E_1^2]\{\Delta_1'\} = [E_1^2][F_1][E_1^1]\{\Delta_0\} = [C_1]\{\Delta_0\}$$

In like manner, transformations can be made across each bay, expressing each state vector in terms of the previous state vector, and thus in terms of the initial state vector.

$$\{\Delta_{N_{STA}}\} = \left(\prod_{N=1}^{N=N_{STA}} [C_N]\right)\{\Delta_0\} = [D]\{\Delta_0\}$$

In expanded form we get,

$$
\left\{\begin{matrix} V \\ M \\ \Phi \\ Y \\ V' \\ M' \\ \Phi' \\ Y' \\ 1 \end{matrix}\right\}_{N_{STA}}
=
\begin{bmatrix}
d_{11} & d_{12} & d_{13} & d_{14} & d_{15} & d_{16} & d_{17} & d_{18} & d_{19} \\
d_{21} & \cdot & \cdot & \cdot & \cdot & \cdot & \cdot & d_{28} & d_{29} \\
d_{31} & \cdot & \cdot & \cdot & \cdot & \cdot & \cdot & d_{38} & d_{39} \\
d_{41} & \cdot & \cdot & \cdot & \cdot & \cdot & \cdot & d_{48} & d_{49} \\
d_{51} & \cdot & \cdot & \cdot & \cdot & \cdot & \cdot & d_{58} & d_{59} \\
d_{61} & \cdot & \cdot & \cdot & \cdot & \cdot & \cdot & d_{68} & d_{69} \\
d_{71} & \cdot & \cdot & \cdot & \cdot & \cdot & \cdot & d_{78} & d_{79} \\
d_{81} & d_{82} & d_{83} & d_{84} & d_{85} & d_{86} & d_{87} & d_{88} & d_{89} \\
0 & 0 & 0 & 0 & 0 & 0 & 0 & 0 & 1
\end{bmatrix}
\left\{\begin{matrix} V \\ M \\ \Phi \\ Y \\ V' \\ M' \\ \Phi' \\ Y' \\ 1 \end{matrix}\right\}_{0}
$$

The resulting above simultaneous equation are reduced to four simultaneous equations by virtue of the four known boundary conditions at each of stations N = 0 and N = NSTA. Then, solving simultaneously the remaining boundary conditions at station N = 0 are evaluated.

For instance, if

$$
-\{\Delta_{N_{STA}}\}- = \begin{bmatrix} O \\ O \\ \Phi \\ Y \\ O \\ O \\ \Phi' \\ Y' \\ 1 \end{bmatrix}_{N_{STA}} \quad AND \quad -\{\Delta_O\}- = -\begin{bmatrix} O \\ O \\ \Phi \\ Y \\ O \\ O \\ \Phi' \\ Y' \\ 1 \end{bmatrix}_O-
$$

The following system of equations are solved:

$$
-\begin{bmatrix} O \\ O \\ O \\ O \end{bmatrix}- = \begin{bmatrix} d_{13} & d_{14} & d_{17} & d_{18} & d_{19} \\ d_{23} & d_{24} & d_{27} & d_{28} & d_{29} \\ d_{53} & d_{54} & d_{57} & d_{58} & d_{59} \\ d_{63} & d_{64} & d_{67} & d_{68} & d_{69} \end{bmatrix} -\begin{Bmatrix} \Phi \\ Y \\ \Phi' \\ Y' \\ 1 \end{Bmatrix}_O-
$$

After the entire conditions of state at N = 0 are known, all other state vectors are evaluated by repeating the chain multiplication.

All $[F_N]$ have elements containing ω. Thus to obtain the dynamic response over the entire shaft speed range of interest, the aforementioned procedure is accomplished first for an initial given shaft whirl frequency ω. Then the procedure is repeated for the additional number of frequencies, separated by the increment $\Delta\omega$, required to define the response of the system in the range of interest.

III. THEORY AND DERIVATION OF EQUATIONS

A. STATE VECTOR

The state vector $\{\Delta\}_N$ is defined as the column matrix of the shear, moment, slope, and deflection of the beam or beams at the end of bay N. The ninth element of the state vector is the constant one which permits the inclusion of the load constant in the transfer matrices.

$$
-\{\Delta\}_N = -\begin{Bmatrix} V \\ M \\ \Phi \\ Y \\ V' \\ M' \\ \Phi' \\ Y' \\ 1 \end{Bmatrix}-
$$

B. MASS TRANSFER MATRIX

Figure A-1 illustrates a free body diagram of the lumped masses at bay N and the forces and moments which act upon the same. The corresponding equations of equilibrium and compatibility are presented in the same

Appendix A

figure.

Some of the terms may require more explanation than is given in the nomenclature. The term $\chi_N \omega^2$ represents the "forcing function" caused by imbalance or conical whirling mode of motion and its associated centrifugal forces. The stator has an element labeled d_N ; this element has infinite stiffness and permits the lumped masses of the rotor and stator at bay N to be located at positions other than immediately above or below the other. The term $(I_{JN} - I_{xN}) \Phi_N \omega^2$ accounts for what is often called the "gyroscopic effect." This term is largest in the bays that contain inducer or turbine wheels. (1)

The transfer matrix across the rotor and stator mass at bay N is given in Figure A-2.

C. ELASTICITY TRANSFER MATRIX

A free body diagram of the elastic elements that connect the adjacent lumped masses is shown in Figure A-3. The resulting equations of equilibrium and deformation are also included in Figure A-3.

The terms in the equation are straightforward with the possible exception of the term

$$\frac{C_N L_N}{G_N} \cdot V_{NR}$$

This component expresses the deflection resulting from shear which may be of importance in short stubby shafts.

The transfer matrix across the rotor and stator elastic element is illustrated in Figure A-4.

D. PROCEDURE FOR NON-LINEAR LOAD-DEFLECTION BEARING SUPPORTS

In applying this program to the lateral vibrations of turbomachinery, the rotor is represented as one beam and the housing as a second beam. The bearings connecting them are represented as springs. However, the load deflection relationships of typical turbomachinery bearings are not linear. One relation given by Palmgren (2) for roller bearings is of the form.

(1) For a more complete discussion, see Den Hartog, J. P., op. cit.
(2) Palmgren, A. Ball and Roller Bearing Engineering, SKF Industries, Inc. 3rd Edition, 1959

Appendix A

$$\delta = C_1 \left(P^{.9} / \ell^{.8} \right)$$

For a given effective length, ℓ ,

$$K = \frac{P}{\delta} = C_2 P^{0.1}$$

which is a non-linear function of P. The force on the bearing, P, is a function of the unbalance in the systems, and is magnified greatly in the neighborhood of resonance. As bearing loads increase, the value of K, or stiffness, increases. The effect upon a plot of bearing load versus shaft speed is to cause a leaning-over of the curve (3).

The computer program treats this effect by calculating a spring rate

$$K = A P^B$$

where A and B are constants. A value of P is assumed (P_0), K is calculated from the above equation and then a forced-vibration analysis is performed. From the resulting deflections, the load in the bearing is calculated $P = KY$ or, $P = KY - KY'$ if working with a flexible housing. This value of P will, in general, not agree with the value P_0 upon which K was based. Thus, a new K is calculated and the cycle repeated until the resulting P agrees with the assumed P. All of this iteration and convergence is based upon a single frequency ω . Once convergence on K is achieved for a given ω , the frequency is changed until the range of interest is investigated. The projected P_0 for subsequent speeds is given by (starting with the 4th ω)

$$P_0^i = 3.0 \left(P^{i-1} - P^{i-2} \right) + P^{i-3}$$

This prediction equation was found to be needed to obtain convergence in a sufficiently small number of iterations as the ω approaches resonant ω .

---

(3) Den Hartog, J. P., op. cit.

Figure A-1
MASS ELEMENT TRANSFER EQUATION

$$V_{NL} = V_{NR} + \frac{W_N}{g} Y_N \omega^2 + \gamma_N \omega^2 - K_N (Y_N - Y_N' - d_N \Phi_N')$$

$$M_{NL} = M_{NR} - (I_{JN} - I_{XN}) \Phi_N \omega^2$$

$$\Phi_{NL} = \Phi_{NR} \quad ; \quad Y_{NL} = Y_{NR}$$

$$V_{NL}' = V_{NR}' + \frac{W_N}{g} Y_N' \omega^2 + K_N (Y_N - Y_N' - d_N \Phi_N') - K_N' Y_N'$$

$$M_{NL}' = M_{NR}' + I_{XN}' \Phi_N' \omega^2 + d_N K_N (Y_N - Y_N' - d_N \Phi_N')$$

$$\Phi_{NL}' = \Phi_{NR}' \quad ; \quad Y_{NL}' = Y_{NR}'$$

Figure A-1
MASS ELEMENT TRANSFER EQUATION
Page A-7

$$
\begin{Bmatrix} V \\ M \\ \Phi \\ Y \\ V' \\ M' \\ \Phi' \\ Y' \\ 1 \end{Bmatrix}_L =
\begin{bmatrix}
1 & 0 & 0 & \frac{W_N}{g}\omega^2 - K_N & 0 & 0 & d_N K & -K_N & \gamma\omega^2 \\
0 & 1 & -(I_{JN} - I_{XN})\omega^2 & 0 & 0 & 0 & 0 & 0 & 0 \\
0 & 0 & 1 & 0 & 0 & 0 & 0 & 0 & 0 \\
0 & 0 & 0 & 1 & 0 & 0 & 0 & 0 & 0 \\
0 & 0 & 0 & K_N & 1 & 0 & -d_N K_N & \frac{W_N}{g}\omega^2 - K_N - K'_N & 0 \\
0 & 0 & 0 & d_N K_N & 0 & 1 & (I'_{XN}\omega^2 - d_N^2 K_N) & -d_N K_N & 0 \\
0 & 0 & 0 & 0 & 0 & 0 & 1 & 0 & 0 \\
0 & 0 & 0 & 0 & 0 & 0 & 0 & 1 & 0 \\
0 & 0 & 0 & 0 & 0 & 0 & 0 & 0 & 1
\end{bmatrix}
\begin{Bmatrix} V \\ M \\ \Phi \\ Y \\ V' \\ M' \\ \Phi' \\ Y' \\ 1 \end{Bmatrix}_R
$$

which may be written more compactly $\left[\Delta\right]_L = \left[F_N\right]\left[\Delta\right]_R$

Figure A-2

MASS ELEMENT TRANSFER MATRIX

Page A-8

$$V_{NL} = V_{NR} \quad ; \quad M_{NL} = M_{NR} + V_{NR} L_N$$

$$\Phi_{NL} = \Phi_{NR} - \frac{L_N^2}{2(EI)_N} V_{NR} - \frac{L_N}{(EI)_N} M_{NR}$$

$$Y_{NL} = Y_{NR} - \Phi_{NR} L_N + \left(\frac{L_N^3}{6(EI)_N} - \frac{C_N L_N}{G_N}\right) V_{NR} + \frac{L_N^2}{2(EI)_N} M_{NR}$$

$$V'_{NL} = V'_{NR} \quad ; \quad M'_{NL} = M'_{NR} + V'_{NR} L'_N$$

$$\Phi'_{NL} = \Phi'_{NR} - \frac{(L'_N)^2}{2(EI)'_N} V'_{NR} - \frac{L'_N}{(EI)'_N} M'_{NR}$$

$$Y'_{NL} = Y'_{NR} - \Phi'_{NR} L'_N + \left[\frac{(L'_N)^3}{6(EI)'_N} - \frac{C'_N L'_N}{G'_N}\right] V'_{NR} + \frac{(L'_N)^2}{2(EI)'_N} M'_{NR}$$

Figure A-3

ELASTICITY ELEMENT TRANSFER EQUATIONS
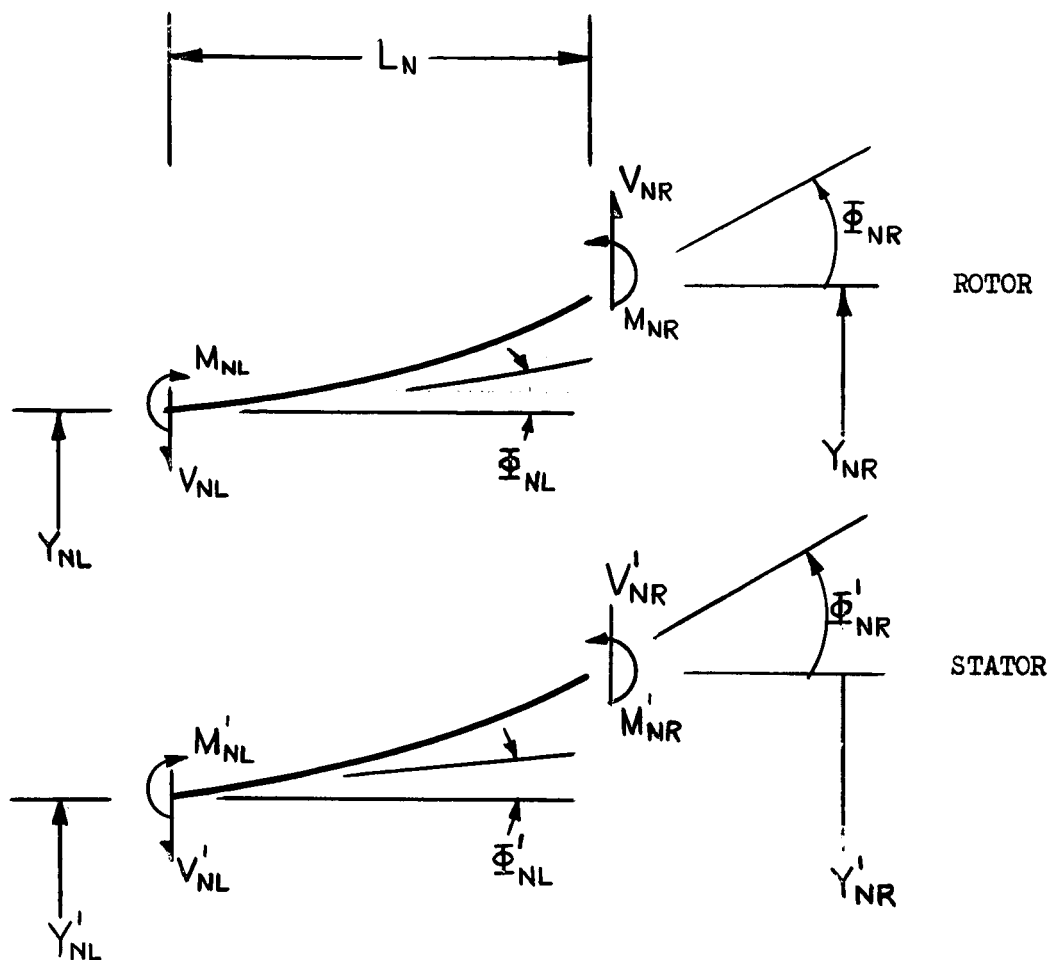
$$
\begin{Bmatrix} V \\ M \\ \Phi \\ Y \\ V' \\ M' \\ \Phi' \\ Y' \\ 1 \end{Bmatrix}_L =
\begin{bmatrix}
1 & 0 & 0 & 0 & 0 & 0 & 0 & 0 & 0 \\
L_N & 1 & 0 & 0 & 0 & 0 & 0 & 0 & 0 \\
-\frac{L_N^2}{2(EI)_N} & -\frac{L_N}{(EI)_N} & 1 & 0 & 0 & 0 & 0 & 0 & 0 \\
\frac{L_N^3}{6(EI)_N} - \frac{C_N L_N}{G_N} & \frac{L_N^2}{2(EI)_N} & -L_N & 1 & 0 & 0 & 0 & 0 & 0 \\
0 & 0 & 0 & 0 & 1 & 0 & 0 & 0 & 0 \\
0 & 0 & 0 & 0 & L'_N & 1 & 0 & 0 & 0 \\
0 & 0 & 0 & 0 & -\frac{(L'_N)^2}{2(EI)'_N} & -\frac{L'_N}{(EI)'_N} & 1 & 0 & 0 \\
0 & 0 & 0 & 0 & \frac{(L'_N)^3}{6(EI)'_N} - \frac{C'_N L'_N}{G'_N} & \frac{(L'_N)^2}{2(EI)'_N} & -L_N & 1 & 0 \\
0 & 0 & 0 & 0 & 0 & 0 & 0 & 0 & 1
\end{bmatrix}
\begin{Bmatrix} V \\ M \\ \Phi \\ Y \\ V' \\ M' \\ \Phi' \\ Y' \\ 1 \end{Bmatrix}_R
$$

which may be written more compactly $\{\Delta\}_L = [E_N] \{\Delta\}_R$

Figure A-4

ELASTICITY ELEMENT TRANSFER MATRIX

Page A-10

APPENDIX B

ROLLER BEARING ANALYSIS

Appendix B

I. INTRODUCTION

During the work for Subcontract E290750[1], Aerojet-General asked New Departure to develop spring rate models for a cylindrical roller bearing. The following Appendix consists basically of material taken from the New Departure Report and summarizes the results of the requested analysis. A computer program based upon the methods presented herein is now in use.

The following is a list of nomenclature pertinent to this computer program:

P_D	Radial Play
θ	Angular Position
θ_L	Angular Limit of the Load Zone
Z	Pitch Circle Diameter
D	Roller Diameter
R	Radial Load
k	Radial Deflection
δ	Deflection
δ_N	Normal Deflection
δ_{ocf}	High Speed, Zero Load Deflection
K	Spring Constant
b	Spring Exponent
CF	Centrifugal Force/Roller
L	Roller Length
Den	Density
P	Normal Load
a	Semi-width of Contact Area
E	Modulus of Elasticity

---

(1) Subcontract to provide analytical support for solving M-1 Engine bearing problems.

μ Poisson's Ratio

r   Radius of Curvature

N   Number of Rollers

n   Error Tolerance

II. ROLLER ELEMENT SPRING EQUATION

A. INTRODUCTION

The solution of the roller bearing mechanics problem is dependent upon a knowledge of the spring equation of the roller element against a raceway. A search of the literature revealed work in this area by Foppl in Germany and Lundberg in Sweden. This report will use Lundberg's work[2].

B. BASIC EQUATION

The basic equation presented by Lundberg relates to the approach between a cylinder and a plane body. This equation is

$$\delta = \frac{2P}{\pi E' L} \ln \frac{\pi L^2 E'}{P} \qquad \text{Equation (1)}$$

where

     P = normal load on cylinder

     L = length of cylinder

     $E' = E/(1-\mu^2)$

where

     E = Modulus of elasticity of the cylinder and plane body.

     μ = Poisson's ratio of the two bodies.

(Note: Equation (1) is independent of the diameter of the cylinder.)

---

(2) Palmgren, A., op. cit.

Lundberg proceeds with the basic equation and after several intermediate steps arrives at an approximate power function relationship.

$$2\delta \approx \frac{0.0062\ P^{0.9}}{L^{0.8}}$$

where δ is in mm and P in Kg. The use of the above approximation is found in Palmgren[2].

C. EXPERIMENTAL CONFIRMATION OF EQUATION (1)

If a roller were placed between two flat plates, their normal approach under load would be twice that given by Equation (1). An experiment of this type was conducted and the results are compared with twice the value as calculated by Equation (1). These results are shown in Figure B-1.

D. POWER FUNCTION REPRESENTATION OF EQUATION (1)

The data upon which the above graph is based are plotted in Figure B-2 on a log-log scale. The data points essentially plot as a straight line. This gives rise to a power function representation, i.e.,

$$P = K\delta^b \qquad\qquad\qquad \text{Equation (2)}$$

where b is the slope of the straight line and may be obtained from any two points (1) and (2) as shown below.
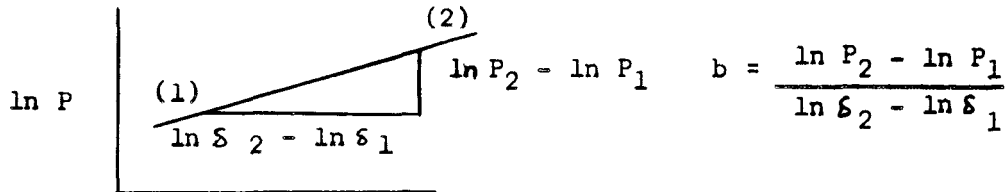
$$b = \frac{\ln P_2 - \ln P_1}{\ln \delta_2 - \ln \delta_1} \qquad\qquad \text{Equation (3)}$$

The constant K is found from

$$K = \frac{P}{\delta^b}$$

Figure B-2 also shows that the slope does change over the range of loading considered. This indicates the need for considering the expected load range which the cylinders will be subjected to if a power function representation is to be used. This aspect of the problem was considered and is discussed in more detail in the discussion of the application of Equation (4).

E. MODIFICATION OF EQUATION (1)

Equation (1) may be modified to account for the effect of curvature of the plane body. This results in

$$\delta = \frac{2P}{\pi E' L} \ \ln \frac{\pi L^2 E'}{2P} \ \left(\frac{2r + D}{r}\right)$$

Equation (4)

where D = diameter of cylinder

r = radius of curvature of other body in the plane perpendicular to the axis of the cylinder; r is positive or negative depending upon its relationship with D in accordance with Hertz theory of contact stress and deflections.

For example,

(a) Negative r
     (outer ring)

(b) Positive r
     (inner ring)
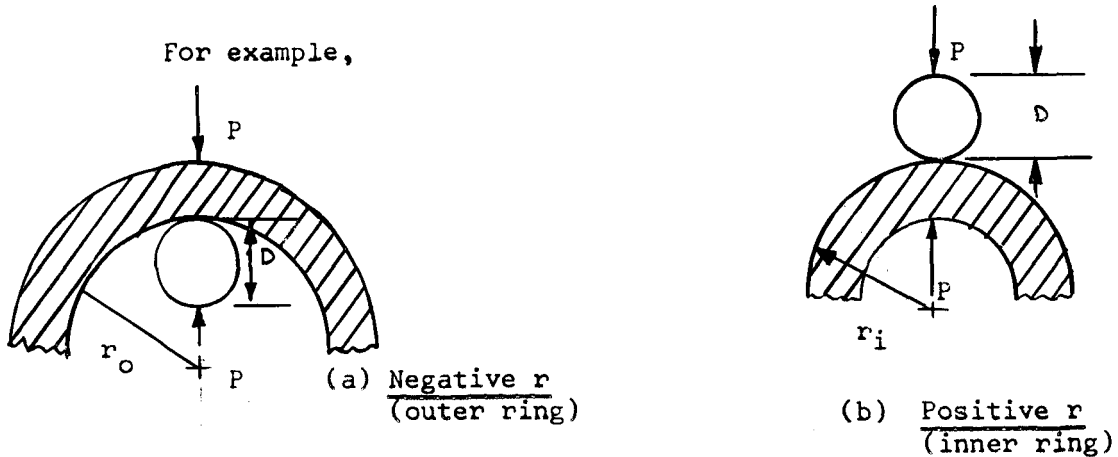
F. APPLICATION OF EQUATION (4) TO A BEARING

The radius r_i of an inner race is a positive curvature (see example above).

$$r_i = \frac{1}{2} \ (Z-D)$$

Z = pitch diameter to roller centers

Then from Equation (4)

$$\frac{2r + D}{r} = \frac{2 Z}{Z-D}$$

therefore

$$\delta i = \frac{2 P_i}{\pi E' L} \quad \ln \left[\frac{\pi L^2 E'}{P_i} \left(\frac{Z}{Z-D} \right) \right] \qquad \text{Equation (5a)}$$

In like manner for the outer race - roller spring

$$\delta o = \frac{2 P_o}{\pi E' L} \quad \ln \left[\frac{\pi L^2 E'}{P_o} \left(\frac{Z}{Z+D} \right) \right] \qquad \text{Equation (5b)}$$

G. ESTIMATE OF LOAD RANGE TO WHICH ROLLERS IN A BEARING WILL BE SUBJECTED

The maximum load which the saddle roller will be subjected to at low speed is approximated by

$$P_{(\theta=0)} \approx \frac{5R}{N} \quad^{(*)} \qquad \text{Equation (6)}$$

where

R = total static radial load on the bearing

N = number of rollers

Equation (6) forms a reasonable basis for the upper limit of roller load used in establishing a power function spring equation.

III. HIGH SPEED MECHANICS OF A ROLLER BEARING UNDER PURE RADIAL LOADING

A. GEOMETRICAL CONSIDERATIONS

In the zero load and speed condition, one may view a roller bearing with its rings concentric and its rollers in line contact with the inner ring. This is shown schematically as follows:

___

(*A Streibeck distribution assuming no diametral looseness in the bearing yields a coefficient slightly larger than 4. Assuming some diametral looseness the coefficient becomes larger. An assumed value of 5 is a reasonable estimate.)

Saddle Roller
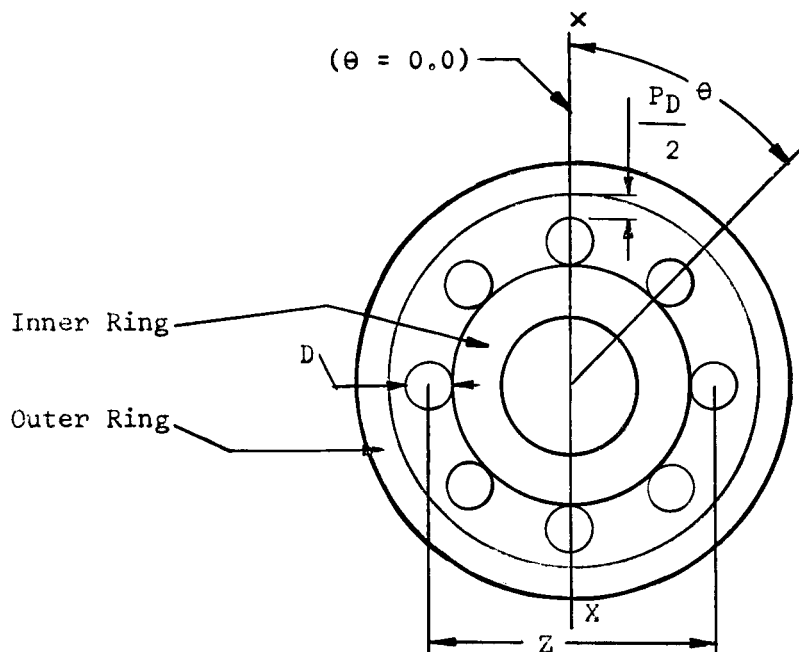
P_D = Free diametral play - (radial play)

θ = Angular position around bearing.

Z = Pitch circle diameter of rollers.

D = Roller diameter.

Schematic (1)

Holding the outer ring stationery, the inner ring may be moved upward along the X-X axis a free amount $P_D/2$ before contact is made by the saddle roller (see Schematic 1) with the outer ring. This displaced position is shown as follows, which defines the position from which deflection shall be measured. For a bearing having zero or a negative radial play, deflection is measured from the symmetric position.

$$\lambda_{(\theta)} \; = \; \frac{P_D}{2} \; (1 - \cos \theta)$$

X - X = Axial of radial load and radial deflection.

Inner Ring

Outer Ring

P_D

R & k
(Positive
Direction)

Schematic (2)
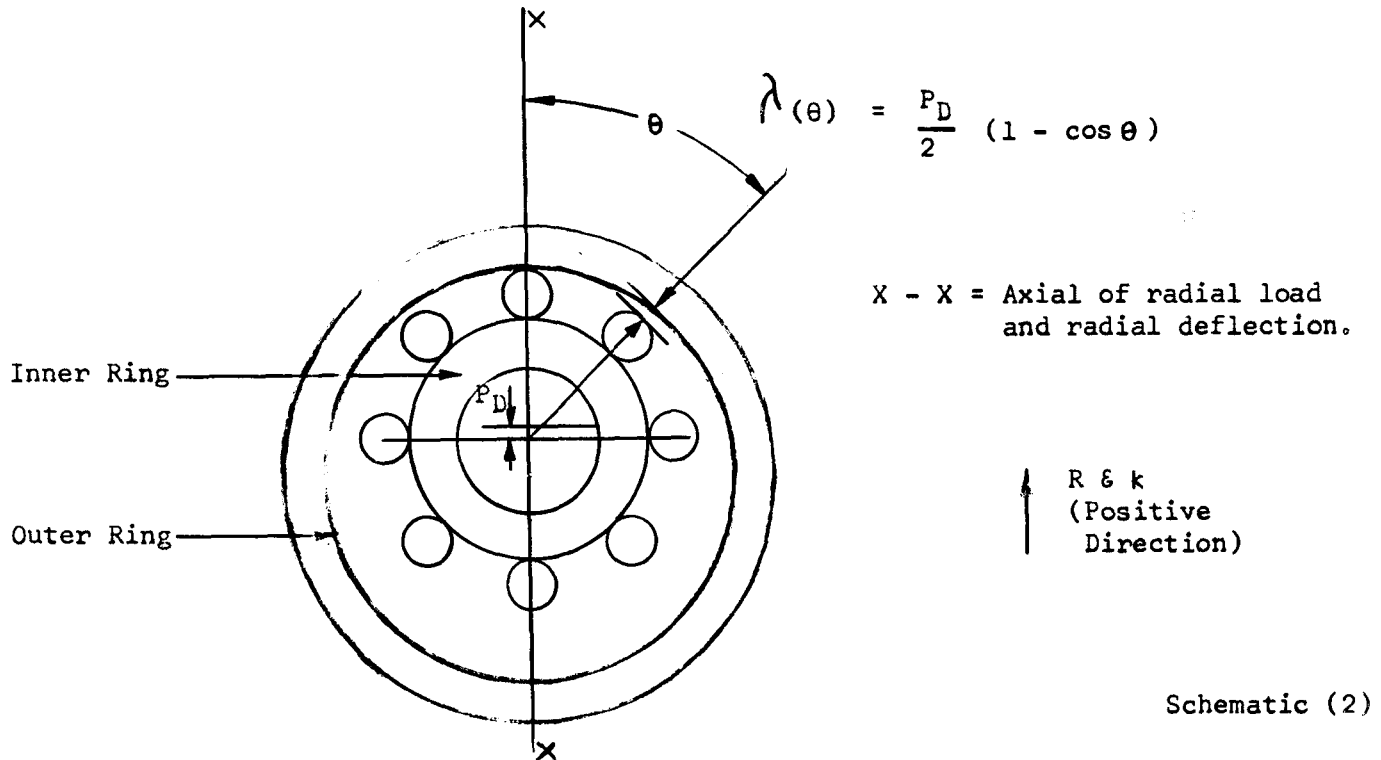
Letting R be equal to a radial load being transmitted by the shaft, the roller bearing will deflect an amount k, where

      k = radial movement of the inner ring of the bearing relative
          to the outer ring along the axis of the radial load as
          defined by the X - X axis of Schematic (2) above.

If the bearing is mounted on a shaft that is essentially solid and in a housing which is massive compared to the thickness of the outer ring, it may be assumed that the rings remain circular in shape with deformations occuring only at the roller-inner race contacts and at the roller-outer race contacts.

Letting,

δ_i = normal approach under load of a roller to the inner ring.

δ_o = normal approach under load of a roller to the outer ring.

The total normal approach under load between the inner and outer rings along a radial line from the bearing center if δ_N where

$$\delta_N = \delta_i + \delta_o \qquad\qquad \text{Equation (7)}$$

For the saddle roller

$$\text{for } P_D \geq 0.0 \qquad \delta_N = k$$

$$\text{for } P_D \leq 0.0 \qquad \delta_N = k - \frac{P_D}{2}$$

For a roller at some position θ around the bearing it may be shown that

$$\text{for } P_D \geq 0.0 \qquad \delta_N(\theta) = \left(\frac{P_D}{2} + k\right) \cos\theta - \frac{P_D}{2} \qquad (a)$$

Equation (8)

$$\text{for } P_D \leq 0.0 \qquad \delta_N(\theta) = -\frac{P_D}{2} + k \cos\theta \qquad (b)$$

Equation (8) is a direct result of geometrical considerations.

B. SPRING EQUATION OF A SINGLE ROLLER

It was shown in the power function representation of Equation (1) that the relationship between load and deflection of a roller against the inner and outer rings may be expressed as

$$P_i = K_i \, \delta_i^{\,b_i} \qquad (a)$$

Equation (9)

$$P_o = K_o \, \delta_o^{\,b_o} \qquad (b)$$

where

P = normal load between a roller and a raceway

K & b = spring constants

Subscript "i" refers to inner ring-roller.

Subscript "o" refers to outer ring-roller.

C. HIGH SPEED EQUILIBRIUM EQUATION FOR ROLLER

For the inner race rotating at some rpm N_i, the centrifugal force acting on each roller is given by

$$CF = .279D^2LZ \; \rho \left(1 - \frac{D}{Z} \right)^2 \; N_i^2 \times 10^{-5} \qquad \text{Equation (10)}$$

where

.279 = constant (assumes lb-in. units)
CF = centrifugal force/roller
L = effective contact length of roller
ρ = density of the roller material

Under constant speed conditions with no cage forces, the required equilibrium condition for each roller is

$$P_i + CF - P_o = 0.0 \qquad \text{Equation (11)}$$
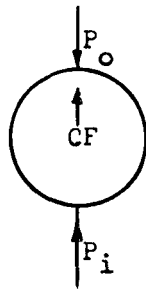
Free body diagram
of a single roller.

Schematic (3)

Equation (11) may be expressed in terms of the deflections δ_i and δ_o by substituting Equation (9) for P_i and P_o.

$$K_i \, \delta_i^{b_i} + CF - K_o \, \delta_o^{b_o} = 0.0$$

From Equation (7) we have

$$\delta_o = \delta_N - \delta_i$$

Then the equilibrium equation for the individual roller becomes

$$K_i \, \delta_i^{b_i} + CF - K_o \left(\delta_N - \delta_i \right)^{b_o} = 0.0 \qquad \text{Equation (12)}$$

A given value of k in conjunction with Equation (8) enables one to evaluate δ_N. Thus, the only unknown in Equation (12) is δ_i.

Solving for δ_i in Equation (12) may be accomplished by any of several numerical techniques. The method used in this part and discussed in the solution to the rolling element equilibrium equation is the Newton-Raphson method.

D. HIGH SPEED ZERO LOAD RADIAL DEFLECTION

If the roller bearing of Schematic (2) is brought up to speed without the application of any radial load, the rollers will deflect normally into the outer race as a result of centrifugal force. This means that the inner race will no longer be in contact with the roller at the saddle position (i.e. $\theta = 0.0$). Neglecting the small effect of unbalance resulting from the eccentric position of Schematic (2) the inner race may move upward under negligible load an amount equal to the normal approach into the outer raceway.

Letting

δ_{ocf} = normal approach of a roller into the outer race due to CF

Then

δ_{ocf} = high speed, zero load radial deflection

Thus at a constant speed, the radial load versus deflection curve of the bearing will have a radial deflection δ_{ocf} under negligible external load.

E.   CRITERIA TO DETERMINE IF A ROLLER IS LOADED

   1.   Zero Speed

      Under zero speed condition, Equation (8) may be used to determine the extent of the loaded zone around the bearing.

      Thus if

$$\delta_N(\theta) > 0.0$$

the roller at that   position will be loaded. In this manner, one may define the limit of the loaded zone in terms of the angle which satisfied the condition.

$$\delta_N(\theta_L) = 0.0$$

Solving Equation (2) for this criteria yields

for $P_D \geq 0.0$ $\theta_L = \pm \cos\left[\dfrac{P_D}{P_D + 2k}\right]$ (a)

for $P_D \leq 0.0$ $\theta_L = \pm \cos\left[\dfrac{P_D}{2k}\right]$ (b)   Equation (13)

   , θ_L = Limit of the Load Zone

   2.   High Speed

      Under high speed conditions the criteria used to determine the angle θ_L at which the inner race becomes unloaded is

$$\delta_N(\theta_L) = \delta_{ocf}$$

      this results in;

for $P_D \geq 0.0$ $\theta_L = \pm \cos\left[\dfrac{P_D + 2\delta_{ocf}}{P_D + 2k}\right]$ (c)

Equation (13)

for $P_D \leq 0.0$ $\theta_L = \pm \cos\left[\dfrac{P_D + 2\delta_{ocf}}{2k}\right]$ (d)

The effect of δ_{ocf} is to reduce the extent of the loaded zone.

F. RADIAL LOAD (R) VERSUS RADIAL DEFLECTION (k)

Based upon the preceeding analysis the following procedure is used to determine the radial load resulting from a given deflection k.

    (a)   Assume a value of k.

    (b)   Determine δ_{ocf} by means of Equations (9b) and (10) for $P_o = CF$.

    (c)   Determine the extent of the loaded zone from Equation (13).

    (d)   For each roller position within the loaded zone evaluate:

        <u>1</u> δ_N from Equation (8)

        <u>2</u>   Solve for δ_i in Equation (12)

        <u>3</u>   Evaluate P_i from Equation (9a)

        <u>4</u>   Evaluate that component of P_i which contributes to the radial load (i.e., $P_i \overline{Cos\theta}$)

    (e)   Sum up the individual contribution of each roller in the loaded zone to arrive at the resulting radial load.

For example:

$$R = \sum_{\theta = -\theta_L}^{\theta = +\theta_L} P_i \, Cos \, \theta \qquad \qquad \text{Equation (14)}$$

G. ACCURACY OF MODEL USED

The accuracy of the mathematical model used in predicting the radial deflection of a roller bearing will depend to varying degrees upon the following factors:

1. <u>Rolling Element Spring Equations</u>

The roller element spring Equations (9a) and (9b) can be established quantitatively either by empirical means or as does this report, from a mathematical model. In the roller element spring equation discussion, it is shown that first order agreement is found between empirical data and a mathematical model derived from advanced theory of elasticity considerations. However, the accuracy of this model can be expected to decrease as the length of the roller becomes smaller and/or if the cylindrical rollers are not properly crowned. Proper crowning reduces but will not completely eliminate stress concentration at the roller ends. As the roller length is decreased, the roller end conditions become more significant.

2. Pure Radial Loading With No Misalignment

The analysis considers only pure radial loading and assumes no relative misalignment of the raceways. Although roller bearings may operate satisfactorily under some small misalignment, at present there is no mathematical basis of predicting the harmful effect of misalignment upon bearing operation or its effect on radial deflection. However, it is expected that increasing misalignment would result in unsatisfactory bearing performance before it would measureably change the bearing's deflection characteristics. Of the different type of roller designs, the cylindrical one is most sensitive to misalignment. Careful consideration should be given to minimize any condition of mounting or loading which will result in misalignment.

3. Assumed Static Positioning of Rollers

Recall that the rollers were assumed to exist at equal intervals around the bearing with one roller being located at the saddle ($\theta = 0°$) position. In the operating state, the rollers will be moving into and out of the saddle position. Under constant load conditions, such an action would produce a pulsating deflection around some average value. While this effect does exist, it is not significant provided the bearing contains a sufficient number of rollers. Generally, approximately ten rollers will eliminate any measurable pulsation. Not considered in this report is any rotating radial unbalance or shaft whip. Either of these two factors could cause a pulsating deflection.

4. Effective Length of the Rollers

The mathematical model used to arrive at the spring Equations (9a) and (9b), depends upon the length of the roller. The effective length of a crowned roller is somewhat less than the actual length. In general, an effective length equal to .9 of the true length is a reasonable representation. However, it must be realized that this is an area of uncertainty. In view of the intended use of this discussion for critical speed studies, an approach which may be useful is to view the effective length over a range which would be expected to bound the true value. A best opinion at this time would be from .85 to .95. Calculations used over these limits would provide a basis for upper and lower bound spring rate values.

IV. SOLUTION TO THE ROLLER ELEMENT EQUILIBRIUM EQUATION

Equation (6) of the discussion is the equilibrium equation of a single roller.

$$\text{For example} \quad K_i\ \delta_i^{\,b_i} + CF\text{-}K_o\ (\ \delta_N - \delta_i)^{\,b_o} = 0.0 \qquad \text{Equation (12)}$$

The only unknown is δ_i. The problem then is to solve for δ_i in Equation (12). To accomplish this the Newton-Raphson iteration technique is used.

Let $\quad \Psi(\delta_i) = K_i \, \delta_i^{\,b_i} + CF - K_o (\delta_N - \delta_i)^{b_o}$ Equation (13)

Then $\quad \Psi'(\delta_i) = b_i K_i \, \delta_i^{(b_i-1)} + b_o K_o (\delta_N - \delta_i)^{(b_o-1)}$ Equation (14)

An initial value of $\delta_i = \dfrac{1}{2}(\delta_N - \delta_{ocf})$ is used.

Successive assumptions for δ_i are

$$(\delta_i)_n = (\delta_i)_{n-1} - \frac{\Psi(\delta_i)_{n-1}}{\Psi(\delta_i)_{n-1}}$$

Equation (14)

The change in δ_i values between two iterations is Δ where

$$\Delta = -\frac{\Psi(\delta_i)}{\Psi'(\delta_i)}$$

The iteration is ended for

$$|\Delta| \leq \eta$$

where

$$\eta = 3 \times 10^{-6} \text{ is used in this report.}$$

The value of η corresponds to a load accuracy of from 5 to 10 lb per inch of roller length.

To prevent negative arguments of unreal significance in Equations (13) and (14), the absolute values of the arguments are used.
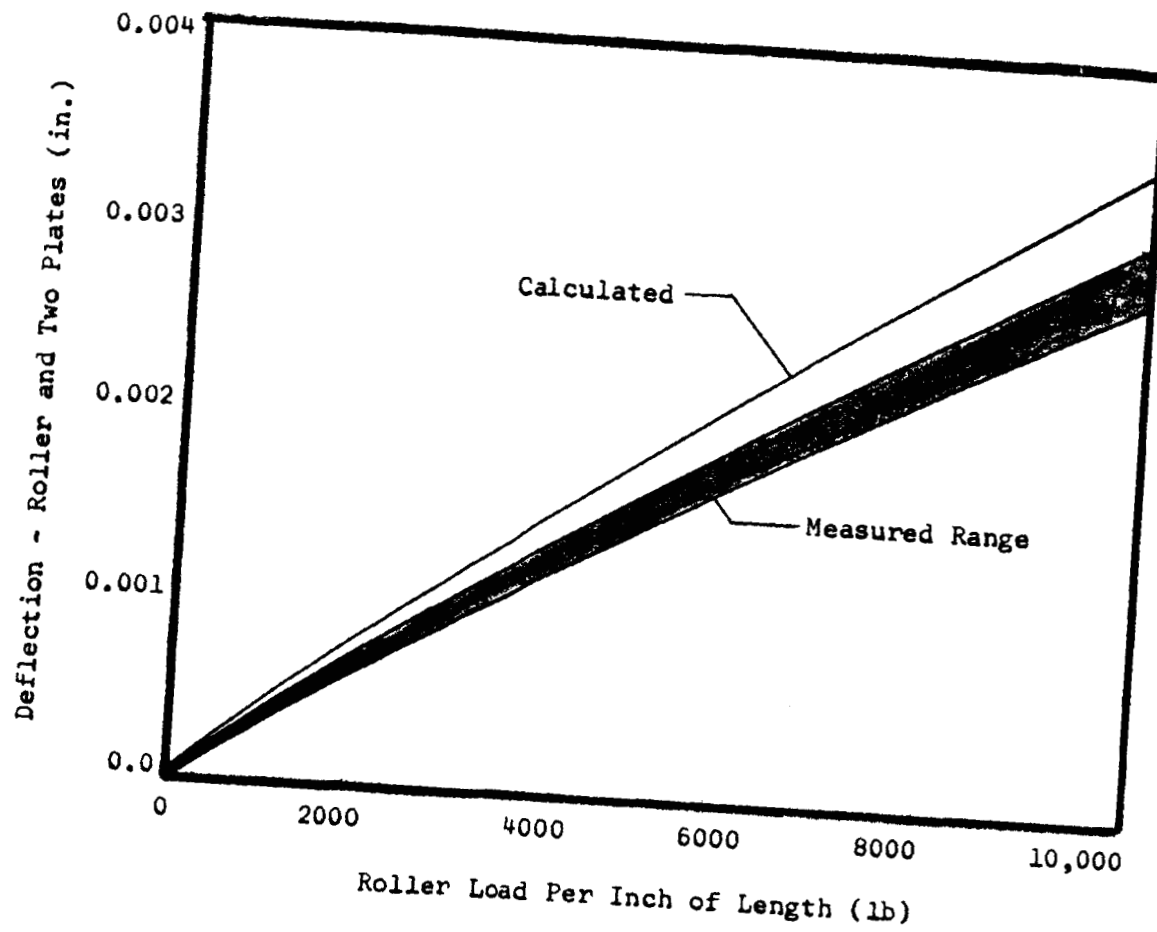
Figure B-1

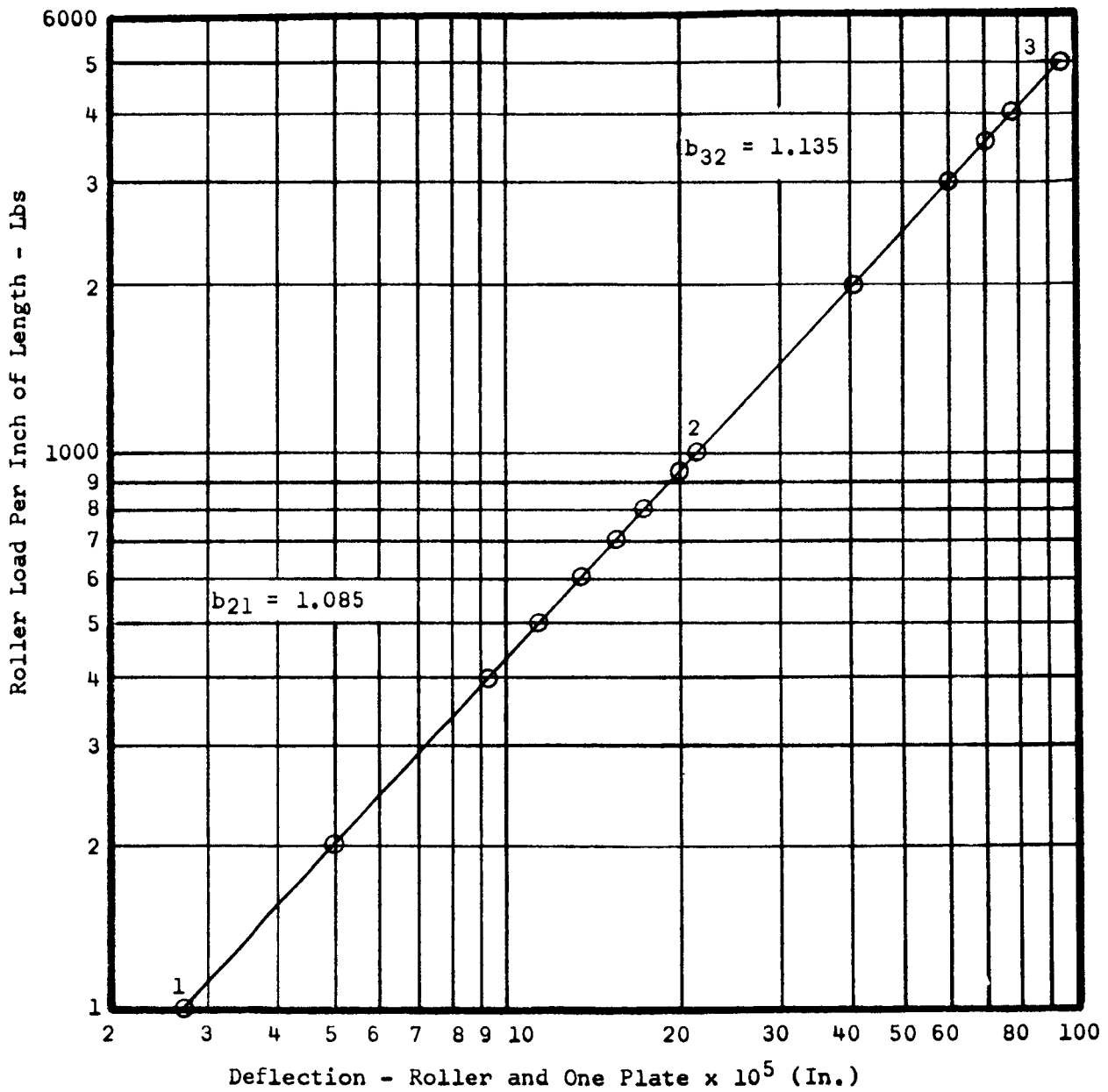CYLINDRICAL ROLLER COMPRESSED BETWEEN TWO FLAT PLATES

Figure B-2

CYLINDRICAL ROLLER COMPRESSED AGAINST A FLAT PLATE

APPENDIX C

TURBINE BEARING HOUSING MODEL TESTS

I. INTRODUCTION

Strain and deflection data[1] obtained from simulated M-1 subscale bearing support housing (P/N 291349) are discussed in this appendix. Five models of various geometrics were tested. However, only the results of the model simulating the actual bearing support housing will be presented.

The tests were conducted to substantiate and aid in the development of theoretical methods for calculating the spring rates of a hollow frustrum-type bearing support housing. The spring rate calculations are used in predicting the critical speeds of the M-1 fuel pump.

Two test conditions were used, and are referred to as the plugged and open conditions. The purpose of the two conditions was to obtain data that could be used in evaluating the amount and type of warping of the end circular shape. This is shown in the sketch below.

PLUGGED   OPEN
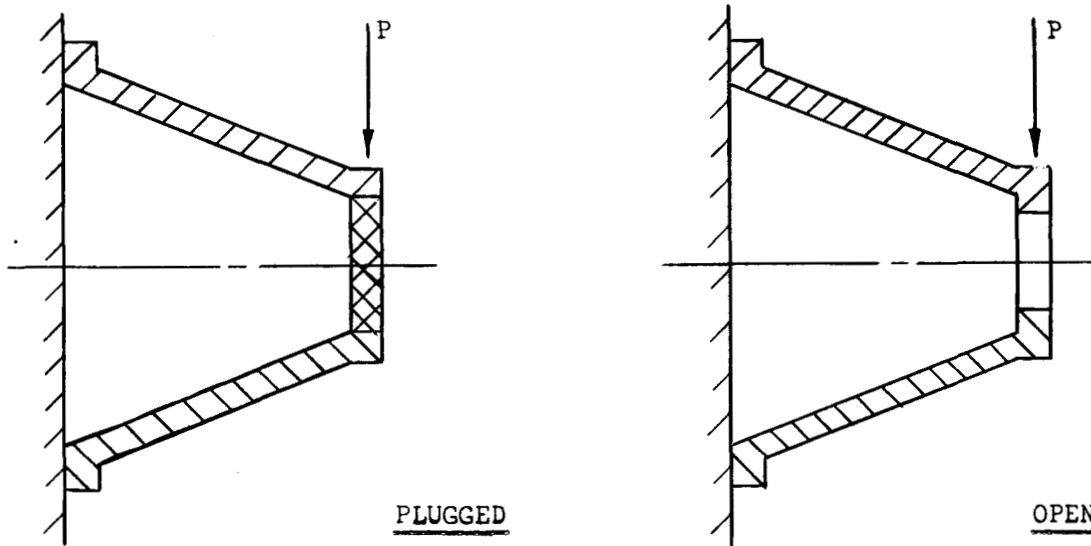
Dial indicators and SR-4 strain gage data were obtained for determination of the model deflections.

---

(1) "Structural Test of the M-1 FTPA Subscale Bearing Support Housings", Aerojet-General Corporation Memorandum 885, Department 9745, 26 June 1964

Appendix C

II. SUMMARY

The spring constant of the frustrum-type bearing housing model obtained for correlation with theoretical analysis is

For the open cone $\quad$ 5.16 $(10)^6$ lb/in.

For the plugged cone $\quad$ 4.12 $(10)^6$ lb/in.

III. TEST SETUP AND INSTRUMENTATION

The 3/8 subscale bearing support housing was instrumented with uni-axial and rosette strain gages, as shown in Figure C-1. The strain gage grid lengths were 0.25 in.

The housings were attached to a rigid deck plate (see Figure C-2) by thirteen 3/8-18 socket head cap screws torqued to 300 in.-lb.

Static loads were applied by a hydraulic actuator, through a 50,000 lb BLH load cell (Model No. U 3XXA) connected to a yoke assembly. A 3/4-in. diameter cable was secured to the yoke and wrapped around the machined groove (from the 90 degree location to the 270 degree location) so that the line of loading went through the zero degree and 180 degree locations of the bearing housing.

Five 0.001-in. division dial indicators were installed at the zero degree and 180 degree locations on the bearing housing to determine the horizontal deflections during loading.

The applied loads were monitored by an SR-4 (Model 120) strain indicator and two 20 channel balancing and switching unit.

IV. TEST PROCEDURE

The bearing housing was subjected to its maximum load to eliminate slippage between the deck plate and the test housing. The load was then released, the bolts retorqued, and the instrumentation zeroed. Incremental loads were then applied to the housing per the following schedule.

Bearing Housing Part Number	Applied Load, (lb)						
291349	0	8000	16,000	24,000	32,000	40,000	0

Dial indicator and strain gage readings were recorded at each incremental load.

A 0.0043-in. to 0.005-in. shrink fit solid steel plug was placed in the upper ring of the bearing housing, and the above test procedure repeated.

V.   DISCUSSION

The data revealed a decrease of the spring rate when the plug was installed in the small end of the cone. Analysis of the strain data indicated a change in the force and moment distribution transmission across the cone diameter. The deflection data measured opposite the point of load application indicated an increase in the rotation of the load ring when the plug was installed which would increase the end moment on the cone resulting in a decrease of the cone spring rate.

The calculated spring rate of the cone, P/N 291349, included the correction for the movement of the cone base. This base movement, which did not occur with the other cones tested, was attributed to the inability of the 3/8-in. diameter bolts to react the 40,000-lb load.

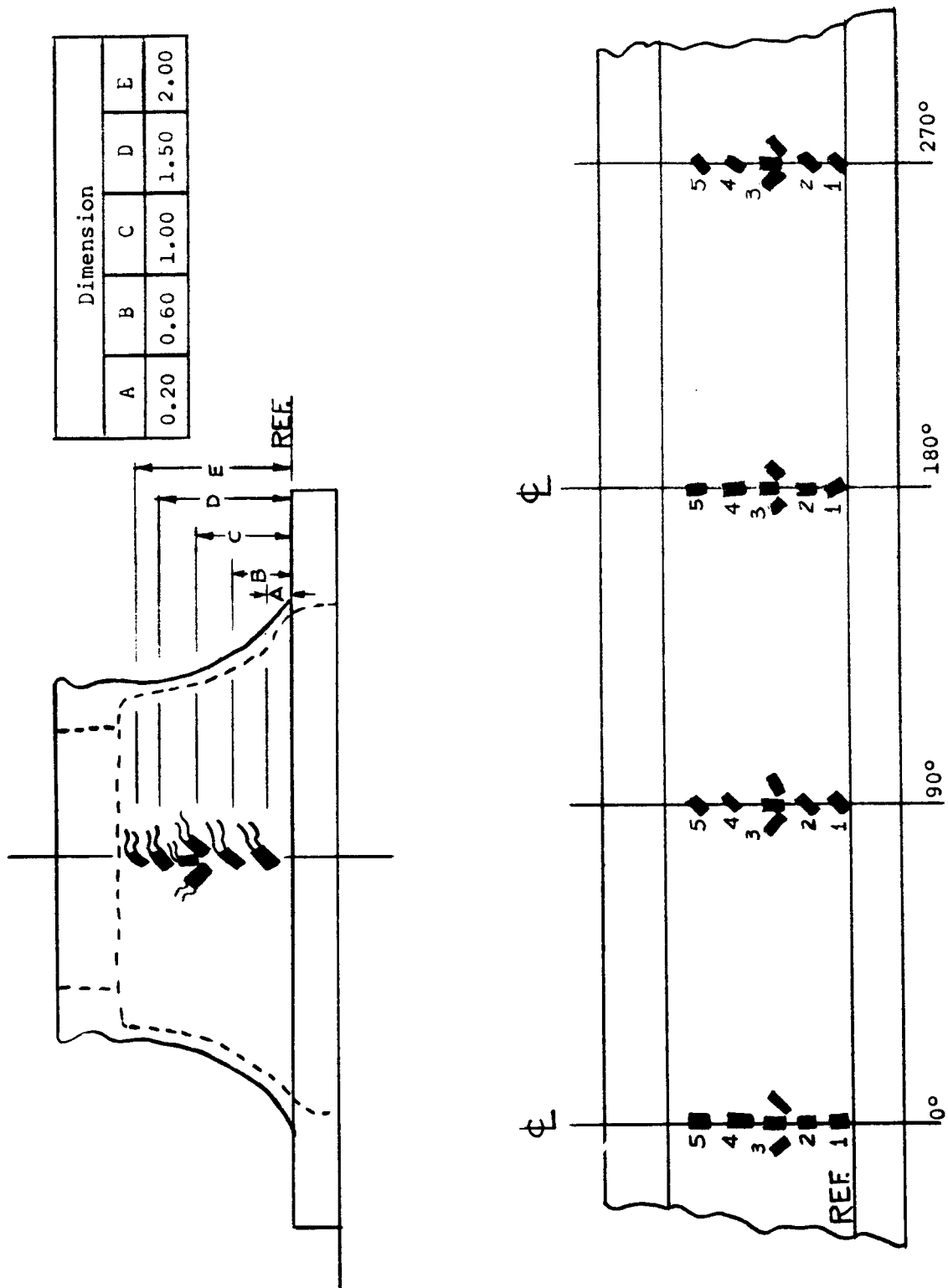| Dimension	A	B	C	D	E
	0.20	0.60	1.00	1.50	2.00

Figure C-1

STRUCTURAL TEST OF THE M-1 TPA SUBSCALE SIMULATED
BEARING SUPPORT HOUSING - LOCATION OF STRAIN GAGES

Figure C-2

Turbine Bearing Housing Test Setup
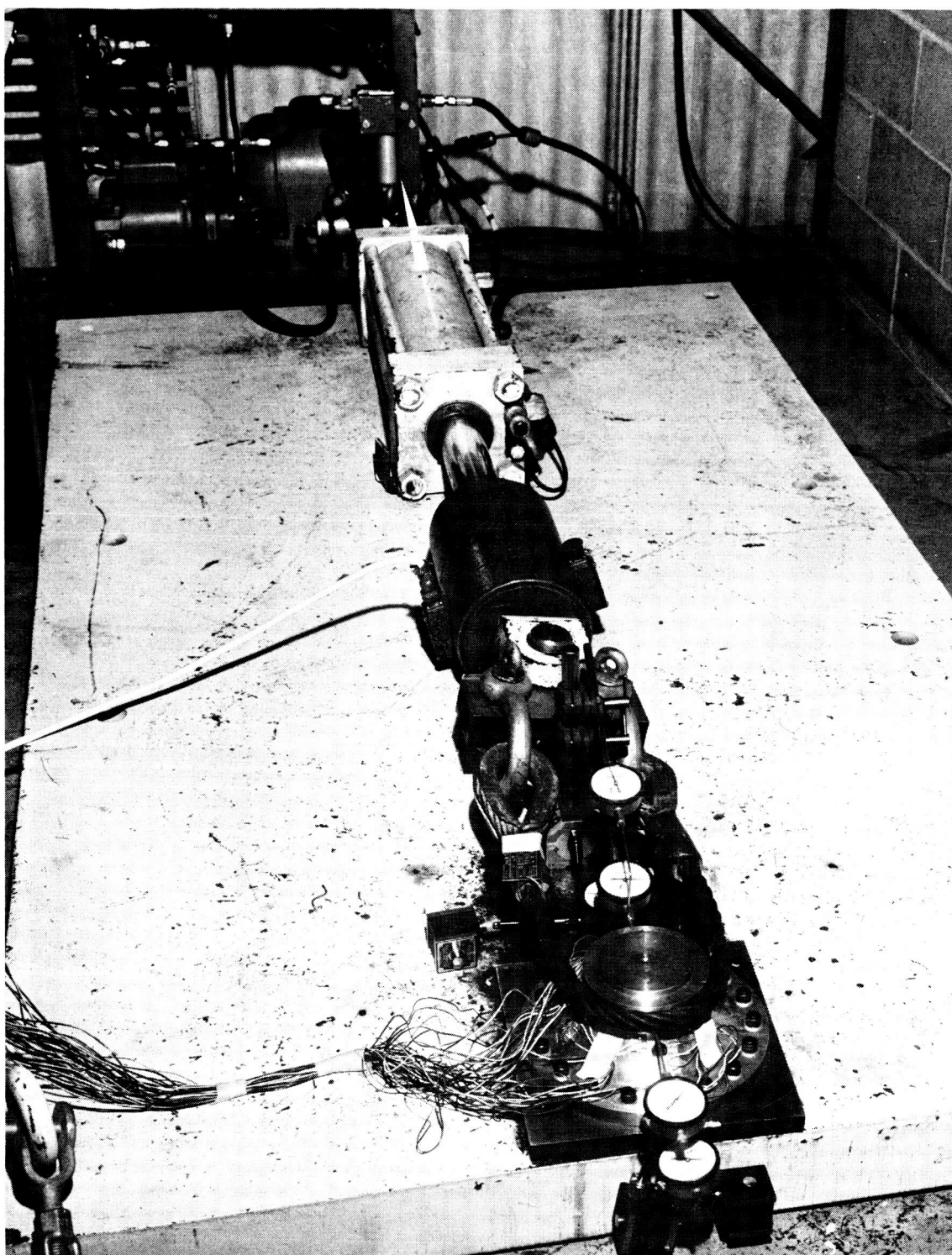
Page C-5

APPENDIX D

BEARING SUPPORT HOUSING ANALYSIS

Appendix D

I. INTRODUCTION

The static spring rate of the turbine bearing housing was analytically predicted based upon three methods of analysis. These methods can be identified as an approximate beam solution, a finite element[1] solution, and scaling model test results. The housing structure and load system are shown in Figure D-1 (top view). The beam and finite element idealizations are given in Figure D-1 (bottom view) and Figure D-2.

II. SUMMARY

The spring constant of the turbine bearing housing was estimated by the various analysis methods as follows:
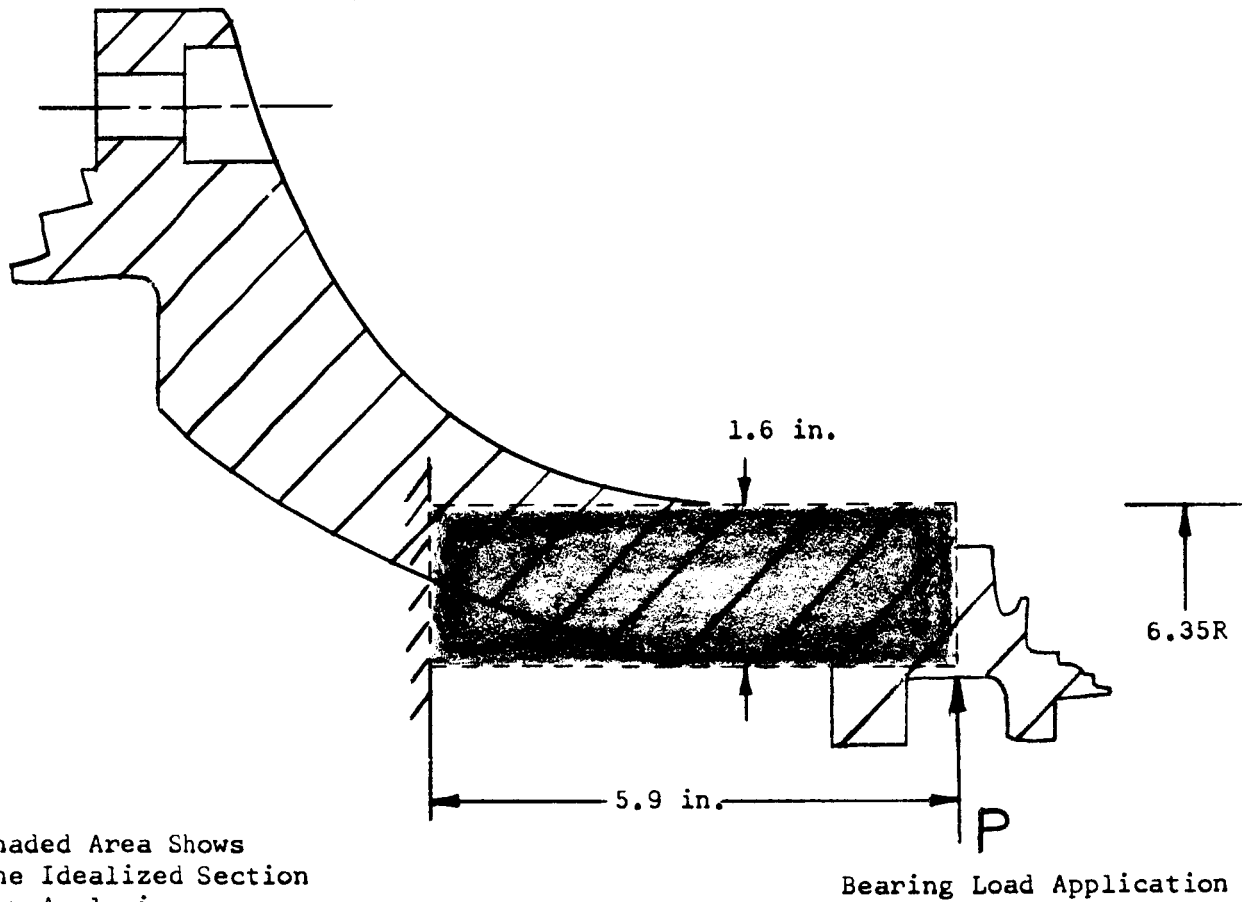
Beam Approximation, $K = 48.1 \ (10)^6$ lb/in.

Finite Element Solution, $K = 19.0 \ (10)^6$ lb/in.

Per Model Tests, $K = 32.3 \ (10)^6$ lb/in.

The model tests, which are discussed in Appendix C, did not entirely simulate the load system. Instead of the sinusoidal-type loading as expected on the prototype, it is believed that the loading on the model was such as to preclude the warping of the end cylindrical shape. Furthermore, when the warping was precluded in the finite element solution, a spring constant within four percent of the model test data was obtained. Thus, the finite element solution which accounts for this warping is considered to yield the best predictions of spring constant. (i.e., $K = 19.0 \ (10)^6$ lb/in.).

---

(1) Holister, G. S. & Zienkiewica, O.D., Stress Analysis, London-New York-Sidney, John Wiley & Sons, 1965

III. <u>APPROXIMATE BEAM ANALYSIS</u>

1.6 in.

6.35R

5.9 in.

P

Shaded Area Shows
The Idealized Section
For Analysis.

Bearing Load Application

It is recognized that the analysis will give a stiffness greater than that of the actual part.

$$\delta_p = \frac{PL^3}{3EI} + 2\frac{PL}{AG}; \quad I = \frac{\pi}{4}\left[\overline{6.35}^{4} - \overline{4.75}^{4}\right] = 900. \text{ in.}^4$$

$$A = \pi\left[\overline{6.35}^{2} - \overline{4.75}^{2}\right] = 56.8 \text{ in.}^2$$

$$= P\left[\frac{207}{3(30)(900)10^6} + \frac{11.8}{56.8(11.5)10^6}\right] = P\left[.00257 + .01813\right]10^{-6}$$

$$= (.0207)10^{-6}P$$

Therefore; Spring Constant $= 48.1\,(10)^6\,\frac{lb}{in.}$

IV. FINITE ELEMENT SOLUTION

A computer program developed to analyze bodies of revolution subjected to non-axisymmetric loading was utilized. This solution is based upon expanding the loading function into a Fourier series representation, obtaining a solution for each Fourier coefficient, and then superposing the solution for each coefficient to obtain the total solution.

The model, which was tested, was analyzed using this finite element computer program. For the condition of zero warping of the circular end, the computer solution yielded a spring rate of $4.0\,(10)^6$ lb/in. as compared to the test value of $4.1\,(10)^6$ lb/in. Allowing end warping, the analytical value was reduced to $2.4\,(10)^6$ lb/in.

The finite element analysis of the prototype indicated a spring rate of $19.0(10)^6$ lb/in.

V. SCALING MODEL TEST RESULTS

According to the finite element solution of the model and prototype the scale factor is

$$S.F. = \frac{19.0(10)^6}{2.42(10)^6} = 7.85$$

It is noted that the model was almost a 3/8 scale model of the prototype. Utilizing the following simplified analysis, the scale factor was determined upon the basis of dimensions and material properties alone.

By definition, $S.F. = \dfrac{K \text{ Prototype}}{K \text{ Model}}$

and: $K = \dfrac{K_f \, K_s}{K_f + K_s}$ where: K_f = Flexure spring rate

K_s = Shear spring rate

$$S.F. = \frac{K_f{}^P \, K_s{}^P}{K_f{}^P + K_s{}^P} \times \frac{K_f{}^M + K_s{}^M}{K_f{}^M \, K_s{}^M} = \frac{K_f{}^P \, K_s{}^P}{K_f{}^M \, K_s{}^M} \, \frac{K_f{}^M + K_s{}^M}{K_f{}^P + K_s{}^P}$$

Rewriting

$$S.F. = \left(\frac{K_f{}^P}{K_f{}^M}\right)\left(\frac{K_s{}^P}{K_s{}^M}\right)\left(\frac{1}{\dfrac{K_f{}^P}{K_f{}^M} + \dfrac{K_s{}^P}{K_f{}^M}} + \frac{1}{\dfrac{K_f{}^P}{K_s{}^M} + \dfrac{K_s{}^P}{K_s{}^M}}\right)$$

Where: $K_f \propto \dfrac{EI}{L^3}$ $\qquad K_s \propto \dfrac{AG}{L}$

$I \propto R^3 t$ $\qquad A \propto Rt$

$K_f \propto \dfrac{R^3 t E}{L^3}$, $K_s \propto \dfrac{RtG}{L}$

Let: $A = \dfrac{K_f{}^P}{K_f{}^M}$ and $B = \dfrac{K_s{}^P}{K_s{}^M}$

Also: $K_f{}^M = Z K_s{}^M$

Then: $S.F. = A \cdot B \left(\dfrac{1}{A + \dfrac{B}{Z}} + \dfrac{1}{B + AZ} \right)$

$+ A \cdot B \left(\dfrac{Z}{ZA+B} + \dfrac{1}{B+AZ} \right)$

$S.F. = A \cdot B \left(\dfrac{Z+1}{ZA+B} \right)$
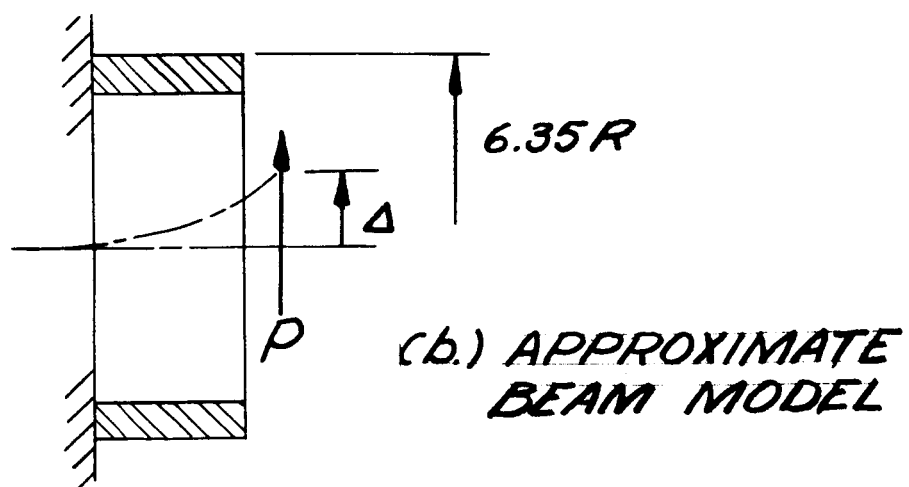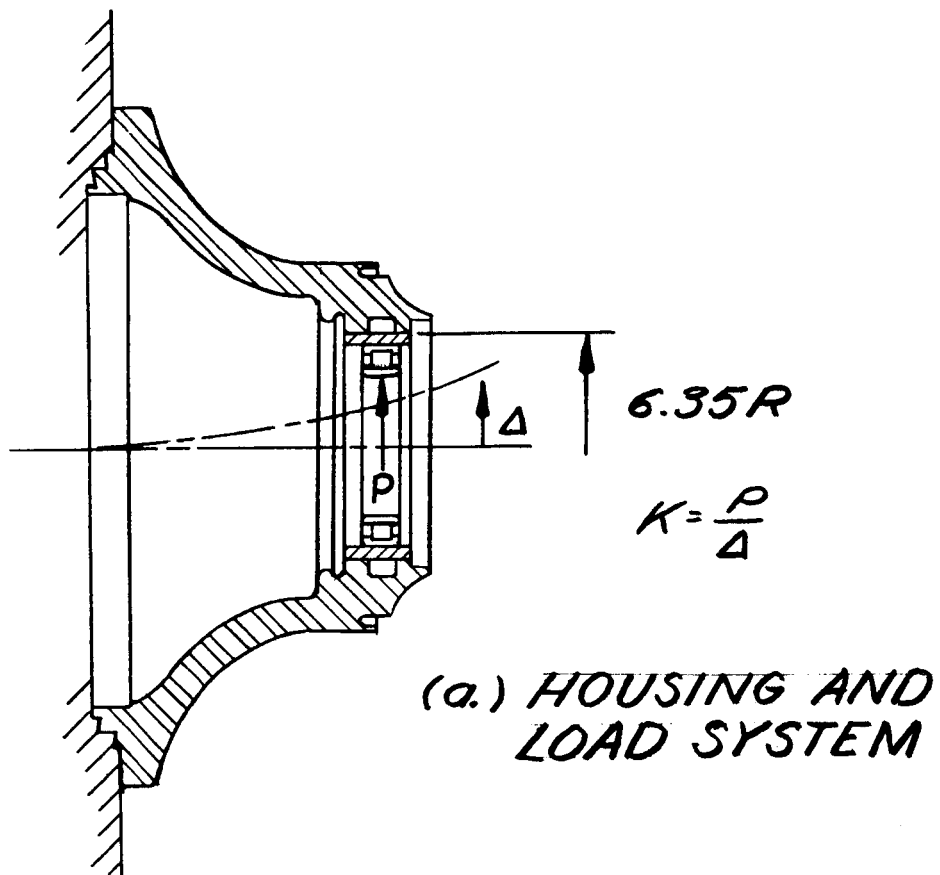
If: A = B as in our case, then:

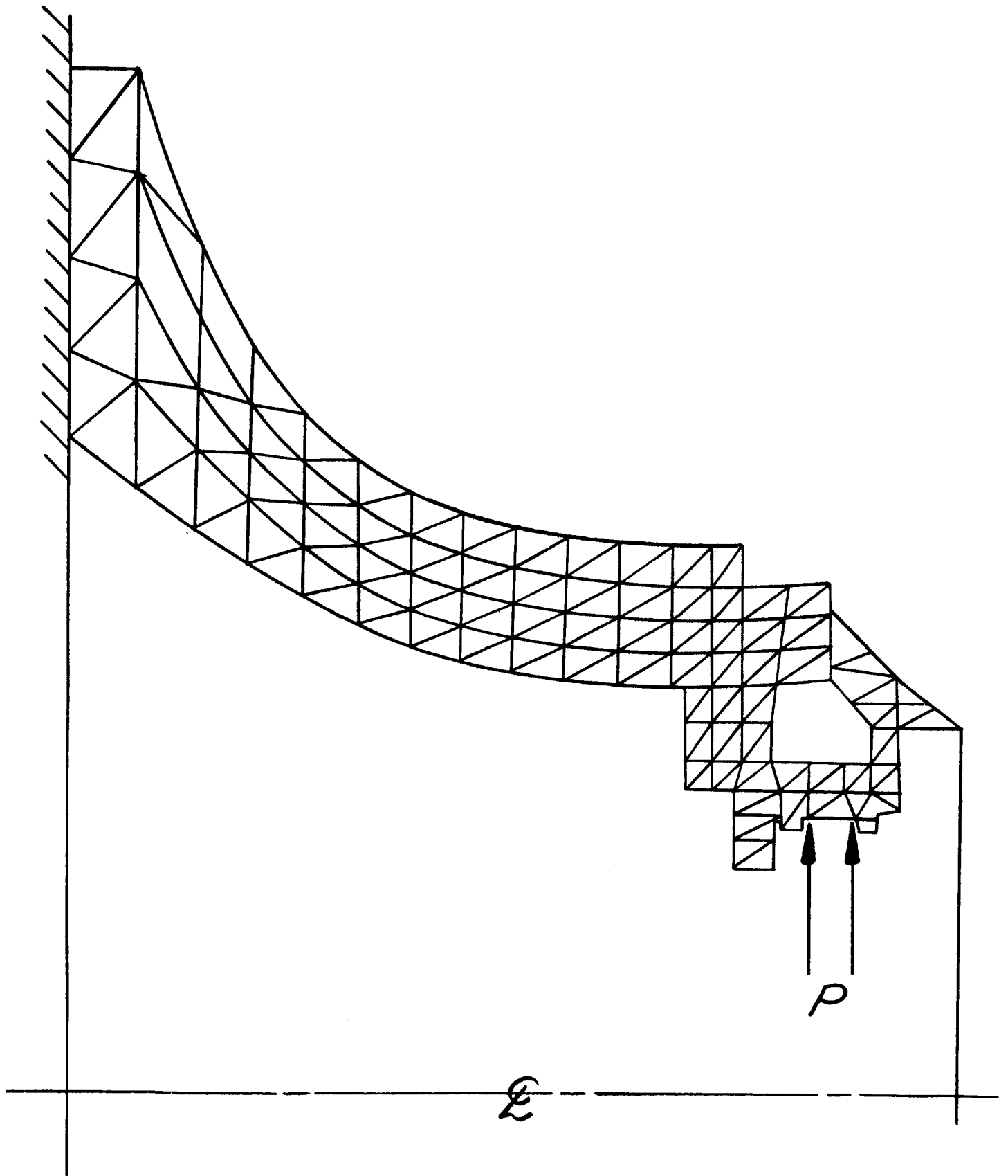$S.F. = A^2 \left(\dfrac{Z+1}{A\,(Z+1)} \right) = A = \dfrac{K_f^P}{K_f^M}$

NUMERICAL CALCULATION OF SCALE FACTOR

Item	Prototype (Inconel 718)	Model (7079 Aluminum)
E	$30(10^6)$ psi	$10.5(10^6)$ psi
G	$11.5(10^6)$ psi	$4.0(10^6)$ psi
R	6.44 in.	2.33 in.
L	5.95 in.	2.16 in.
t	1.65 in.	0.6 in.

$\dfrac{K_f^P}{K_f^M} = S.F. = \left(\dfrac{R^p}{R^m} \right)^3 \left(\dfrac{L^m}{L^p} \right) \left(\dfrac{t^p}{t^m} \right) \left(\dfrac{E^p}{E^m} \right)$

$= \left(\dfrac{6.44}{2.33} \right)^3 \left(\dfrac{2.16}{5.95} \right)^3 \left(\dfrac{1.65}{0.6} \right) \left(\dfrac{30}{11.5} \right)$

$S.\ F. = 7.85$

$6.35R$

$K = \dfrac{P}{\Delta}$

(a.) HOUSING AND
LOAD SYSTEM

$6.35R$

(b.) APPROXIMATE
BEAM MODEL

Turbine Bearing Housing Stiffness Estimate

P

$\mathcal{CL}$

Page D-7

Finite Element Model

APPENDIX E

BEARING CLEARANCES AND ASSOCIATED CONICAL WHIRL UNBALANCE FORCES

I.   INTRODUCTION

The following analysis determines the magnitude of the forcing functions that can exist at the principal masses due to bearing clearances at operating conditions (i.e. -423°F & 13,225 RPM).

II.   SUMMARY

The forcing function caused by conical whirl is defined as ' γ ' where
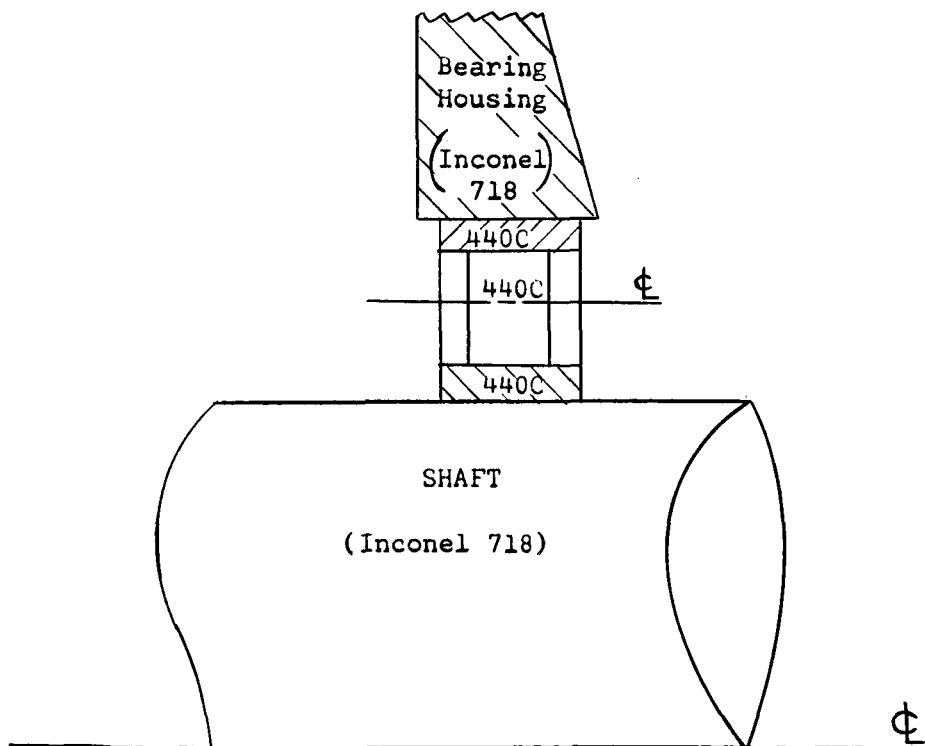
$$F = me\omega^2 = \gamma\omega^2$$

The maximum computed value of forcing functions are

$$\gamma_I = 4.83 \ (10^{-4}) \text{ lb-sec}^2 \text{ at the Inducer}$$

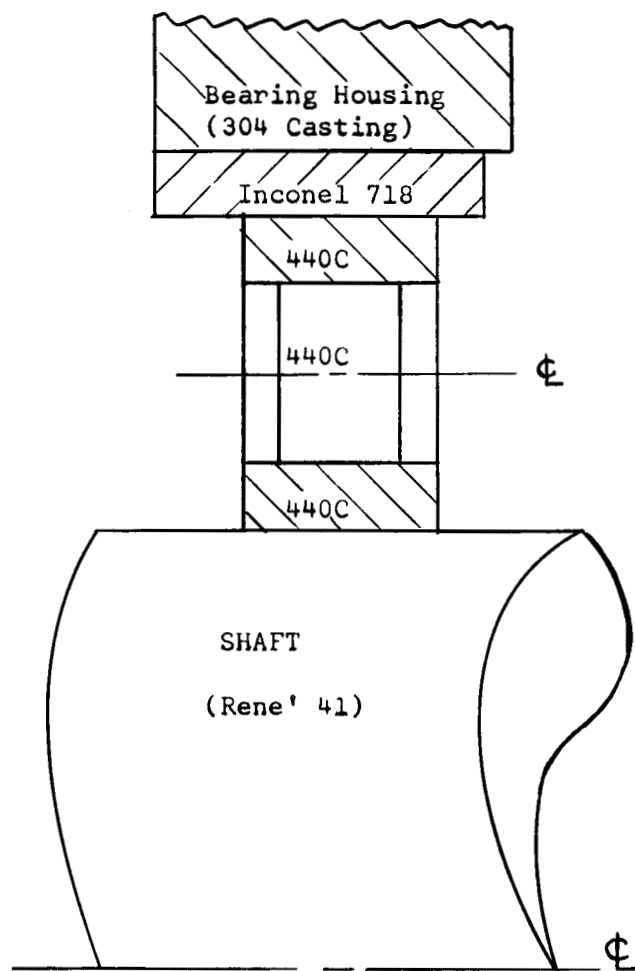$$\gamma_{T_1} = 3.70 \ (10^{-4}) \text{ lb-sec}^2 \text{ at the Turbine No. 1}$$

$$\gamma_{T_2} = 4.31 \ (10^{-4}) \text{ lb-sec}^2 \text{ at Turbine No. 2}$$

III.   CONFIGURATION   (Pump Bearing, P/N 288260) (110mm)

III. <u>CONFIGURATION</u> (Turbine Bearing, P/N 288340) (120mm)

V. FORCING FUNCTIONS

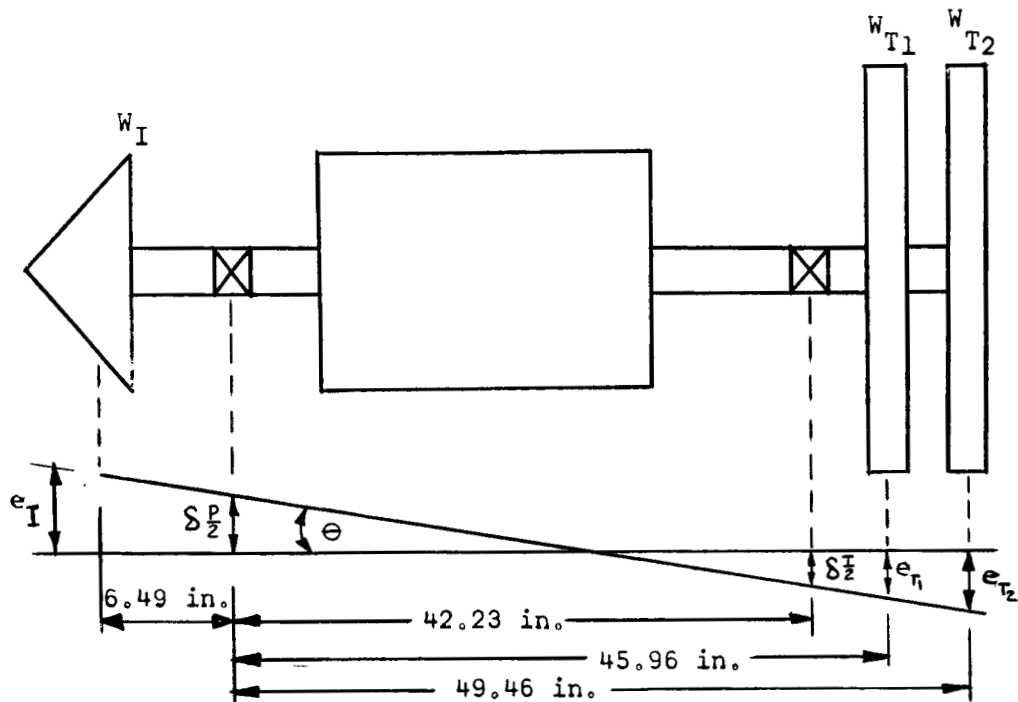The nominal bearing clearances[1] at -423°F and 13,325 RPM are

$$\delta_P = 0.0017 \longrightarrow 0.0022 \text{ in.}$$

$$\delta_T = 0.0008 \longrightarrow 0.0017 \text{ in.}$$

$$W_I = 133. \text{ lb}$$

$$W_{T_1} = 130. \text{ lb}$$

$$W_{T_2} = 128. \text{ lb}$$

$$\theta_{max} = (\delta_P + \delta_T)/2(42.2) = 0.0039/84.4 = 0.462 \, (10^{-4}) \text{ Rad}$$

$$e_I = \frac{\delta_P}{2} - 6.49 \, \theta = -0.0011 - 0.000315 = -0.0014 \text{ in.}$$

$$e_{T_1} = \frac{\delta_T}{2} + 3.73 \, \theta = 0.00095 + 0.000181 = 0.0011 \text{ in.}$$

$$e_{T_2} = \frac{\delta_T}{2} + 7.23 \, \theta = 0.00095 + 0.000352 = 0.0013 \text{ in.}$$

(1) "Design & Development of Liquid Hydrogen Cooled 120mm Roller, 110mm Roller, & 110mm Tandem Ball Bearings for the M-1 Fuel Turbopump", NASA CR-54826,

The Centrifugal Forces are:

$$F \quad = \quad me\omega^2 \quad = \quad \gamma\omega^2$$

$$F_I \quad = \gamma_I\omega^2 \quad = \quad -\frac{133.}{386.} (1.4)(10^{-3})\ \omega^2 = -4.83(10^{-4})\ \omega^2$$

$$F_{T_1} = \gamma_{T_1}\omega^2 = \frac{130.}{386.} (1.1)(10^{-3})\ \omega^2 = 3.70(10^{-4})\ \omega^2$$

$$F_{T_2} = \gamma_{T_2}\omega^2 = \frac{128.}{386.} (1.3)(10^{-3})\ \omega^2 = 4.31(10^{-4})\ \omega^2$$

$$\gamma_I \quad = \quad -4.83(10^{-4})\ \text{lb-sec}^2$$

$$\gamma_{T_1} = \quad 3.70(10^{-4})\ \text{lb-sec}^2$$

$$\gamma_{T_2} = \quad 4.31(10^{-4})\ \text{lb-sec}^2$$

The only forcing functions considered are caused by the inducer and two turbines. All other components are relatively small.

W. F. Dankhoff (3 copies)
NASA
Lewis Research Center
21000 Brookpark Road
Cleveland, Ohio 44135
Mail Stop 500-305

J. A. Durica (1 copy)
Mail Stop 500-210

Patent Counsel (1 copy)
Mail Stop

Lewis Library (2 copies)
Mail Stop 3-7

Lewis Technical Information
   Division (1 copy)
Mail Stop 5-5

D. W. Drier (1 copy)
Mail Stop 21-4

M. J. Hartmann (1 copy)
Mail Stop 5-9

J. C. Montgomery (1 copy)
SNPO-C
Mail Stop 501-1

Major E. H. Karelis (1 copy)
AFSC Liaison Office
Mail Stop 4-1

Lewis Office of Reliability
   and Quality Assurance (1 copy)
Mail Stop 500-203

F. J. Dutee (1 copy)
Mail Stop 21-4

D. F. Lange (1 copy)
Mail Stop 501-1

D. D. Scheer (1 copy)
Mail Stop 500-305

W. J. Anderson (1 copy)
Mail Stop 6-1

NASA Headquarters (6 copies)
NASA Scientific and Technical
   Information Facility
Technical Information Abstracting
   and Dissemination Facility
Box 5700
Bethesda, Maryland

Library (1 copy)
NASA
Ames Research Center
Moffett Field, California 94035

Library (1 copy)
NASA
Flight Research Center
P. O. Box 373
Edwards AFB, California 93523

Library (1 copy)
NASA
Goddard Space Flight Center
Greenbelt, Maryland 20771

Library (1 copy)
NASA
Langley Research Center
Langley Station
Hampton, Virginia 23365

Library (1 copy)
NASA
Manned Spacecraft Center
Houston, Texas 77058

Library (1 copy)
NASA
George C. Marshall Space Flight Center
Huntsville, Alabama 35812

Library (1 copy)
NASA
Western Operations Office
150 Pico Boulevard
Santa Monica, California 90406

Library (1 copy)
Jet Propulsion Laboratory
4800 Oak Grove Drive
Pasadena, California 91103

A. O. Tischler (2 copies)
NASA Headquarters
Code RP
Washington, D. C. 20546

J. W. Thomas, Jr. (5 copies)
NASA
George C. Marshall Space Flight Center
I-E-E
Huntsville, Alabama 35812

W. W. Wilcox (1 copy)
NASA
Lewis Research Center
21000 Brookpark Road
Cleveland, Ohio 44135
Mail Stop 500-305

Dr. E. B. Konecci (1 copy)
National Aeronautics and Space Council
Executive Office of the President
Executive Office Building
Washington, D. C.

H. V. Main (1 copy)
Air Force Rocket Propulsion Laboratory
Edwards Air Force Base
Edwards, California

T. Iura (1 copy)
Aerospace Corporation
2400 East El Segundo Blvd.
P. O. Box 95085
Los Angeles, California 90045

Pratt and Whitney Aircraft
   Corporation (1 copy)
Florida Research and Development
   Center
P. O. Box 2691
West Palm Beach, Florida 33402

Rocketdyne (1 copy)
(Library Department 586-306)
Division of North American Aviation
6633 Canoga Avenue
Canoga Park, California 91304
Attention: Dr. Kurt Rothe

Hudson Scheifle (1 copy)
Bower Roller Bearing Division
3040 Hart Avenue
Detroit, Michigan

R. P. Remorenko (1 copy)
The Fafnir Bearing Company
37 Booth Street
New Britain, Connecticut

H. Hanau (1 copy)
Industrial Tectronics, Inc.
18301 Santa Fe Avenue
Compton, California

John H. Johnson (1 copy)
Marlin-Rockwell Corporation
402 Chandler Street
Jamestown, New York

Richard Matt (1 copy)
New Departure Division of
  General Motors Corporation
269 N. Main Street
Bristol, Connecticut

Tibor Tallian (1 copy)
SKF Industries, Inc.
1100 First Avenue
King of Prussia, Pennsylvania

Richard Shevchenko (1 copy)
Pratt & Whitney Aircraft
Division of United Aircraft Corp.
400 Main Street
E. Hartford 8, Connecticut

Myles Butner (1 copy)
Rocketdyne
Division of North American Aviation
6633 Canoga Avenue
Canoga Park, California 91304

H. J. Macke (1 copy)
General Electric Company
Flight Propulsion Division
Large Jet Engine Department
Cincinnati 15, Ohio